POLITECNICO DI TORINO

Corso di Laurea Magistrale in Ingegneria Biomedica

Tesi di Laurea Magistrale

Tailored design of multifunctional bioactive glasses for bone tissue applications

Relatori:

Prof.ssa Enrica Vernè

Prof. Francesco Baino

……. **Candidato:**

Carla Anna Migneco

…… …….

Ottobre 2020

Sommario

1. Introduction

The structure of human body is assured by a skeleton made of 206 bones [1].

Mechanical properties of bones are given by their complex internal structure, made of an organic phase, composed mainly by collagen, and a mineral phase constituted by carbonated apatite, plus other proteins that stimulate cellular functions [1].

At difference with the other tissues, most of bony fractures fixes without scar formation and the regenerate bone matches perfectly to the pre-existing one. In fact, bones are characterized by their intrinsic capacity for regeneration. The bone regeneration process occurs during normal fracture healing, but can also be due to physiological load conditions, which produce micro-damage and lead to continuous remodelling, known as bone turnover [2].

Moreover, there are special clinical conditions that require enhancement of bone regeneration. For example, skeletal reconstruction of large bone defects due to abnormalities, infections, trauma, tumour resections, or pathologies related to age and sex, in which regenerative processes are compromised, such as osteoporosis and avascular necrosis, osteopenia and as several dental problems [2].

Persons with bone defects may also suffer from huge social and psychological handicap, with a significative impact on their life quality [3].

Therefore, bone defects due to trauma and to pathological bone resorption represent a major challenge and are to be considered as a global health problem [1].

There are different clinical approaches aimed at enhancing bone regeneration when the physiological healing process is not sufficient or compromised. They can be divided into invasive methods, as bone-grafting, induction of cement spacer (Masquelet technique), and non-invasive, which reproduce biophysical stimulation, thanks to low-intensity pulsed ultrasound and pulsed electromagnetic fields [2].

In orthopaedic and maxillofacial applications, bone grafting is a common surgical procedure to improve bone regeneration and it can be realized by autologous bone grafts, allografts and bone graft substitutes, combined or not with growth factors. The ‘golden standard’ choice is certainly represented by autologous bone grafts where the bone tissue is usually taken from anterior and posterior iliac crests of the pelvis of the patient [4]. In this case, side effects due to immunoreactions and infections are greatly reduced. On the other

hand, the bone tissue collection requires additional surgical interventions, with possible complications for patients and substantial cost increase. These disadvantages can be overcome by allografts, obtaining bone tissue from human cadavers or living donors. Contrary to autografts, tissues coming from different source from own patient may involve issues of immunogenicity and rejection reactions, possibility of infection transmission, and costs [1], [5] [6].

Another alternative possibility to autologous or allogeneic grafting is represented by bone grafts substitutes. They often consist of three-dimensional porous structures, known as scaffolds, made of synthetic or natural biomaterials that stimulate migration, proliferation and differentiation of bone cells while providing mechanical support for bone regeneration. These methods are already used in clinical practice for their excellent osteoconduction, especially for regeneration of large bone injuries. Most of these current procedures are relatively satisfactory but present some limits [6].

Bioactive glasses have been extensively studied with a growing interest by scientists all over the world due to their appealing characteristics that allow tissue engineering improvement which is of outmost importance for bone regenerative medicine [7].

The goal is to generate new, cell-driven, functional tissues, rather than just to implant non-living scaffolds. This would overcome limitations of current therapies combining knowledges from different sciences, such as engineering, materials science, physics, chemistry and biology [7].

The reproduction of physiological bone regeneration would offer novel strategies to treat many bone diseases, due to trauma, ablative surgery, ageing, genetic or metabolic disorders [7].

2. Biomaterials

Human body can immediately react to "invader" introduction by a biological response through two different reactions: the innate immune response (nonantigen specific) and the adaptive immune response (antigen specific) [8]. Innate immune response is the first reaction of the body triggering a defence strategy whenever a foreign material is introduced into the organism. The *foreign body reaction* occurs with a complex and uncontrollable cascade of events which can appear in different degree of severity on dependence of the material nature. In the worst case, implant can be completely surrounded by a fibrotic capsule and rejected comporting dangerous side effects as material degradation, chronic inflammation, cell apoptosis or tissue necrosis (**Table 1**) [9] [10] .

Table 1. Major characteristics of the generic host response to biomaterials [3].

Protein adsorption and desorption characteristics
Generalised cytotoxic effects
Neutrophil activation
Macrophage activation, foreign body giant cell production, granulation tissue formation
Fibroblast behaviour and fibrosis
Microvascular changes
Tissue/organ specific cell responses
Activation of clotting cascade
Platelet adhesion, activation, aggregation
Complement activation
Antibody production, immune cell responses
Acute hypersensitivity/anaphylaxis
Delayed hypersensitivity
Mutagenic responses, genotoxicity
Reproductive toxicity
Tumour formation

The need of materials to be implanted without triggering this negative response lead to an increasing interest in the development of new biomaterials.

Biomaterials early definition goes back to 1976 thanks to European Society for Biomaterials (ESB): *"a nonviable material used in a medical device intended to interact with biological system"*. Since then, biomaterials science and technology have been stimulated and guided by progress in chemistry, biology and engineering. In this way,

biomaterials evolution can distinguish three biomaterials generation partially overlapped [11].

The first generation of biomaterials was developed in the ‘50s, the goal of this early biomaterials was to be as bioinert and biocompatible as possible. Biocompability can be defined as *“the ability of a material to perform with an appropriate host response in a specific application.”*[11]. Biomaterials belonging to the first generation were selected because of their ability to minimize the negative effects associated to innate response.

In the second biomaterial generation the concept of biocompatibility evolved to a pronounced bioactivity, that is the ability to trigger a controlled and favourable reaction in the tissue into which they are implanted. This new feature makes biomaterials of second-generation therapeutic devices.

Further progresses have been made with a third-generation of biomaterials aiming at functional tissue regeneration. In fact, this third generation is bio-interactive, bio-integrative, completely resorbable and capable to stimulate specific cell responses at the molecular level.

Biomaterials can be also classified by their nature: polymers, metals, composites and ceramics [7].

Polymers biomaterials are characterized by a unique composition flexibility that allows to realize many different formulations according to different requirements. They are also available in different forms, from solids to films and gels, making them very appealing for a wide variety of clinical applications. Unfortunately, they have poor mechanical properties that make them not suitable to applications which require stress resistance [2].

On the contrary, metals have high strength and ductility, but they are characterized by a low biocompatibility [2] .

Composite materials are corrosion-free and they have high elastic moduli thanks to cross-linked elastomers. These features are beneficial for biocompatibility, but their limit is represented by their short-term durability which make them not adapt to permanent solutions[2]

Finally, glass, ceramic and glass-ceramic biomaterials combine an excellent biocompatibility with good resistance to corrosion and compression. For this reason, they

are highly appreciated in biomedicine and research is still underway to overcome their brittleness, high density and low fracture strength [2].

3. Bioactive Glass Origin

3.1 Definition and general characteristics of glasses

Glasses are defined as amorphous solid materials produced by progressive cooling of a fluid and characterized by the absence of long-range regular periodic arrangement at atomic level. This lack of order does not represent an equilibrium state and the glass solid appears as *frozen* into a unstable condition (**Figure 1**) [12].

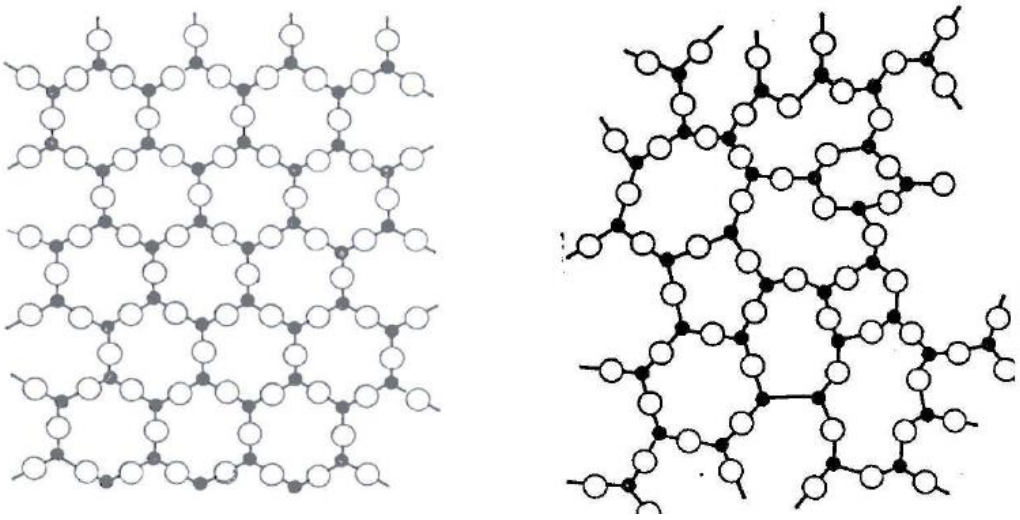

Figure 1. Comparison between well-ordered crystalline silica network and amorphous silica network characterized by lack of long-range order [12].

The structure may be defined as thermodynamically *metastable* since it may evolve to a more ordered crystalline structure under specific kinetics conditions [13]. Crystallization rate is the main factor able to determine the formation of amorphous or crystalline phases, in fact when this rate is much lower than cooling rate the fluid can vitrify. The opposite process is the "devitrification", that is the nucleation and development of crystalline

species within the glassy matrix. This phenomenon takes place when the crystallization rate reaches quite high value and the growth of clusters of few hundred atoms leads progressively to a glass-ceramic material.

As amorphous materials glasses exhibit a region of behaviour transformation correlated to a transition temperature (T_g). Above the T_g the glass shows typical fluid properties and below it the material is in rigid form [14]. The transition temperature value is defined by both cooling rate and melting temperature (T_m) as shown **Figure 2**.

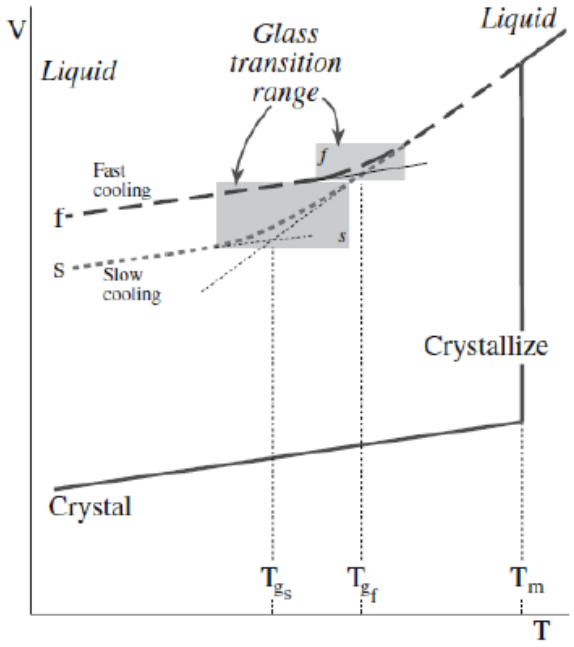

Figure 2. Plot of volume versus temperature for a liquid that forms a glass on cooling and one that forms a crystalline solid. As represented, the glass transition temperature, T_g, depends on the cooling rate and is not fixed like T_m. Cooling rate increase corresponds at T_g and specific volume incrementation [13].

Glass structure appears as a disordered network composed by oxides, which can be classified into three different classes depending on their coordination number, namely the number of atoms that surround a central atom:

- Glass formers (3<n<4) which form the amorphous network, as silica, boron oxide and phosphorous oxide;

- Glass modifiers(n>6), weakly bonded to the network, as alkali oxides and zinc oxide;

- Intermediates(4<n<6), strongly bonded to the network even if they are not able to form the glass alone. In low concentration they can co-participate to the structure within former oxide network, as alumina, zirconia and titanium oxide [15].

X-ray diffraction analysis of a glass material is characterized by the absence of spikes and the presence of an amorphous halo due to lack of long-range order.

Glass materials have quite low mechanical properties strongly influenced by their composition and surface conditions.

Regarding chemical stability, they are corrosion-free, making them appealing to several applications. One of the most attractive features of glasses is their capability to release alkalyn ions once in contact to specific environments [15].

Thanks to the above-mentioned properties, glass materials are used in several applications providing excellent results in many fields.

3.2 Brief History of Bioactive Glasses

Bioactive glasses are biomaterials of third generation [5]. Their origin has to be found in 1967 thanks to the discovery of Bioglass® by Professor Larry L. Hench who began his studies about glass-ceramics at the University of Florida, giving a particular attention to the mechanism of glass nucleation. Hench's interest about materials able to regenerate human tissue was triggered by a casual conversation with Colonel Klinker, as reported in his article "The story of Bioglass®" [13] . Colonel Klinker had just came back from Vietnam where he was enlisted with the Army Medical Corps. The Professor described him his recent studies about polymeric and metal implants and the problem derived from their use. Moreover, he mentioned other experiments about gamma rays applied to vanadia-phosphate semiconductors. These results caught the attention of the officer: the studies had proved these new materials can survive to high dose of high energy radiation [13]. It is from the description of these two different material applications that Colonel Klinker naturally formulate a question which will inspire Hench and his future discoveries: "If you can make a material that will survive exposure to high energy radiation, can you make a material that will survey exposure to human body?" [16]. Especially in USA, in that period after an excruciating war, a growing number of people needed to be treated because of

amputated limbs or damaged tissue, they needed materials able to regenerate defects without being rejected.

In his report, Hench described how he and his co-workers based their research upon a simply hypothesis: “The human body rejects metallic and synthetic polymeric materials by forming scar tissue because living tissue are not composed of such materials. Bone contains a hydrated calcium phosphate component, hydroxyapatite (HA) and therefore if a material is able to form a HA layer in vivo it may not be rejected by the body.” [16].

On the base of this hypothesis, Professor Hench and his research group had the intuition to study and test different glass compositions based on SiO_2-Na_2O-CaO-P_2O_5 oxide system. Between the other, the formulation 45 SiO_2- 24.5Na_2O- 24.5 CaO- 6 P_2O_5 (wt.%), (referred to as 45S5 and trademarked as Bioglass® by University of Florida) was selected because of its easiness of melting and its CaO/ P_2O_5 high ratio which improves material surface ability to react into a physiological environment.

Experiments carried on 45S5 Bioglass® showed an excellent biocompatibility and new osteoconduction and osteoinduction abilities: this new material played an active role in the process of bone tissue regeneration, becoming the first example of bioactive glasses (BGs) and therefore the first biomaterial belonging to third generation. Different *in vitro* and *in vivo* tests were conducted on 45S5 bioactivity in bone regeneration process, proving its extraordinary ability to induce formation of a HA layer which forms a strong bone-implant bond and finally leads to completely restore the bone tissue.

Since that moment, many other compositions and different bioactive glasses have been studied and developed by scientists all over the world, leading to the development of three main classes of bioactive glasses divided by their former oxides [17]:

i) Silicate bioactive glasses;
ii) Phosphate bioactive glasses;
iii) Borate bioactive glasses.

The 45S5 Bioglass® is a silica-based composition and it has been demonstrated that silicon plays a fundamental role in bone regeneration process by the gene activation [7].

In these glasses, the network is formed by basic units of SiO_4 tetrahedron and its connectivity can widely vary into 1-, 2-, and 3- dimensional structures. Each oxygen anion

is coordinated by two silicon cations (Si-O-Si) resulting in relatively open structures which can be easily broken once in contact with biological fluids.

In 1990, Brink proposed the first borosilicate glass for biomedical application [7][18]. In its composition the amount of B_2O_3 was carefully tailored to achieve a pronounced bioactivity. Glassed based on borate as network former oxide are very reactive and characterized by lower chemical durability, which allows them to create the hydroxyapatite layer more rapidly than the silica-based ones.

P_2O_5 was used as former oxide for the first time in 1980, when Anderson decided to study and develop the first phosphate-based glasses. In nature, phosphate group [PO_4] is present in tetrahedron structural unit which is intrinsically asymmetric [7] Thanks to its property, phosphate bioactive glasses are characterized by low durability and more solubility in biological fluids.

Flexibility of bioactive formulation is a strongly appealing characteristic which has permitted the realization of a huge number of BGs, exhibiting different features depending to their composition, processing method and additive manufacturing.

4. Bioactivity Process

In 1987 European Society for Biomaterials defines as bioactive material *"one which has been designed to induce specific biological activity"* [3]. This definition may be declined to different application fields in medicine. Focusing in particular on bone regeneration, bioactive glasses are considered attractive bone substitutes for their property of chemically bonding the living bone through the formation of bone-like apatite on implant-bone interface [17].

To better understand the complex mechanisms of bioactivity occurring in bone regeneration process, a brief summary of bone tissue structure and hydroxyapatite properties is reported below.

4.1 Structure and Main Properties of Bone Tissue

Bone is a nanocomposite material characterized by a hierarchical structure (**Figure 3**). Its tissue appears as highly heterogeneous and dynamic thanks to bone ability to re-adapt its structure in reaction of mechanical and biological application of stimuli.

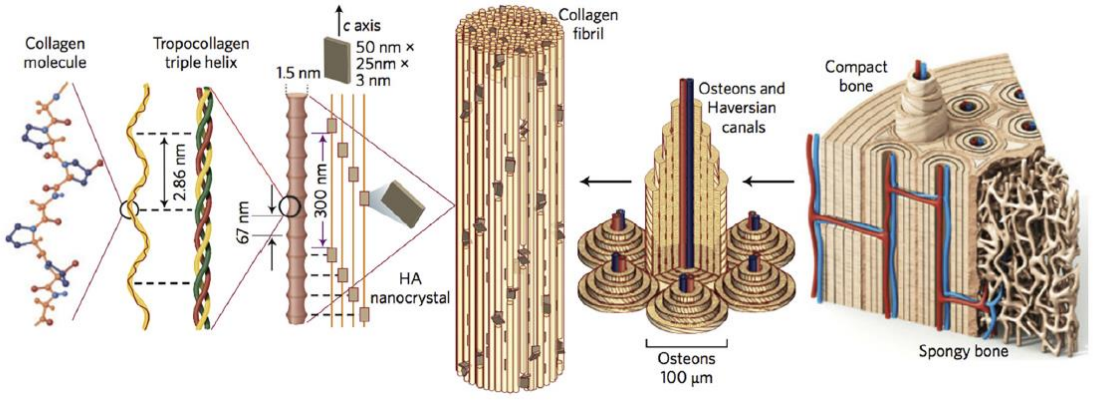

Figure 3. Hierarchal structure of the bone [19].

On a macrostructural perspective, bones are usually described in terms of an external **cortical** (or compact) **bone** which is very dense and internal **cancellous** (or **trabecular**) **bone**. At the microscopic level, the cortical bone is composed by osteons and Haversian canals surrounded by blood vessels which provide nutrition to the tissue. At the nanoscopic level, the fibrils are arranged into geometrical patterns and comprise collagen molecules formed by three chains of amino acids and nano crystals of hydroxyapatite [19].

Bone is also defined as mineralized tissue because of its intracellular matter, rich of mineral crystals. The coexistence in bone of an organic phase (30-35 wt.%) and an inorganic phase (60-65wt. %) confers different properties: the organic component provides strength and elasticity, while the inorganic one gives hardness and compactness.

The **organic matrix** is prevalently composed of collagen fibers in which bone cells are immersed, i.e. osteo-progenitor cells, osteoclasts, osteoblasts and osteocytes [1].

Osteo-progenitor cells are highly proliferative and they can differentiate into osteoblasts which are responsible for the synthesis of new tissue (*osteogenesis*). Once osteoblasts have fulfilled their role in the bone synthesis, they could be trapped within the matrix, becoming osteocytes which are responsible for the preservation of the extracellular matrix.

Of great interest for tissue engineering is the phenomenon leading to changes in the osteoblast progenitor cells population in presence of biologically active ionic dissolution, as illustrated in **Figure 4**.

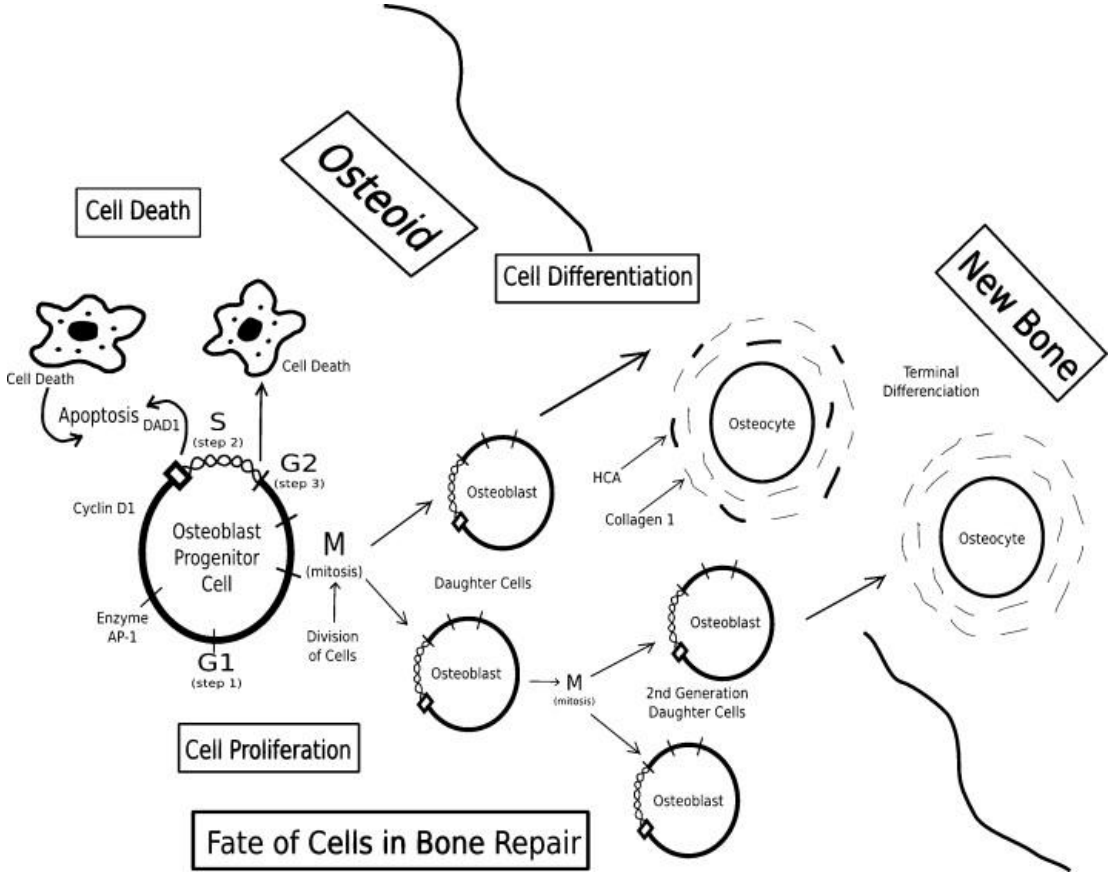

Figure 4. Schematic of osteogenic progenitor cell cycle leading to (1) programmed cell death; (2) mitosis and cell proliferation; or (3) terminal differentiation into osteocytes [20].

The **inorganic phase** is mainly composed by calcium salts crystals, mostly calcium phosphates but also calcium carbonates, while calcium fluorides and magnesium phosphates are present in lower quantity. Calcium phosphates take the form of ***hydroxyapatite*** *crystals* [$(Ca_{10}(PO_4)_6(OH)]$ which are responsible of bone tissue mechanical properties. In bone tissue, crystals appear elongated and their dimensions are nanometrics, about 2×20×40 nm **(Figure 5)** [21].

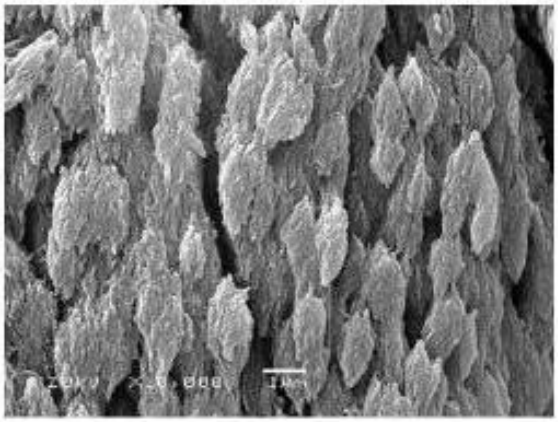

Figure 5. Hydroxyapatite crystals [12].

Bone regeneration process continuously occurs in physiological condition, leading to perpetual cellular renovation and changes of the bony morphology. But bone tissue can be subjected to a myriad of pathologies (as *osteoporosis,* metabolic and autoimmune bone disorders and tumours) and trauma creating large defects within the bone tissue. Bone implant is required in these severe cases when the natural repair process is insufficient due to the above-mentioned causes.

Although Tissue Engineering (TE) has successfully developed several biomaterials to realize bone implants, side effects related to their implantation may occur. Failure usually originates at the interface between the biomaterial and the host bone: this combination of *foreign body reaction* of the immune system and deterioration of the bone-implant may have catastrophic effects causing the failure of the orthopaedic implants (**Table 2**).

Table 2. Problems, side effects and possible solutions related to bone implants [22].

Problem	**Leads to**	**Solution**
Stability of the bone-implant interface Stress shielding of bone	Wear debris Implant loosening Deterioration of bone Fracture Pain Revision surgery	A new generation of implants designed to: - Achieve interfacial stability by bonding to bone and soft connective tissue - Minimize stress shielding by having an elastic modulus similar to bone - Assist in the augmentation and regeneration of tissues instead of replacing tissues

4.2 Bioactivity mechanisms in bone regeneration process

The invention of bioactive glasses represents a turning point for bone TE. The most appealing characteristic of the third generation of biomaterials is certainly their pronounced bioactivity.

Once implanted into the body bioactive materials stimulate a specific biological reaction at the interface of the material, resulting in the formation of a strong bone-implant bond. (**Figure 6**)

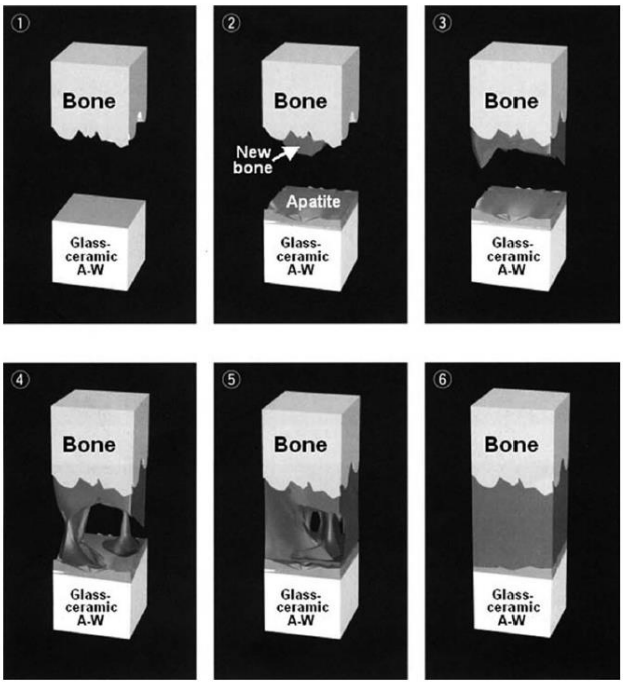

Figure 6. Bioactivity processes in bone-implant interface [23].

At the basis of bioactivity process there are complex interactions driven by inorganic chemical (Stage 1-5) and biochemical (Stage 6-12) mechanisms which can be classified in 12 reaction stages (**Figure 7**).

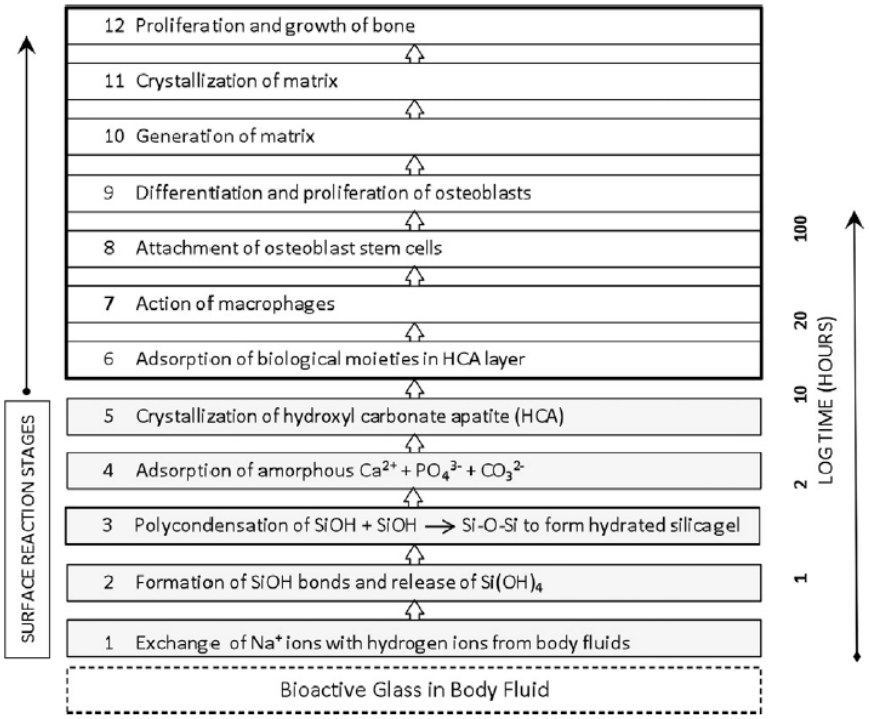

Figure 7. Sequence of interfacial reactions between bone and a bioactive glass [24].

In the first reaction, exchange of Na^+ ions from the glass with H^+ and $H3O^+$ from body fluids rapidly occurs. The second step involves the breaking of Si-O-Si bonds and formation of Si-OH (silanols) at the interface between the material and the bone tissue. In the third stage condensation takes place followed by a migration of Ca^{2+} and PO_4^{3-} to the surface, forming a layer rich of calcium oxide and phosphate oxide on top of the silica layer. Stage number five represents the progressively crystallization of hydroxyapatite, at this moment the surface is covered by nanometric hydroxyapatite crystals [24], [25].

Biochemical adsorption of growth factors has been observed on the formed HCA layer [26]. Macrophages do not recognize the hydroxyapatite as foreign material, due to its similarity to the mineral phase of bone tissue, and simulate stem cells attachment on HCA surface. Stem cells progressively differentiate into different cells of the bone tissue, allowing the generation of bone matrix. The crystallized matrix represents the final product of bioactivity process, permitting the proliferation and growth of bone tissue [26].

Some studies have recently shown that bioactive resorbable glasses and their dissolution products stimulate osteogenesis by regulating osteoblast proliferation, differentiation and also **gene expression** [12][20].

As illustrated in **Figure 8**, bioactive glasses enhance bone cell gene expression depending on four main factors:

1. Surface chemistry;
2. Topography;
3. Rate and type of dissolution ions released;
4. Mechanical properties of glass/bone interfaces [12].

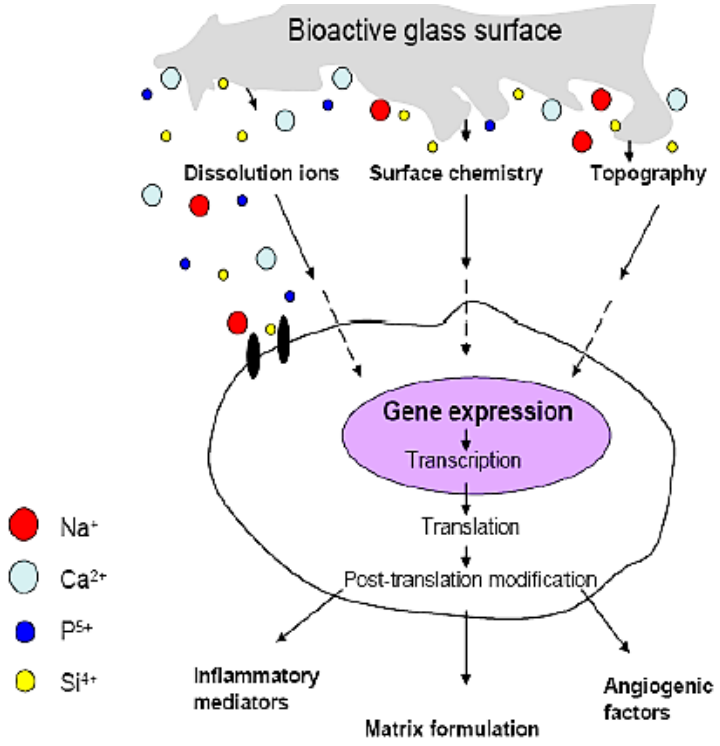

Figure 8. Main mechanisms proposed to determine bone cell gene expression [12].

The bioactivity process can be evaluated through *in vitro* experiments immerging the biomaterial into a Simulated Body Fluids (SBF) developed by Kokubo which recreates the physiological environments [27]. However, in vitro bioactivity tests using SBF do not always represent a realistic prediction of the bioactive potential of the material in vivo [2].

5. Bioactive Glass Processing Methods

The glass is a very attractive material for several applications from optoelectronics to biotechnologies and for this reason different processing techniques have evolved. The most

common preparation methods of bioactive glasses are the melt-quenching techniques and the sol-gel technique [28](**Figure 9**).

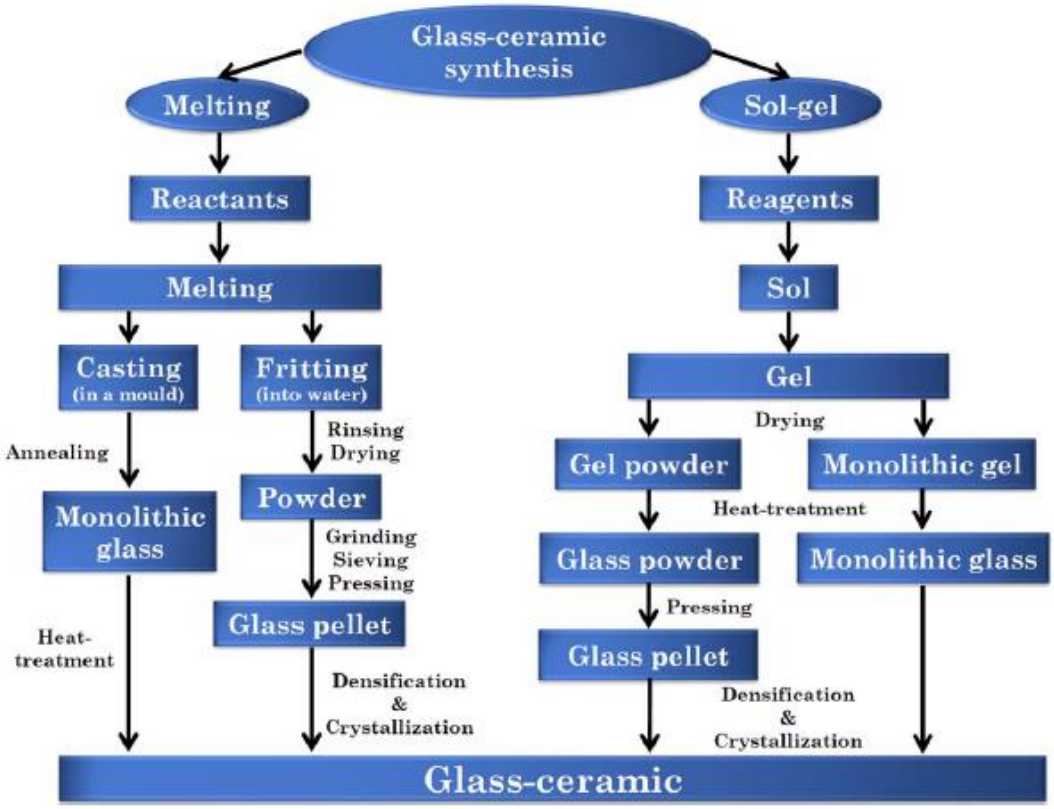

Figure 9. Glass-ceramic synthesis chart [23].

In this paragraph these two processing methods are illustrated with a focus on sol-gel synthesis.

5.1 Melting technique

The first bioactive glass was realized through melt-quench conventional technique. This first processing method is the most common way to obtain glasses by fusion of two or more components. Melting procedures begin from raw precursors powders which should be very pure to avoid contaminations. Sometimes after mixing the precursors, they are versed in the ball mill with acetone to break agglomerates in order to obtain the final products as homogenous as possible providing homogeneity in glass structure.

The resulting mixed powders are dried in air. Once raw materials are dry, they can be melted in aluminium crucibles in the furnace or in platinum ones if higher temperatures are required (up to 1500 °C) [28], [29].

The molten product can be casted in air into moulds (**Figure 10**), obtaining a monolithic glass, or be casted into water to obtain a glass frit, then rinsed and air-dried.

Figure 10. Casting into a cylindric mould during melt-quenching process (Glance Group-DISAT, Politecnico di Torino).

5.2 Sol-gel Synthesis

In 1991, Hench, Rounan Li and Clark realized 45S5 Bioglass® by sol-gel technique [16], [30]. This technique was first mentioned in 1866 by Ebelman and Graham. The two scientists focused their attention on tetraethyl ortosilicate (TEOS) hydrolysis discovering that the process could lead to the formation of SiO_2 based glasses [26].

To better understand sol-gel procedure, it is necessary to introduce some definitions: the term *sol* refers a colloid particles suspension while the term *gel* is referred to a more rigid and interconnected network in which pores and chains are usually immersed into a liquid phase. Different classifications of gels have been also defined. For example, in 1974, Flory divided gels into four classes: ordered and lamellar gels, covalent polymer networks, networks aggregated polymers and disordered particulate gels. Successively, in 1996 Kakihana introduced a new gels classification based on five different classes, strictly based on key features of sol-gel chemistry (**Figure 11)**.

Type of gel	Bonding	Source	Gel schematic
Colloidal[7]	Particles connected by Van der Waals or hydrogen bonding	Metal oxide or hydroxide sols	
Metal-oxane polymer[4]	Inorganic polymers interconnected via covalent or intermolecular bonding	Hydrolysis and condensation of metal alkoxides e.g. SiO_2 from tetramethyl orthosilicate	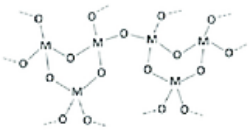
Metal complex[8]	Weakly interconnected metal complexes	Concentrated metal complex solution e.g. aqueous metal citrate or ethanolic metal urea Often form resins or glassy solids rather than gels	
Polymer complex I *In situ* polymerizable complex ('Pechini' method)[9,10]	Organic polymers interconnected by covalent and coordinate bonding	Polyesterification between polyhydroxy alcohol (e.g. ethylene glycol) and carboxylic acid with metal complex (e.g. metal-citrate)	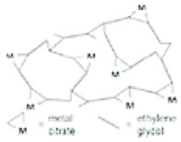
Polymer complex II Coordinating and crosslinking polymers[11]	Organic polymers interconnected by coordinate and intermolecular bonding	Coordinating polymer (e.g. alginate) and metal salt solution (typically aqueous)	

Figure 11. Kakihana classification of gels synthetized via sol-gel procedure.

Depending on the modality of liquid removal, 'aereogels', 'xerogels' and 'alcogels' can be distinguished (**Figure 12**). In aereogels the liquid phase is removed in form of gas under hypercritical condition, xerogels are monoliths formed by liquid removal thanks to thermal evaporation and, finally, alcogels are defined gels in which liquid phase is constituted by alcohols [31].

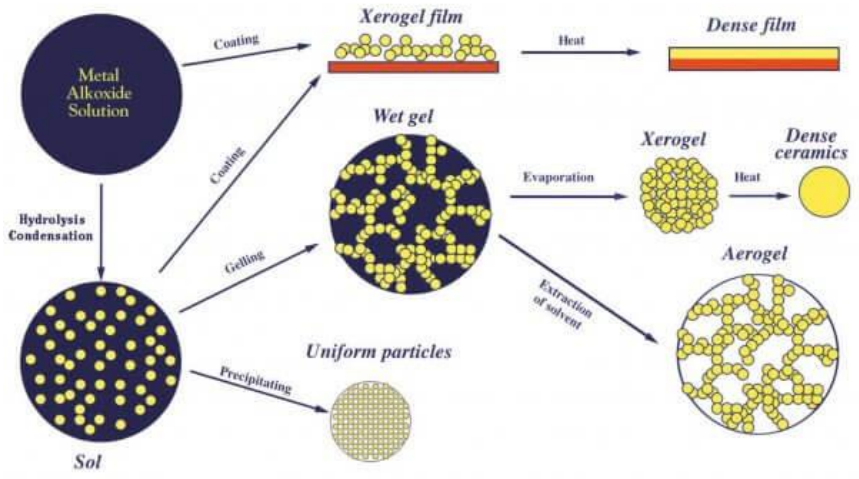

Figure 12. Gels classification according modality of liquid removal.

The possibility of different treatments of the gelled sol is maybe the most appealing advantage of this technique because this permits the formation of several different morphologies just simply modifying processing parameters [26].

Sol- gel products can be realized through:

i) Sol colloidal powder gelation
ii) Precursors, as alkoxides or nitrates, hydrolysis and poly-condensation under hypercritical conditions
iii) Alkoxides hydrolysis and poly- condensation in ambient atmosphere [26].

Three main phases can be defined in sol-gel processing method:

1) Sol preparation
2) Sol gelation
3) Solvent removal

Bioactive glasses are usually produced through hydrolysis and poly-condensation process of alkoxide precursors in ambient atmosphere.

A deeper analysis allows to identify seven different reaction steps in sol-gel process for biomedical applications:

1) Alkoxide or organometallic reagents **mixing** at room temperature leads to the formation of the sol through covalent bonding between the elements. In this step hydrolysis and poly-condensation reactions are competitive and proceed simultaneously.
2) **Sol casting** into a proper mould, if the one used for the synthesis is not appropriate or if special geometries are required.
3) In **gelation** the glass network is formed accompanied by consequential increase of fluid viscosity. Gelation time depends on solvent concentration, oxide group and water amount in the synthesis.
4) In **aging** poly-condensation prevails over hydrolysis reaction causing a decrease in gel porosity and increase of mechanical properties. This process usually occurs at 25-80 °C for several hours influencing also density, surface area and pore volume of the gel.
5) In **drying** liquid phase is removed: colloidal gels should be easily dried, but originating great capillary stress which can provoke cracking problems.

6) In **dehydration**, also known as **chemical stabilization**, silanol bonds are removed from the network reaching the final chemical stability of the glass.
7) The **densification** occurs by thermal treatment in furnace at relatively high temperatures (about 500-700 °C, definitely lower than the ones required for melt-quenching technique) [26].

Hydrolysis and polycondensation processes are the key of sol-gel synthesis allowing the formation of the glass network through different bonds recombination (**Figure 13**).

The two chemical reactions are represented below:

a) Hydrolysis is defined as a nucleophilic attack in which -OH group substitutes -OR group (*Equation 1*):

$$\equiv Si - OR + H_2O \leftrightarrow \equiv Si - OH + ROH \ (1)$$

b) Condensation can produce as final products, water or alcohol, through the formation of silanol bonds, as it is shown in *Equations 2 and 3*:
   i) Condensation with alcohol elimination:
   $$\equiv Si - OR + OH - Si \equiv \leftrightarrow \equiv Si - O - Si \equiv + ROH \ (2)$$
   ii) Condensation with water elimination:
   $$\equiv Si - OH + OH - Si \equiv \leftrightarrow \equiv Si - O - Si \equiv + H_2O \ (3)$$

In these reactions, R group indicates an alkyl functional group in the form C_xH_{2x+1} [6], [26].

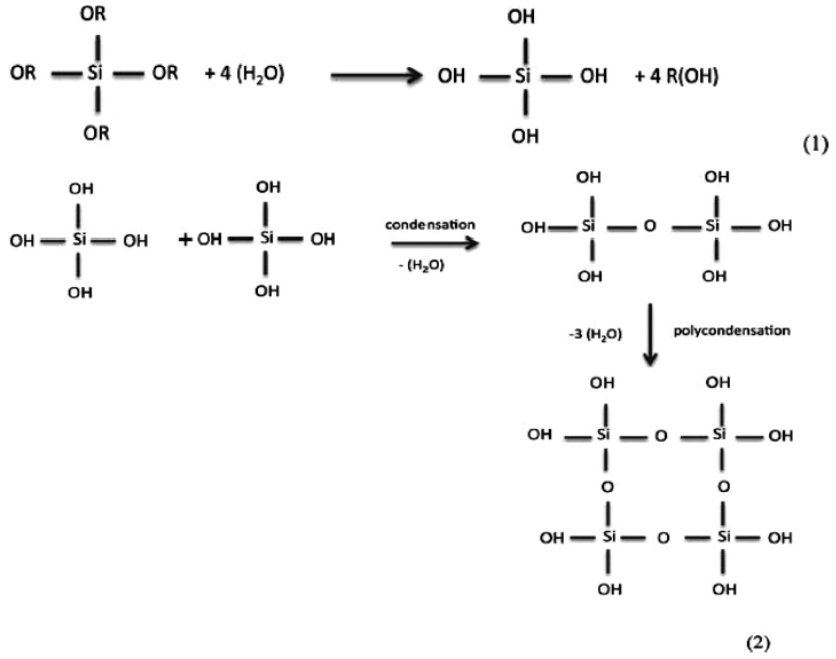

Figure 13. (1) Hydrolysis process; (2) Poly-condensation process.

5.2.1 Properties of sol-gel bioactive glasses

Bioactive glasses produced by sol-gel technique have shown an enormous potential in tissue engineering applications compared to the traditional melting route. Above sol-gel is considered as appealing processing method for the lower temperatures required and the higher versatility of products realizable.

Sol-gel products are also characterized by:

1) High surface area which reflects into higher solubility and higher reactivity in biological environments.
2) Specific pore size which can be tailored modifying processing parameters.
3) Simpler compositions avoid the addition of high amount of Na_2O to lower the melting temperature and facilitate the glass processing.
4) Possibility to adjust the composition during the synthesis.
5) Variety of products realizable just modifying some processing parameters [6][32].
6) Bioactive properties in a wider compositional range, compared to melt-derived glass products

In a chemical perspective, sol-gel based bioactive glasses allow easily achieving different properties by bonding functional groups on the surface of the material due to the high

presence of silanol groups. The grafting of functional groups usually occurs to enhance biocompatibility, binding affinity, adsorption of biomolecules and load capacity.

As described before, the improved bioactivity of these materials is one of the most appealing characteristics to mention when discussing about sol-gel derived biomaterials.

Sol-gel derived bioactive glasses are characterized by lower mechanical properties than the melt-derived glasses with the same composition due to their porous structure. Hence, porosity is an intrinsic characteristic of BGs produced by sol-gel synthesis which has been classified by IUPAC into three macro categories:

- Microporous materials: pore diameters < 2.0 nm
- Mesoporous materials: pore diameters between 2.0 nm and 50.0 nm
- Macroporous materials: pore diameters > 50.0 nm.

Chapter 2 is focused on mesoporous bioactive glasses because of their appealing characteristics in several biomedical application, as drug-delivery systems.

The porosity features as pore sizes, pore shapes and their interconnectivity can be evaluated through X-ray diffraction analysis at lower angles.

5.2.2 Impacting factors on properties of sol-gel based BGs

The kinetics of hydrolysis and poly-condensation reaction is the most impacting factor on the gel structure and consequently on the final product formation. Different factors play a significative role on sol-gel synthesis outcomes: synthesis conditions, use of acid or base catalysts, gelation agents, solvent type and concentration, precursors are key elements which can strongly influence sol-gel process [26].

Temperature and pressure

Sol-gel conditions, as temperature and pressure, have a direct impact on gel structure and final product features in each step of the synthesis. Considering the aging stage, time, pH and temperature of this step influence directly the gel morphology: increasing aging terms the size of pores in gel increase and specific area decrease. The evaporation rate is strictly connected to the temperature and fluctuations of this parameter can lead to different gel structures. Other large structural changes may be observed treating the gel in critical conditions (as in autoclave under pressure or reaching temperatures of 100 °C). Hence, the

thermal process and aging have been observed to loss in specific surface area and increase in pore size [7], [26], [28].

Catalyzing agents

Different studies have been also conducted on catalyst agents influence in sol-gel process. The main role of catalysts, both acids and bases, is to accelerate the hydrolysis and poly-condensation reactions lowering their activation energy. It is quite difficult to precisely define effects of both acid and base catalysts on hydrolysis and poly-condensation rates because of reverse reactions which simultaneously occur [33].

Since the isoelectric point of silica is pH= 2.5, it is possible to distinguish acidic conditions (pH< 2.5), in which hydrolysis is promoted by protonation of the leaving groups, and basic conditions (pH> 2.5) in which condensation is favourited through deprotonation of -OH groups. The choice of catalyst agents reflects on gel properties and impacts the features of the final solid product [34].

In acidic conditions the first step of hydrolysis is the fastest one and hydrolysis rate progressively decrease. In this case, polymeric sol is weakly branched and the gel is a fine network of linear chains which form well-ordered, hexagonal mesopores in the structure. Gel produced by addition of acid catalysts are characterized by higher reactivity of the chain ends which result in easier approaches to the reaction groups and higher flexibility which allow rotating, bending and plastically deforming the glass network [33]–[35].

Contrary in basic conditions, hydrolysis step rate progressively increases and sol appears highly condensed while gel is composed by more dense colloidal particles [27], [36].

In sol-gel process different agents, as mineral acids for acid catalyst and ammonia as basic catalyst, are commonly used to catalyse TEOS hydrolysis while the use of catalysts is considered useful but not necessary for the condensation reactions. The choice of catalyst agents is determinant for the products of the sol-gel process: the strength of the acids or basis added and their concentration play a significant role in the synthesis outcomes. Catalyst role in sol-gel process has been deeply studied since 1985 focusing also how catalysts can affect gelation rate as reported in **Table 3** [33], [35] [37].

Table 3. Gelation times and pH of solutions for six different catalysts [34], [38]

Catalyst	TEOS (mol/L)	Initial pH of the solution	Gelation time (h)
HF	0.05	1.90	12
HCl	0.05	0.05	92
HNO_3	0.05	0.05	100
H_2SO_4	0.05	0.05	106
HOAc	0.05	3.70	72
NH_4OH	0.05	9.95	107
None	-	5.00	1000

.

Gelation agents

Different gels can be produced using the same precursors and changing just one condition in sol-gel synthesis. Several studies have shown the incidence of temperature and H_2O: TEOS ratio in gelation process: the increase of this factor corresponds to a decrease of gelation times [35], [39]. To improve gelation process in sol-gel synthesis, chelating agents as citric acid have been mostly used in synthesis with metal nitrate precursors. Other experiments have been conducted using small molecule gelators as tartaric acid, glycolic acid and oxalic acid or propylene oxide in synthesis of hydrated metal salts in ethanol [35].

Precursors

Even the precursors choice can have a strong impact on structure of the final solid product. Mechanical properties are directly influenced by this choice as different studies have shown using TEOS or TMOS in same concentrations but obtaining derived glasses with same porosity while different mechanical strength [26].

Alkoxides suitability for sol-gel synthesis depends on electronegativity between oxygen and metal and on electron donating/withdrawing ability of alkyl and aryl chain. Furthermore, the nature of R can affect structure determining inductive effects which change the morphology of the gel. Usually sol-gel synthesis is based on hydrolysis and polycondensation of metal alkoxides, but metal chlorides can be also used as precursors which react with alcohols forming alkoxide and hydrogen [39].

Solvents

Just few data are available about solvent effects on the condensation rate and researches about their influence are actually underway. Solvent use in the primary steps has surely the goal to increase TEOS and precursors solubility in aqueous solutions [40], [41]. Four classes of solvents may be classified depending on dipolar moment and polarity: polar, non-polar, protic and aprotic solvents [38][26].

Different studies have shown the effects of H_2O: TEOS or EtOH: TEOS molar ratios and solvent concentrations on TEOS hydrolysis: increase of H_2O: TEOS ratio or decrease of EtOH-TEOS ratio improves solvent polarity and interfacial energy with silica particles forming bigger primary particles [35].

When high amount of water is used in the synthesis bioactive glasses are also characterized by lower density and lower elastic, shear and bulk moduli[35]].

In conclusion, several factors have to be considered as final products can be differently tailored just changing one parameter of sol-gel process [26].

6. Glass-based 3D scaffolds for bone regeneration

Before beginning to discuss about BG scaffolds, it is useful to introduce some concept related at **Tissue Engineering (TE)** and its latest developments.

Tissue Engineering and regenerative medicine are considered the new frontier of biomedicine aimed at repairing and regenerating damaged biological tissues. These multidisciplinary fields of research concern the development of biocompatible tissue substitutes to be implanted in the defected site and able to stimulate the growth of functional tissue [32].

Figure 14 schematically shows the regenerative process highlighting three main elements considered in TE approach.

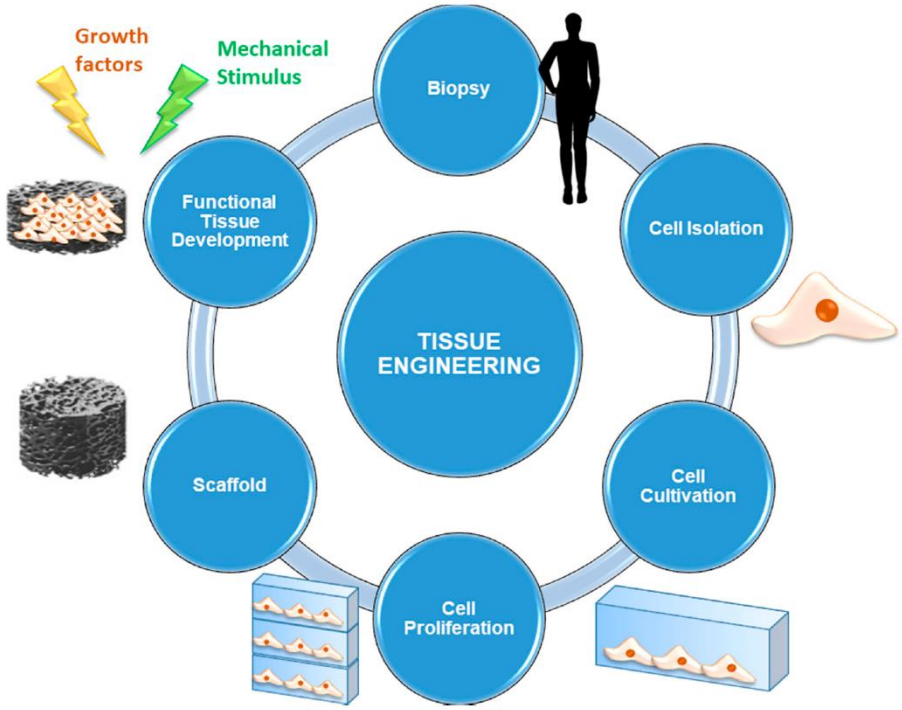

Figure 14. schematic illustration of a tissue engineering approach from patient biopsy to tissue substitutes implantation [32].

- **Cells** are the first element to be studied into details before developing a tissue substitute. Cells are responsible of tissue synthesis and trigger regeneration mechanisms.
- **Scaffolds** are 3D porous structures that provide support to cells allowing them to adhere, migrate, proliferate and differentiate.
- Biological, chemical or physical-mechanical **signals** influence cell pathways during each steps of cell proliferation and differentiation[32], [38], [42].

Nowadays, BGs are considered the gold standard materials used to realize 3D scaffolds for TE clinical applications.

The appealing properties of bioactive glasses have caught the attention of scientists all over the world and nowadays man-made bone substitutes are available in several forms as monoliths, granules or porous scaffolds [38].

The term '*scaffold*' literally means a supporting framework and can be used in different fields. In tissue engineering *"scaffolds are materials that have been engineered to cause desirable cellular interactions contributing to the formation of new functional tissues for medical purposes"*.

In bone regeneration applications, glass derived scaffolds are porous 3D structures which should mimic as much as possible the healthy bone (**Figure 15**) and its architecture in order to optimize the integration with the host tissue. At the moment, there are not standard design criteria for the develop of 3D scaffolds with specific mechanical properties. This because both the variability in structural and mechanical features of bones and differences in age, activity and pathologies of patients represent a major challenge in the design of scaffolds for specific defect sites (**Figure 16**) [43].

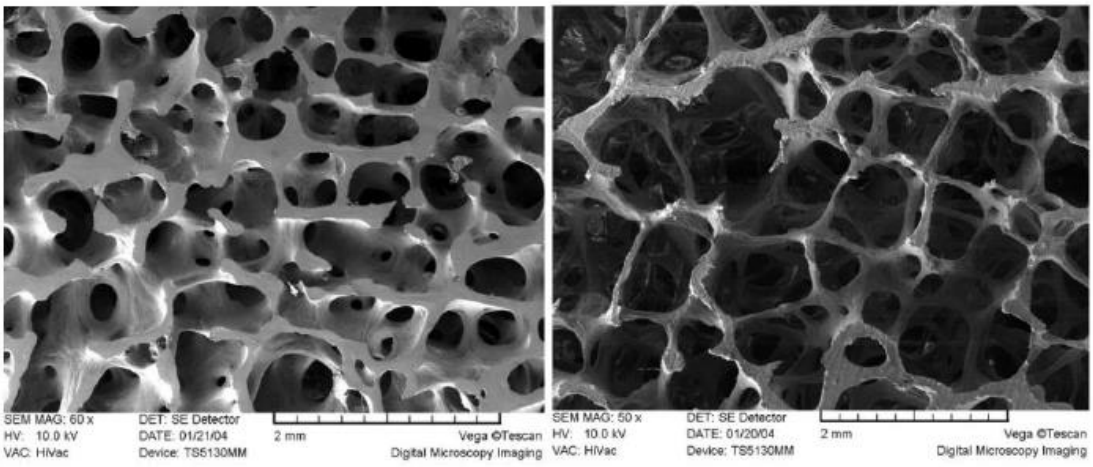

Figure 15. Comparison between SEM image of a healthy bone and a defected bone. A) a young (22-year old) male human bone while B) an elderly bone of osteoporotic woman 80 years old. Because of the aging process trabeculae are subjected to collapse and thinning, affecting both morphological and mechanical properties.

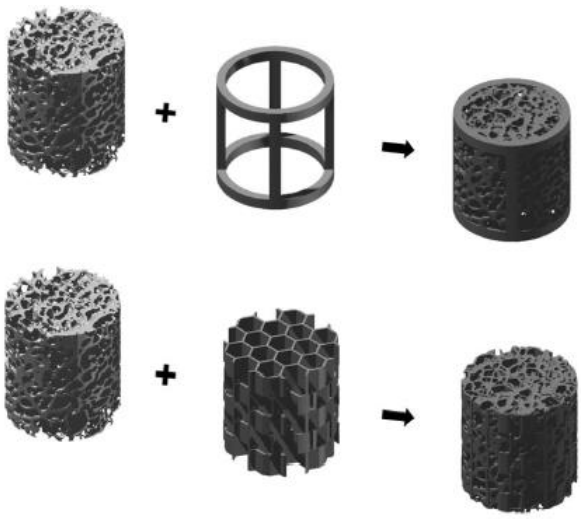

Figure 16. CAD files of trabecular bone scaffold with different artificial supports [29].

The goal of scaffolds is to deliver bio-factors as cells, genes and proteins to the defected sites with the aim of induce the regeneration process into the surrounding tissue. The ideal scaffold should certainly:

1) Provide the correct anatomic geometry
2) Support mechanical load typical of the interested site
3) Have high regeneration capability [2].

In fact, according to the final application, scaffolds should match structural and mechanical properties with those of the host tissue and optimize the micro-environment of the defected site. For these reasons, the design and develop of a scaffold should considered different requirements (**Figure 17**), such as:

1) Biocompatibility and bioactivity
2) Capability to bond the host tissue without scar formation
3) Porous and interconnected structure
4) Mouldability in different shapes and sizes
5) Suitable degradation rate
6) Maintenance of mechanical properties
7) Easy fabrication
8) Sterilization [6], [32].

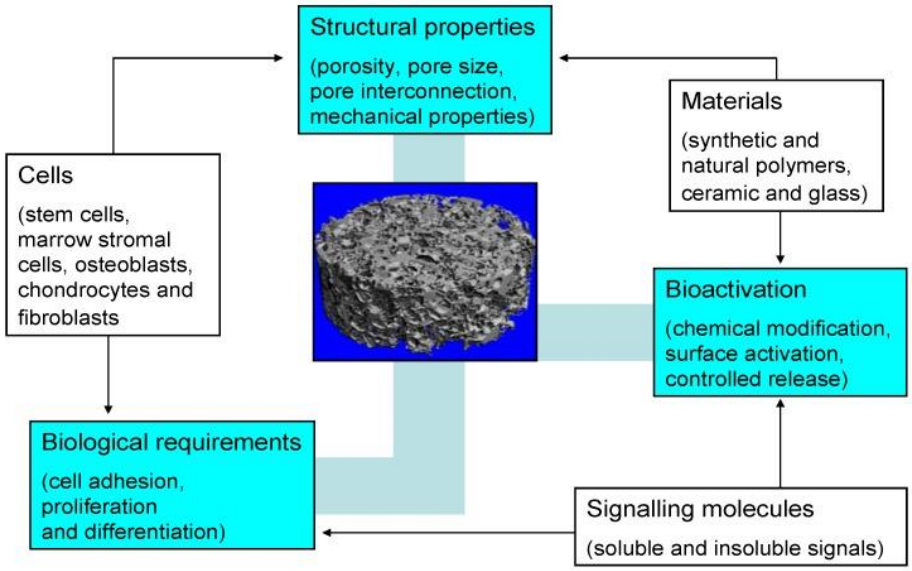

Figure 17. Schematic diagram of key factors involved in the design of optimal scaffold for bone tissue engineering [44].

Table 4 shows required properties of a bioactive glass-made 3D scaffold for bone regeneration applications.

Table 4. Overview of the key properties for a scaffold aimed at regenerating bone [38].

Property	**Effect/ explanation**
Ability to deliver cells	The material should not only be biocompatible but also foster cell attachment, differentiation and proliferation
Osteoconductivity	Osteoconductivity does not only eliminate the formation of fibrous tissue encapsulation but it also brings about a strong bone between the scaffold and host bone
Biodegradability	The composition of the material, combined with the porous structure of the scaffold, should lead biodegradation *in vivo* at rates appropriate to tissue regeneration
Mechanical properties	The mechanical strength of the scaffold, which is determined by both the properties of the biomaterial and the porous structure, should be sufficient to provide mechanical stability to build in loading-bearing sites prior to synthesis of the new extracellular matrix by cells
Porous structure	The scaffold should have an interconnected porous structure with porosity > 90% and diameters between 300 and 500 μm for cell penetration, tissue ingrowth and vascularization
Fabrication	The material should possess desired fabrication capability, for example, being readily produced into irregular shapes of scaffolds that match the defects in the bone of individual patients
Commercialization potential	The synthesis of the material and fabrication of the scaffold should be reproducibly suitable for commercialization. The scaffold should also be sterilizable and accessible at a reasonable cost

The first bioactive glass based on a sol-gel synthesis was produced by Sepulveda in 2002 in order to obtain a microporous structure [45] [38].

Since then, a lot of experiments have already realized bioactive glass-based scaffolds in infinity shapes and sizes to best fit into the damaged bone. With the evolution of manufacturing processes, major issues concerning the intrinsic brittleness of glass-ceramic materials have been successfully overcome and scaffolds with mechanical properties comparable to those of human bone have been produced (**Table 5**) [38].

Table 5. Mechanical properties of trabecular and cortical bone compared to 45S5 BG composition [46].

Material property	**45S5 Bioglass®**	**Trabecular bone**	**Cortical bone**
Compressive strength [MPa]	500	0.1-16	130-200
Tensile strength [MPa]	42	n.a.	50-151
Compressive modulus [GPa]	n.a.	0.12-1.1	11.5-17

Young's modulus [GPa]	35	0.05-0.5	7-30
Fracture toughness [MPa·m$^{1/2}$]	0.7-1.1	n.a.	2-12

Major limits of scaffolds realized with BG materials are the intrinsic brittleness of the glasses and the lack of an interconnected and porous structure needed for TE applications. These two factors seem to be intrinsically correlated, in fact some studies have demonstrated that high porosity in glass-ceramic scaffolds results in low mechanical properties. A deeper analysis has shown a strong anti-correlation between scaffold porosity and compressive strength, characterized by coefficients of determination R^2 between 0.80-0.99 [32]. This result means that the systematic impact of porosity on the variability of compressive strength is at least 80% (**Figure 18**) [44].

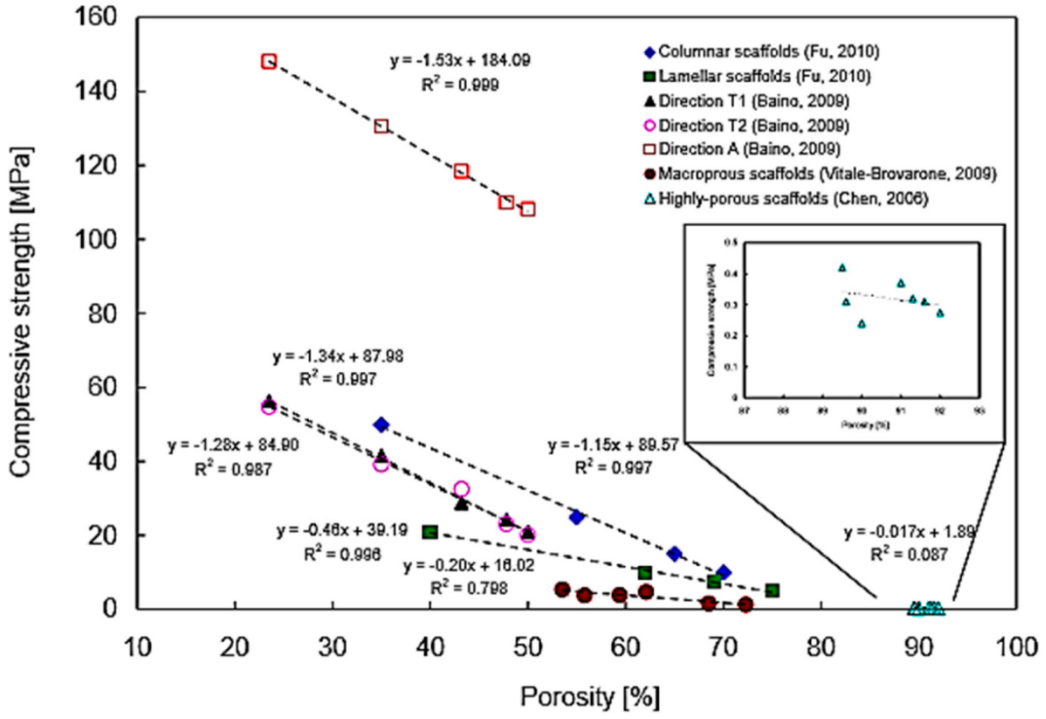

Figure 18. Compressive strength vs porosity curve for glass-ceramic scaffolds. The negative slope shows how increase in porosity percentage reduces mechanical compressive strength according to a linear relationship. It can be noticed also that for very high values of porosity percentage (≈ 85-95%) the relation does not fit a linear curve and the mechanical performances of the scaffold are almost inexistent [32], [44].

In this scenario, one possible solution to solve mechanical limits of BG scaffolds was represented by the use of multifunctional BG composite structures. These are realized by the integration of a biodegradable polymer matrix with BG particles as filler phase or of a

polymeric coating on BG surface [32], [38]. In this way, the polymeric component strongly improves BGs mechanical properties thus should allow to overcome brittleness problem of BG scaffolds.

However, some recent studies have shown that composite BGs and polymeric coatings introduce significant side effects in scaffolds features. For example, the polymeric coating negatively affects scaffold bioactivity performances due to its covering role. Furthermore, the introduction of the coating also influences environment conditions by its premature degradation which releases acidic products reducing pH. Finally, mechanical strength and properties are not constant after the scaffold implantation *in vivo*, but rapidly decrease because of the interaction between polymeric coating and glass and the influence of reciprocal degradation mechanism [32].

7. BG Manufacturing Methods

Since the realization of the first scaffold in 2002, a lot of researchers had focused their studies on the optimization of manufacturing processes to realize the "perfect" scaffold [38]. The perfect manufacturing process should be easily repeatable and should give same outputs guaranteeing constant scaffold characteristics and allowing a mass production. The processing route should also be economically sustainable and health-safe for all workers who participate at the process [38].

In the last two decades, different technologies have been developed to produce glass-based scaffolds. Principal manufacturing methods may be divided into two different major categories, known as conventional methods and additive manufacturing techniques **(Table 6).**

Table 6. overview of the manufacturing techniques used for the production of glass-based scaffold in bone tissue engineering [38].

Manufacturing methods	Technological class	Specific methods
Conventional	Foaming techniques	Gel-casting foaming, sol-gel foaming, H_2O_2 foaming
	Thermal consolidation of particles	Organic phase burning-out: polymeric porogens, starch consolidation, rice husk method
	Porous polymer replication	Coating methods, foam replication

	Freeze- drying	Freeze-casting of suspensions, ice-segregation-induced self assembly
	Thermally induced phase separation	
	Solvent casting and particulate leaching	
Additive manucturing	Selective laser sintering	
	Stereolithography	
	Direct ink writing	3D printing, ink-jet printing, robocast

Conventional methods are characterized by a top-down approach in which the realization of the desired form occurs by the progressive removal of material from a bigger bulk piece [38].

While **Additive Manufacturing Technologies** (AMTs) is the currently used term to indicate those bottom-up approaches where 3D structures are fabricated by progressively adding materials in the form of ultrathin layers to obtain the desired morphology.

7.1 Scaffold manufacturing by "conventional methods"

Conventional manufacturing methods are the first routes used to realized glass-based 3D-scaffolds.

Foaming techniques belongs to conventional technology family. These techniques take their name from the use of a foaming agent in the manufacturing process [38]. The foaming agent is generally introduced in a slurry to create air bubbles which are responsible of porosity in the final product. The use of these technique may lead to some side effects, such as high brittleness of derived scaffolds, low interconnectivity, or the lack of pores in the outer layer [38].

In this family should be certainly cited *gel-cast foaming, sol-gel foaming, H_2O_2 foaming.* Gel-casting foaming includes foaming technique in which are used melt-derived powders mixed into a solution forming the slurry [38].

Differently to gel-casting, in sol-gel foaming the foaming agent is simultaneously introduced into sol-gel synthesis. The introduction of this method was due to an initial difficulty to produce melt-derived BGs that could resist to another sintering step without induce crystallization into the material [38].

Last foaming approach is the H_2O_2 foaming process which includes the use of a peroxide solution, as foaming agent [38]. This route shows excellent results as the H_2O_2 content increases leading to increment in interconnectivity, pore size and porosity of the final 3D scaffold.

Methods based on **thermal consolidation of particles** includes all those processes which require the introduction of templates/particles, usually polymeric, before the sintering procedure [38]. These techniques allow to properly tailor the porosity degree controlling process parameters and templates/particles introduction.

The process could also occur without the introduction of sacrificial particles just varying sintering parameters. Other techniques include polymeric fillers or polymeric foams as porogen particles [38].

In alternative to the use of organic particles as porogen agent, **freeze-drying methods** have been developed in which the formation of ice-crystals generates porosity in final 3D-scaffolds [38]. In these methods, the solution containing glass particles is freezed into crystals, then solvents are removed showing porous structures and scaffold architecture is consolidated [38].

Another conventional method involves **thermally induced phase separation** based on the change of solubility between different polymers in relation of temperature variations [38]. This process mainly produces polymeric scaffolds, but it can be also extended to the fabrication of polymer/glass composite [38]. The main step regards polymers solution cooling which reveals phase separation, then porous structure is obtained through latter phase removal [38].

7.2 Scaffold manufacturing by "additive manufacturing methods"

On the contrary of conventional methods, Additive Manufacturing Technologies (AMT) includes all techniques which involve the use of a CAD model or a computed tomography (CT) of the final product [38].

Therefore, two main classes of techniques to produce ceramic materials by AMT can be individuated: direct fabrication technique which produces sintered ceramic parts without needing any further thermal treatments and indirect fabrication technique which involves three different steps as 3D printing, thermal de-binding and sintering [29].

Selective laser sintering is included into direct fabrication techniques because just one step is necessary to realize the 3D scaffold. In fact, the CAD model of the object is followed by a computer which controls a laser over a bed of powders realizing the desired path [38].

Stereolithography represents probably the most precise AMTs, reaching high resolution values up to 20 μm. In this process a liquid UV-sensible polymer, UV-laser and a movable platform are used to realize layer by layer the 3D objecy [38]. The major limitation of this technique is the poor availability of UV-curable polymers which usually turn out into very brittle final materials [38].

Direct ink writing methods include many different AMTs, such as 3D printing, ink-jet printing and robocasting. In all these techniques a print head or nozzle builds up a 3D object by following computer instructions which translate a pattern-generating device [38]. *3D printing (3DP)* setup is fundamentally similar to select laser sintering ones in which a print head follows a CAD model. While in 3DP the ink is formed by the binder and glass particles are in the building bed, in *ink-jet printing* the ink contains all the components [38]. *Robocasting* is probably the most common technique between AMTs. Its main advantage is the possibility to change ink viscosity through chemical and physical processes achieving strong 3D structures [38].

8. Bioactive Glass Applications

In 1985 the first implant realized by bioactive glass (45S5 Bioglass®) received the approval from Food and Drug Administration (FDA). Since then over 1.5 million patients have been treated implanting Bioglass®-made medical devices and nowadays synthetic bone substitutes and biomaterials with several compositions are widely used in clinical applications [4] [47]. **Table 7** reports a brief overview of bioactive glass main applications and commercial products:

Table 7. Chronological overview of the key applications of bioactive glasses in medicine [47].

Year (First Experimental Use)	**Achievement/ Application**
1969	Invention of the 45S5 glass composition (45S5 Bioglass®)
1977	Replacing of middle ear small bones using Ceravital® glass-ceramics

1978	Ocular implant (biocompatibility with corneal tissue)
1985	Approval by FDA of the first 45S5 Bioglass® implant
1987	Treatment of liver cancer (radioactive glasses)
1988	Clinical use of the 45S5 Bioglass®- based Endosseous Ridge Maintenance Implant (ERMI) in human patients
1993	FDA approval of PerioGlas (45S5 Bioglass® particulate used for bone and dental repair)
1998	Peripheral nerve repair
1999	FDA approval of radioactive glasses (TheraSphere®) for cancer treatment
2000	Wound healing
2002	FDA approval of Medpor®-Plus™ (polyethylene/ 45S5 Bioglass® composite porous orbital implants).
2003	Antibacterial (Zn-containing) bone/ dental cements
2004	Lung tissue engineering
2004	Use of mesoporous bioactive glass (MBG) as a drug delivery system
2005	Skeletal muscle and ligament repair
2005	Treatment of gastrointestinal ulcers
2010	Cardiac tissue engineering
2011	Commercialization of a cotton-candy borate bioactive glass for wound healing in veterinarian medicine
2012	Embolization of uterine fibroids
2012	Spinal cord repair
2018	Use of radioactive glasses (TeraSphere®) in patients with metastatic colorectal carcinoma of the liver

Thanks to their appealing properties bioactive glasses have been employed in several fields of medicine from the original purpose of bone regeneration to completely different clinical applications.

Orthopaedics and Dental Applications

In bone tissue engineering, the applications of BGs is constantly increasing and several studies aiming at improving the biological and mechanical properties of bioactive glass-made scaffolds are conducted all over the world [48]. The results of bioactive glasses *in vivo* applications have already demonstrated their huge potential as bone substitutes able to restore large orthopaedics defects caused by trauma, tumours, congenic pathologies, implant revisions or infections (**Figure 19)** [7].

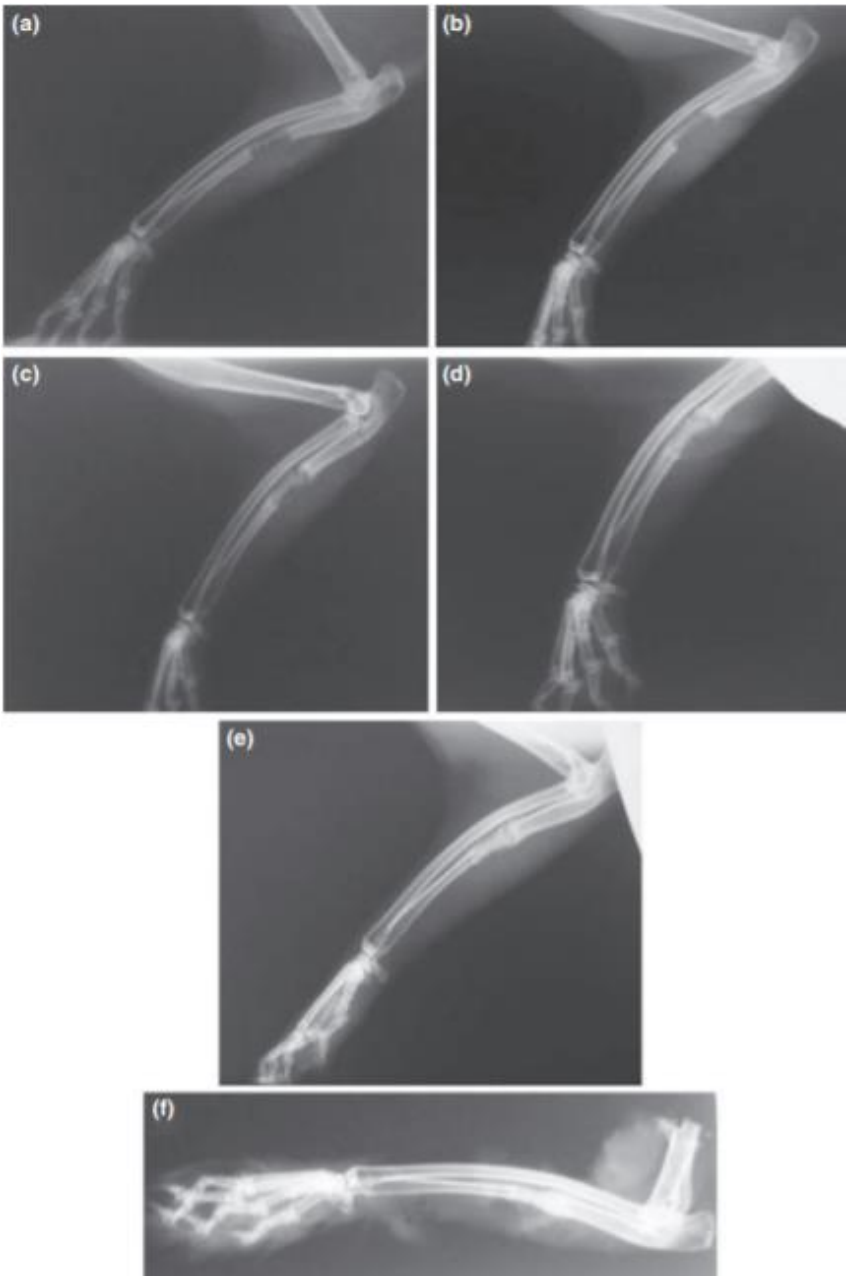

Figure 19. Results of the *in vivo* study on nanosized bioactive glass/gelatin scaffolds. (a) Radiograph of the defect immediately after surgery showing the removal of the segment of ulna and the creation of a segmental defect in the ulna. (b-e) typical radiographs of the defect site at 2 weeks (b), 4 weeks (c), 6 weeks (d), 8 weeks (e), and 10 weeks (f) post-operation [48].

Bioactive glasses made implants are currently available for different clinical application in bone tissue engineering. They may be developed in several forms for specific applications as granular porous or dense bone substitute in combination with autogenous bone (**Figure 20**), and also in forms of coating for joint prothesis or bioactive cement [49]. Applying a

BG coating on implant surface allows to achieve additional properties to the ones of the uncoated device. These coatings are able to both enhance the substrate corrosion resistance and inhibit the release of potentially toxic metal ions. BG coatings have also the potential to stimulate implant stability thanks to the binding with the host bone [47]. The major issue of bioactive glass coatings concerns their natural biodegradability which make them unsuitable for long-term implants. This topic is nowadays one of the most attractive challenges of bioactive glass research for orthopaedic and dental applications.

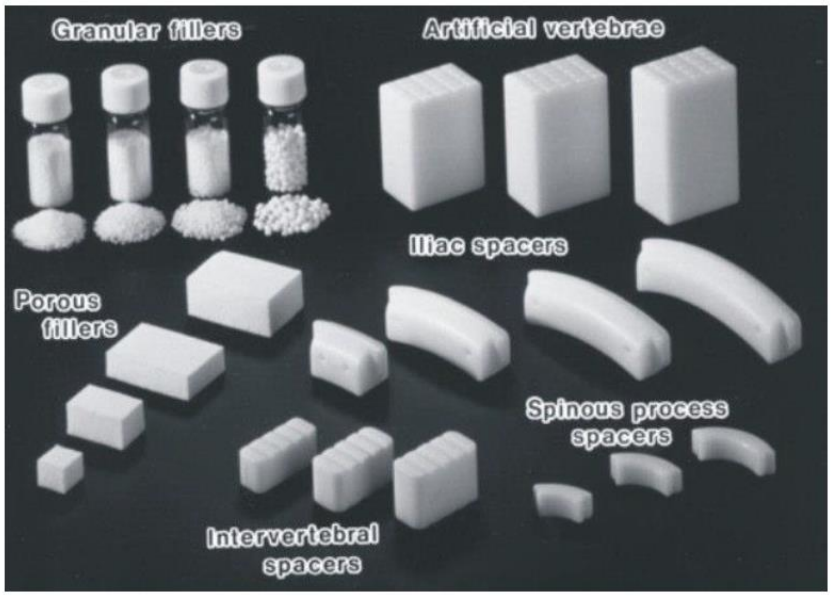

Figure 20. Different bioactive glasses forms available in commerce [13], [49].

Nowadays bioactive glasses are also often mixed with cements or composites aiming at the realization of harder applications in dentistry and orthopaedics. Moreover, in dental surgery BGs are considered very promising materials for restorative applications and they are already used as scaffolds fitting large defects [50].

Chondrogenesis

Different experiments have recently shown that bioactive glasses may be able to stimulate not only the osteogenesis process, but also chondrogenesis which is the process responsible of the formation of cartilage. Thanks to their osteogenic properties, BGs have been proposed as suitable substrates for chondrocyte culture and chondrogenic differentiation aiming at repairing osteochondral defects at the interface between bone and cartilage. This topic represents one of the most challenging tissue engineering applications due to the very

limited self-repair capability of cartilage tissue [51]. The development of engineered synthetic cartilage able to mimic the shock-absorbing and load bearing properties of real cartilage tissue is an ongoing appealing research.

Soft tissue applications

The successful applications of bioactive glasses as replacement, regeneration and repair of hard tissues, as bones and teeth, have more recently caught the eye on the possibility to use BGs also in soft tissue regeneration. An increasing number of experiments have observed the reactions of bioactive glasses in contact with soft tissues showing how the BGs ionic dissolution in body fluids may enhance both osteogenesis and angiogenesis in particular conditions [52]. This demonstrated suitability of bioactive glasses have opened the field of research to infinity of medical applications, as vascularization, cardiac, lung, nerve, gastrointestinal, urinary etc medical devices (**Figure 21**) [52]. These fascinating therapeutic horizons will be further discussed in the following paragraph.

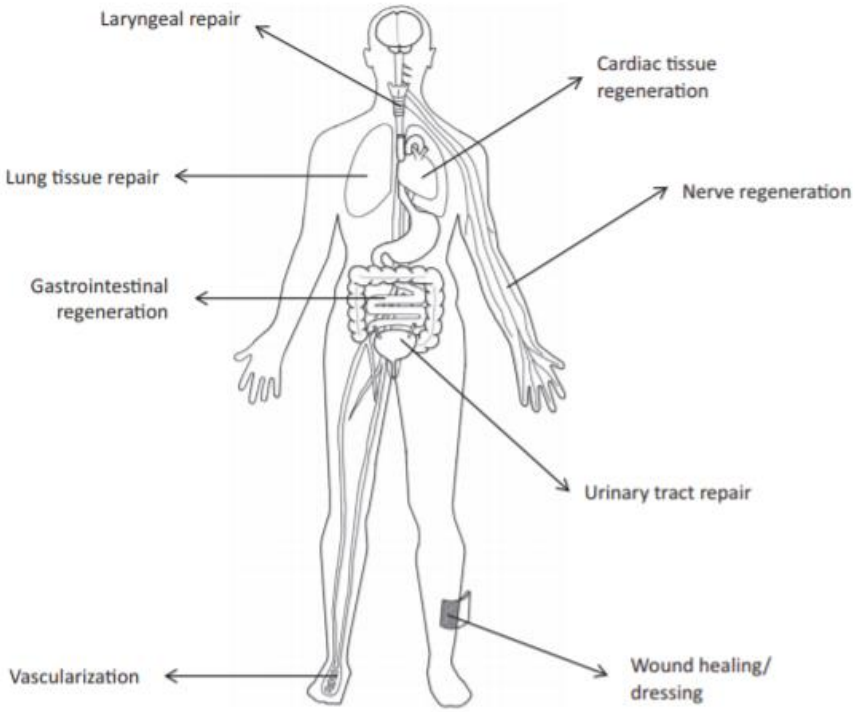

Figure 21. Schematic diagram of emerging bioactive glasses applications in soft tissue regeneration [52].

Tumor therapy

In addition to applications in tissue regeneration processes, different 3D scaffolds have been tested to validate their potential features in tumor therapies. These bioactive glass-made scaffolds have been recently functionalized to absolve a dual function: both repair bone defects induced by surgery and kill the residual tumor cells in the implantation site (**Figure 22**) [53]. The composition of bioactive glasses has been tailored doping with specific elements which confer to the scaffold desired properties becoming adapt to magnetothermal and photothermal therapies.

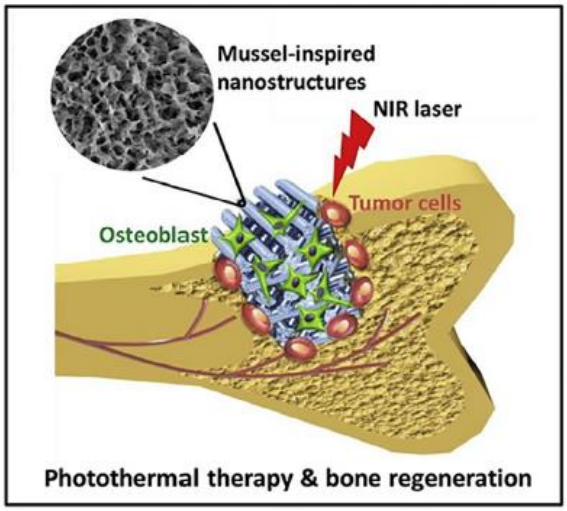

Figure 22. Potential application in bone tumor therapy: a bifunctional scaffold exhibiting capability for both bone tissue regeneration and tumor therapy [53].

Bio-nanotechnologies and Drug Delivery Systems

The structural, mechanical and biochemical properties of bioactive glasses have led to consider them as appealing biomaterials which may be functionalized in drug delivery applications. The loading and delivery systems represent the future of medical therapies as base for a patient-specific and targeted medicine and have involved a greater number of studies, experiments and investments. The topic, particularly related to mesoporous bioactive glasses which have demonstrated greater loading efficiency thanks to their porous and well-ordinated structure, is deeply analysed in Chapter 2 [54].

9. Towards new therapeutic scenarios: Ion-Doped Bioactive Glasses

Between the appealing above-mentioned features of bioactive glasses, an important role is played by their high flexibility which allows several modifications on the original system.

The composition of bioactive glasses greatly influences the physiochemical and biological properties exhibited from these biomaterials. Furthermore, by opportunely tuning the BGs formulation it is possible to achieve different desired effects for the intended applications [17] . For this reason, since 1985 in literature appeared several studies about incorporation of different ion on the composition, named as **doping process**.

Doping elements are defined elements added in low concentration (few percentages respect to elements forming the original system) into the main composition giving a new functionality, strictly correlated with the element itself, to the material. The doping process directly impacts on material architecture creating structural modifications in the glassy network.

Nowadays incorporation of ions able to add new therapeutic skills to original bioactive glasses is considered a very attractive perspective for tissue engineering.

8.1 Main Doping Elements

In the early experiments, the choice of doping elements was conducted according to their similarity with elements already present in trace into the human body. Several inorganic ions (**Table 8**) as calcium, phosphorous, silicon, strontium, zinc, boron and magnesium also affect the bone metabolism, for example metal ions act as coenzyme factors directly impacting on signalling pathways and enhancing bone regeneration mechanisms [5].

Table 8. Acts of different inorganic ions in human body [5].

Ion	**Biological acitivity**
Si	• Metabolic processes, formation of bone tissue • Intake of Si increase bone mineral density • HAP precipitation • Helps to stimulate collagen I formation and osteoblastic differentiation
Ca	• Favours osteoblast proliferation, differentiation and mineralisation • Activates Ca-sensing receptors in osteoblast cells
P	• Matrix gla protein (MGP) stimulation
Mg	• Helps to form new bone • Increases bone-cell adhesion and stability
Zn	• Shows anti-inflammatory effect

	• Bone formation *in vitro* by activation of protein synthesis in osteoblasts • Increases ATP's activity
Sr	• Beneficial effects on bone formation *in vivo* • For treating osteoporosis
Cu	• Promotes synergic stimulating effects on angiogenesis when associated with angiogenic growth factor FGF-2 • Stimulates proliferation of human endothelial cells
Ag	• Antimicrobial properties • Anti-inflammatory properties
Li	• Treatment of both bipolar and unipolar depressive disorder • Effects on blood and brain • Enhances immunological activities of monocytes and lymphocytes

In order to enhance the bioactivity, stimulating osteogenesis, angiogenesis and antibacterial effects of BGs, different experiments have been conducted adding dopant elements in the silicate network. For this reason, recent trends show an increasing use of doping process to realize biomaterials for several clinical applications.

Magnesium-doped Bioactive Glasses

Magnesium is essential to bone metabolism and it has been shown to have stimulating effects on new bone formation interacting with integrins of osteoblast cells which are responsible for cell adhesion and stability. As demonstrated from magnesium depletion which result in impaired bone growth, increased bone resorption and loss in trabecular bone [13], [55], [56].

Both bone and dental tissue contain around 1% of magnesium which participate at over 300 reactions into human organism. For these reasons, from first bioactive glass to nowadays many composition comprising magnesium ions have been developed (**Table 9**).

The dual role of magnesium, which may be both former or modifier ion, sometimes weaken the glassy structure.

Table 9. Role of magnesium in three different BGs compositions [13].

Compositions	**Activities**
45.98SiO_2- 43.3CaO- 10.72MgO	Increased viability and proliferation of osteoblasts
64SiO_2- 26CaO- 5P_2O_5- 5MgO	Increased proliferation and differentiation of osteoblast cells
52.7SiO_2- 10.3Na_2O- 18CaO- 6P_2O_5- 2.8 K_2O- 10.2MgO	Enhanced stimulation of osteogenic marker expression

Zinc-doped Bioactive Glasses

Zinc and magnesium have almost same effect [17]. Zinc is already present in human body; it absolves the role of cofactors for many enzymes and plays also an essential role in bone cells development and differentiation because of its ability to inhibit osteoclast cells. Some experiments have also shown zinc anti-inflammatory effects due to antibacterial properties inhibiting the bacteria lipase, the enzymatic metabolism and the fibrin formation [57] [13].

Strontium-doped Bioactive Glasses

Addition of strontium not results in any structural alteration of the glass network due to the similar role of SrO compared with that of CaO [58]. Strontium exhibits beneficial effects on bone cells and bone formation *in vivo* and it has also been shown to be a promising agent in treating osteoporosis [13]. Nowadays, strontium is included in compositions of marketed anti-osteoporotic oral drugs. The concentration of Sr ions in the glass composition, in fact an excessive amount of strontium can lead to out of control of osteoclast cells which may even lead to bone necrosis [31][59].

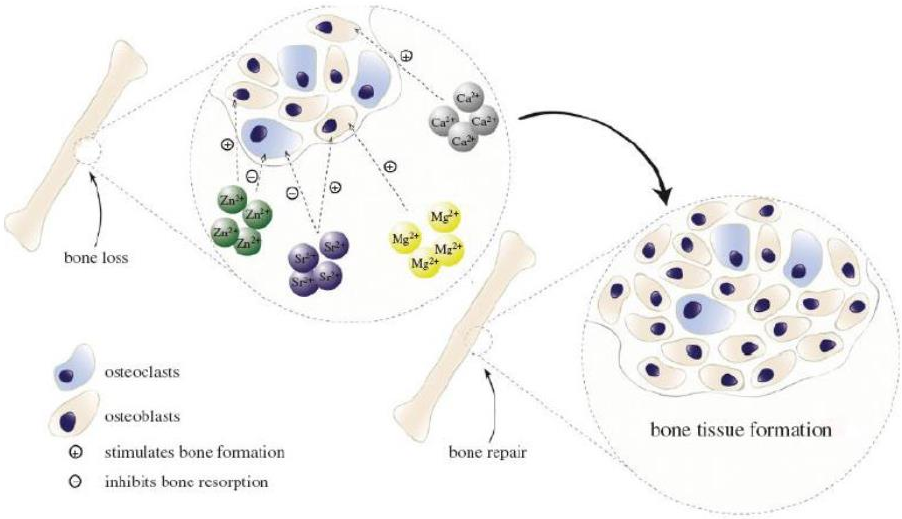

Figure 23. Doping with specific ions stimulates bone mineralization and inhibits bone resorption [13].

Silver-doped Bioactive Glasses

Silver is not one of the trace elements, but it is toxic only at high concentrations (2 wt.% of Ag ions shows cytotoxicity while the range of 0.75-1 wt.% has no shown toxic influence). In bone reconstruction surgeries, Ag-doped bioactive glasses absolve fundamental roles: both chemical binding with living bone and prevention of bacterial infections. Thanks to its antimicrobial properties, the recent trends on development of silver-doped implants is increasing, especially in wound healing applications [5].

8.2 Lithium-doped Bioactive Glasses

Lithium (Li) is a chemical element with atomic number 3 belonging to alkali metal elements which are highly reactive. Lithium and its compounds have several industrial applications as lithium-ion batteries, flux additives, heat-resistant glass and ceramics [31].

Lithium is present in biological systems in trace and its use as therapeutic element has a longer medical history [60]. For moreover 100 years, lithium salts have been used as mood stabilising oral drug to cure maniac depression, both bipolar and unipolar depression disorders. Its effects as mood stabilizer seem to be correlated to lithium capability of enhancing remyelination of peripheral nerves and increasing proliferation of neural progenitor cells [61] [62].

Several studies have shown lithium has also effects on human blood increasing white blood cells counts (granulocytosis) and decreasing lymphosite counts (lymphomenia) [63]. Scientists have also discovered lithium enhances immunological activities of monocytes and lymphocytes developing excellent antibacterial properties, as against *Enterococcus faecalis* a bacteria gram positive responsible of several threatening infections in humans [64]. More recently the lithium role has been investigated also for bone regeneration applications. Different studies evidenced that lithium may affect bone mineral metabolism promoting osteoblastogenesis and inhibiting osteoclastogenesis [61], [63].

Bioactivity in Li-doped BGs

Several experiments have been performed developing bioactive glasses based on doped composition where Li_2O substitutes an equal amount of Na_2O (**Figure 24**). Lithium ions have a strong affinity with oxygen and their ionic radius is smaller than the one of Na^+. These properties lead to a decrease of the free space in the silicate network reducing the rate of glass dissolution [59] .

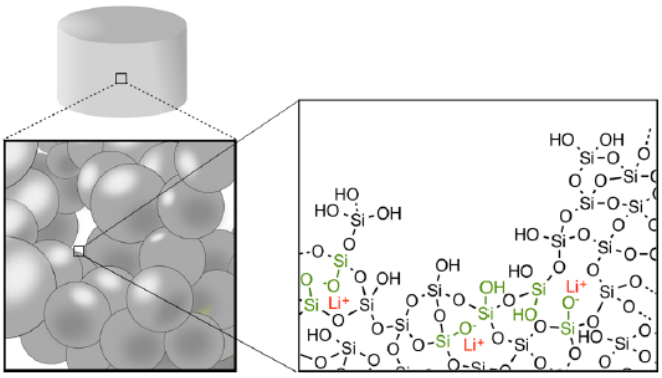

Figure 24. Structure of sol-gel bioactive glass containing lithium [64].

Bioactivity performances of Li-doped bioactive glasses have been studied by different authors. In 2011 Khorami et al. studied 45S5-doped compositions with different concentration of lithium (0-12 wt.%) and discovered that bioactivity depends on Li content within the glass composition. Doping the 45S5 Bioglass® with maximum concentration of Li_2O in substitution of Na_2O, the formation of nanoapatite phase was observed on the glass surface, while at low substitutions of Li a slight inhibition of apatite formation was noted [61]. But an earlier study has demonstrated increased *in vitro* proliferative activity only at low lithium concentration (0.25 wt.%) [31]. Some authors correlated reactivity response to glass solubility dependent on change of Li_2O amount. **Figure 25** shows SEM analysis of various glasses containing lithium in different amounts immersed into SBF solution up to 21 days.

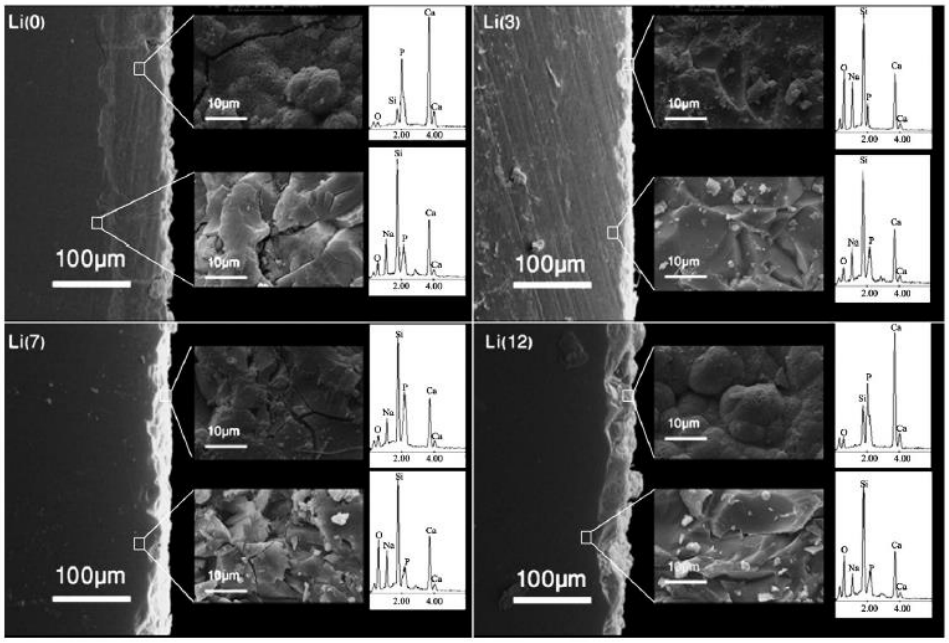

Figure 25. SEM images from the transverse section of various glasses soaked in SBF solution for 21 days [61].

In vivo experiments about Li-doped BGs implants in rats have reported enthusiastic results showing anabolic effects on bone mass [63]. Therefore, other studies supported the idea of a correlation between lithium content in BGs composition and bone mineral density; for example, clinical reports about lithium carbonate use for maintenance post-surgical therapy have shown positive effects on bone density preservation and enhancement [63].

Deeper investigations on biological effects of lithium ions revealed that lithium plays an important role in osteoblast proliferation and cementogenic differentiation by stimulating Wnt signalling pathways. Wnt are a group of transduction pathways where proteins pass signals into cell through surface cell receptors. The open question is if this osteogenic behaviour shall be assigned solely at lithium presence or if its release acts in combination with other ions already present in biological fluids [59]. However, these appealing features make lithium-doped bioactive glasses suitable for several applications in both orthopaedics and dentistry, as bone regeneration devices or dental bridges, crown and veneers.

10. Conclusions

As seen in this chapter, BGs had represented and continue to represent one of the most attractive biomaterials for clinical applications.

Their appealing properties, their relatively easy fabrication methods, the possibility to propertly functionalize them open a new frontier of opportunities in regenerative medicine.

Extensive studies have been conducted on mesoporous bioactive glasses, a BG evolution, and will be deeply analysed in *Chapter 2*.

Bibliography

[1] S. E. Componenti, D. E. Follow-up, and I. L. T. Osseo, “Tessuto ossseo.”

[2] K. Arvidson *et al.*, “Bone regeneration and stem cells,” *J. Cell. Mol. Med.*, vol. 15, no. 4, pp. 718–746, 2011, doi: 10.1111/j.1582-4934.2010.01224.x.

[3] D. F. Williams, “On the mechanisms of biocompatibility,” *Biomaterials*, vol. 29, no. 20, pp. 2941–2953, 2008, doi: 10.1016/j.biomaterials.2008.04.023.

[4] J. Henkel *et al.*, “Bone Regeneration Based on Tissue Engineering Conceptions-A 21st Century Perspective,” *Bone Res.*, vol. 1, no. 3, pp. 216–248, 2013, doi: 10.4248/BR201303002.

[5] M. N. Rahaman *et al.*, “Bioactive glass in tissue engineering,” *Acta Biomater.*, vol. 7, no. 6, pp. 2355–2373, 2011, doi: 10.1016/j.actbio.2011.03.016.

[6] J. R. Jones, “Review of bioactive glass: From Hench to hybrids,” *Acta Biomater.*, vol. 9, no. 1, pp. 4457–4486, 2013, doi: 10.1016/j.actbio.2012.08.023.

[7] G. Kaur, O. P. Pandey, K. Singh, D. Homa, B. Scott, and G. Pickrell, “A review of bioactive glasses: Their structure, properties, fabrication and apatite formation,” *J. Biomed. Mater. Res. - Part A*, vol. 102, no. 1, pp. 254–274, 2014, doi: 10.1002/jbm.a.34690.

[8] E. Gibon *et al.*, “The biological response to orthopedic implants for joint replacement. II: Polyethylene, ceramics, PMMA, and the foreign body reaction,” *J. Biomed. Mater. Res. - Part B Appl. Biomater.*, vol. 105, no. 6, pp. 1685–1691, 2017, doi: 10.1002/jbm.b.33676.

[9] F. Velard, J. Braux, J. Amedee, and P. Laquerriere, “Inflammatory cell response to calcium phosphate biomaterial particles: An overview,” *Acta Biomater.*, vol. 9, no. 2, pp. 4956–4963, 2013, doi: 10.1016/j.actbio.2012.09.035.

[10] J. W. Hench, *Inflammation and wound healing*. Woodhead Publishing Limited, 2005.

[11] B. D. Ratner, A. S. Hoffman, F. J. Schoen, and J. E. Lemons, *Introduction - Biomaterials Science: An Evolving, Multidisciplinary Endeavor*, Third Edit.

Elsevier, 2013.

[12] E. Vern, “I vetri.”

[13] “I CERAMICI AMORFI : I VETRI.”

[14] M. Ткач, “No TitleТайны католических монашеских орденов,” pp. 1–23.

[15] D. Pugliese, “Glass systems Glass structure,” pp. 1–20.

[16] L. L. Hench, “The story of Bioglass®,” *J. Mater. Sci. Mater. Med.*, vol. 17, no. 11, pp. 967–978, 2006, doi: 10.1007/s10856-006-0432-z.

[17] F. Baino, “Bioactive glasses – When glass science and technology meet regenerative medicine,” *Ceram. Int.*, vol. 44, no. 13, pp. 14953–14966, 2018, doi: 10.1016/j.ceramint.2018.05.180.

[18] E. Pirhonen, L. Moimas, and M. Brink, “Mechanical properties of bioactive glass 9-93 fibres,” *Acta Biomater.*, vol. 2, no. 1, pp. 103–107, 2006, doi: 10.1016/j.actbio.2005.08.008.

[19] C. Wu and J. Chang, “Mesoporous bioactive glasses: Structure characteristics, drug/growth factor delivery and bone regeneration application,” *Interface Focus*, vol. 2, no. 3, pp. 292–306, 2012, doi: 10.1098/rsfs.2011.0121.

[20] L. L. Hench, “Genetic design of bioactive glass,” *J. Eur. Ceram. Soc.*, vol. 29, no. 7, pp. 1257–1265, 2009, doi: 10.1016/j.jeurceramsoc.2008.08.002.

[21] “Biomateriali in ortopedia.”

[22] L. L. Hench, *Bioactive Ceramics: Theory and Clinical Applications*, vol. 7, no. July. Butterworth-Heinemann Ltd, 1994.

[23] M. Montazerian and E. Dutra Zanotto, “History and trends of bioactive glass-ceramics,” *J. Biomed. Mater. Res. - Part A*, vol. 104, no. 5, pp. 1231–1249, 2016, doi: 10.1002/jbm.a.35639.

[24] L. L. Hench, N. Roki, and M. B. Fenn, “Bioactive glasses: Importance of structure and properties in bone regeneration,” *J. Mol. Struct.*, vol. 1073, no. C, pp. 24–30, 2014, doi: 10.1016/j.molstruc.2014.03.066.

[25] P. Sepulveda, J. R. Jones, and L. L. Hench, “Bioactive sol-gel foams for tissue

repair," *J. Biomed. Mater. Res.*, vol. 59, no. 2, pp. 340–348, 2002, doi: 10.1002/jbm.1250.

[26] F. Baino, E. Fiume, M. Miola, and E. Verné, "Bioactive sol-gel glasses: Processing, properties, and applications," *Int. J. Appl. Ceram. Technol.*, vol. 15, no. 4, pp. 841–860, 2018, doi: 10.1111/ijac.12873.

[27] T. Kokubo, "Bioactive glass ceramics: properties and applications," *Biomaterials*, vol. 12, no. 2, pp. 155–163, 1991, doi: 10.1016/0142-9612(91)90194-F.

[28] G. Kaur, G. Pickrell, N. Sriranganathan, V. Kumar, and D. Homa, "Review and the state of the art: Sol–gel and melt quenched bioactive glasses for tissue engineering," *J. Biomed. Mater. Res. - Part B Appl. Biomater.*, vol. 104, no. 6, pp. 1248–1275, 2016, doi: 10.1002/jbm.b.33443.

[29] R. Gmeiner *et al.*, "Additive manufacturing of bioactive glasses and silicate bioceramics," *J. Ceram. Sci. Technol.*, vol. 6, no. 2, pp. 75–86, 2015, doi: 10.4416/JCST2015-00001.

[30] L. L. Hench, "Bioglass and Similar Materials," *Encycl. Mater. Sci. Technol.*, no. 4, pp. 563–568, 2001, doi: 10.1016/b0-08-043152-6/00108-x.

[31] P. K. Khan *et al.*, "Influence of single and binary doping of strontium and lithium on in vivo biological properties of bioactive glass scaffolds," *Sci. Rep.*, vol. 6, no. February, pp. 1–18, 2016, doi: 10.1038/srep32964.

[32] E. Fiume, J. Barberi, E. Verné, and F. Baino, "Bioactive glasses: From parent 45S5 Composition to Scaffold-Assisted Tissue-Healing Therapies," *J. Funct. Biomater.*, vol. 9, no. 1, 2018, doi: 10.3390/jfb9010024.

[33] T. H. E. Role, O. F. The, C. P. Of, and S. Glass, "H Apter - the Role of the Catalyst in Sol-Gel Processing of Silica."

[34] E. J. A. Pope and J. D. Mackenzie, "Sol-gel processing of silica. II. The role of the catalyst," *J. Non. Cryst. Solids*, vol. 87, no. 1–2, pp. 185–198, 1986, doi: 10.1016/S0022-3093(86)80078-3.

[35] Ö. Kesmez, E. Burunkaya, N. Kiraz, H. E. Çamurlu, M. Asiltürk, and E. Arpaç, "Effect of acid, water and alcohol ratios on sol-gel preparation of antireflective amorphous SiO2 coatings," *J. Non. Cryst. Solids*, vol. 357, no. 16–17, pp. 3130–

3135, 2011, doi: 10.1016/j.jnoncrysol.2011.05.003.

[36] J. Musgo, J. C. Echeverría, J. Estella, M. Laguna, and J. J. Garrido, "Ammonia-catalyzed silica xerogels: Simultaneous effects of pH, synthesis temperature, and ethanol:TEOS and water:TEOS molar ratios on textural and structural properties," *Microporous Mesoporous Mater.*, vol. 118, no. 1–3, pp. 280–287, 2009, doi: 10.1016/j.micromeso.2008.08.044.

[37] M. A. Fardad, "Catalysts and the structure of SiO2 sol-gel films," *J. Mater. Sci.*, vol. 35, no. 7, pp. 1835–1841, 2000, doi: 10.1023/A:1004749107134.

[38] F. Baino *et al.*, "Processing methods for making porous bioactive glass-based scaffolds—A state-of-the-art review," *Int. J. Appl. Ceram. Technol.*, vol. 16, no. 5, pp. 1762–1796, 2019, doi: 10.1111/ijac.13195.

[39] A. E. Danks, S. R. Hall, and Z. Schnepp, "The evolution of 'sol-gel' chemistry as a technique for materials synthesis," *Mater. Horizons*, vol. 3, no. 2, pp. 91–112, 2016, doi: 10.1039/c5mh00260e.

[40] S. S. Soni, G. Brotons, M. Bellour, T. Narayanan, and A. Gibaud, "Quantitative SAXS analysis of the P123/water/ethanol ternary phase diagram," *J. Phys. Chem. B*, vol. 110, no. 31, pp. 15157–15165, 2006, doi: 10.1021/jp062159p.

[41] A. J. Rossiter, "Mixed Alcohol-Water Solvents Declaration," no. August, 2009.

[42] F. Baino, J. Barberi, E. Fiume, G. Orlygsson, J. Massera, and E. Vern, "Glass Scaffolds," *J. Healthc. Eng.*, vol. 2019, 2019.

[43] Q. Fu, E. Saiz, M. N. Rahaman, and A. P. Tomsia, "Bioactive glass scaffolds for bone tissue engineering: State of the art and future perspectives," *Mater. Sci. Eng. C*, vol. 31, no. 7, pp. 1245–1256, 2011, doi: 10.1016/j.msec.2011.04.022.

[44] L. C. Gerhardt and A. R. Boccaccini, "Bioactive glass and glass-ceramic scaffolds for bone tissue engineering," *Materials (Basel).*, vol. 3, no. 7, pp. 3867–3910, 2010, doi: 10.3390/ma3073867.

[45] P. Sepulveda and J. G. P. Binner, "Processing of cellular ceramics by foaming and in situ polymerisation of organic monomers," *J. Eur. Ceram. Soc.*, vol. 19, no. 12, pp. 2059–2066, 1999, doi: 10.1016/s0955-2219(99)00024-2.

[46] J. Barberi *et al.*, “Robocasting of SiO2-based bioactive glass scaffolds with porosity gradient for bone regeneration and potential load-bearing applications,” *Materials (Basel).*, vol. 12, no. 7, 2019, doi: 10.3390/ma12172691.

[47] F. Baino, S. Hamzehlou, and S. Kargozar, “Bioactive glasses: Where are we and where are we going?,” *J. Funct. Biomater.*, vol. 9, no. 1, 2018, doi: 10.3390/jfb9010025.

[48] M. Erol-Taygun, K. Zheng, and A. R. Boccaccini, “Nanoscale Bioactive Glasses in Medical Applications,” *Int. J. Appl. Glas. Sci.*, vol. 4, no. 2, pp. 136–148, 2013, doi: 10.1111/ijag.12029.

[49] H. O. Ylänen, *Clinical application of bioactive glasses*. Woodhead Publishing Limited, 2008.

[50] T. De Caluwé, C. W. J. Vercruysse, H. A. Declercq, D. Schaubroeck, R. M. H. Verbeeck, and L. C. Martens, “Bioactivity and biocompatibility of two fluoride containing bioactive glasses for dental applications,” *Dent. Mater.*, vol. 32, no. 11, pp. 1414–1428, 2016, doi: 10.1016/j.dental.2016.09.014.

[51] E. Littmann *et al.*, “Cobalt-containing bioactive glasses reduce human mesenchymal stem cell chondrogenic differentiation despite HIF-1α stabilisation,” *J. Eur. Ceram. Soc.*, vol. 38, no. 3, pp. 877–886, 2018, doi: 10.1016/j.jeurceramsoc.2017.08.001.

[52] V. Miguez-Pacheco, L. L. Hench, and A. R. Boccaccini, “Bioactive glasses beyond bone and teeth: Emerging applications in contact with soft tissues,” *Acta Biomater.*, vol. 13, pp. 1–15, 2015, doi: 10.1016/j.actbio.2014.11.004.

[53] H. Ma, C. Feng, J. Chang, and C. Wu, “3D-printed bioceramic scaffolds: From bone tissue engineering to tumor therapy,” *Acta Biomater.*, vol. 79, pp. 37–59, 2018, doi: 10.1016/j.actbio.2018.08.026.

[54] M. Vallet-Regí, C. Victoria Ragel, and A. J. Salinas, “Glasses with medical applications,” *Eur. J. Inorg. Chem.*, no. 6, pp. 1029–1042, 2003, doi: 10.1002/ejic.200390134.

[55] H. Zreiqat, P. Evans, and C. R. Howlett, “Effect of surface chemical modification of bioceramic on phenotype of human bone-derived cells,” 1998.

[56] T. Yamasaki *et al.*, “Meniscal regeneration using tissue engineering with a scaffold

derived from a rat meniscus and mesenchymal stromal cells derived from rat bone marrow," 2005, doi: 10.1002/jbm.a.30369.

[57] P. Balasubramanian, L. A. Strobel, U. Kneser, and A. R. Boccaccini, "Zinc-containing bioactive glasses for bone regeneration, dental and orthopedic applications," *Biomed. Glas.*, vol. 1, no. 1, pp. 51–69, 2015, doi: 10.1515/bglass-2015-0006.

[58] Y. C. Fredholm, N. Karpukhina, R. V Law, and R. G. Hill, "Strontium containing bioactive glasses : Glass structure and physical properties," *J. Non. Cryst. Solids*, vol. 356, no. 44–49, pp. 2546–2551, 2010, doi: 10.1016/j.jnoncrysol.2010.06.078.

[59] I *et al.*, "We are IntechOpen , the world ' s leading publisher of Open Access books Built by scientists , for scientists TOP 1 %," *Intech*, vol. i, no. tourism, p. 13, 2012, doi: 10.1016/j.colsurfa.2011.12.014.

[60] A. L. B. Maçon *et al.*, "Lithium-silicate sol–gel bioactive glass and the effect of lithium precursor on structure–property relationships," *J. Sol-Gel Sci. Technol.*, vol. 81, no. 1, pp. 84–94, 2017, doi: 10.1007/s10971-016-4097-x.

[61] M. Khorami, S. Hesaraki, A. Behnamghader, H. Nazarian, and S. Shahrabi, "In vitro bioactivity and biocompatibility of lithium substituted 45S5 bioglass," *Mater. Sci. Eng. C*, vol. 31, no. 7, pp. 1584–1592, 2011, doi: 10.1016/j.msec.2011.07.011.

[62] V. Miguez-Pacheco *et al.*, "Development and characterization of lithium-releasing silicate bioactive glasses and their scaffolds for bone repair," *J. Non. Cryst. Solids*, vol. 432, pp. 65–72, 2016, doi: 10.1016/j.jnoncrysol.2015.03.027.

[63] P. Han, C. Wu, J. Chang, and Y. Xiao, "The cementogenic differentiation of periodontal ligament cells via the activation of Wnt/β-catenin signalling pathway by Li + ions released from bioactive scaffolds," *Biomaterials*, vol. 33, no. 27, pp. 6370–6379, 2012, doi: 10.1016/j.biomaterials.2012.05.061.

[64] R. J. Kavitha, B. Subha, S. Shanmugam, and K. Ravichandran, "Synthesis and Invitro Characterisation of Lithium Doped Bioactive Glass through Quick Alkali Sol - Gel Method," *IJIRSE) Int. J. Innov. Res. Sci. Eng. ISSN (Online)*, pp. 2347–3207.

Chapter 2- Mesoporous Bioactive Glasses

1. Introduction

For almost 50 years, bioactive glasses (BGs) have been extensively studied for their extremely appealing characteristics, leading, day by day, to a rapid increase in new application fields and, as a result, life quality and expectancy [1].

In fact, recent studies showed that kinetics deposition process of hydroxyapatite (HCA) on BGs may be improved by modifying glass surface properties [1], [2]. Extensive researches conducted on this topic have come out with a handful of modifications: the possibility to get control over porosity, pore size and internal pore connectivity, as well as to increase the external surface area of bioactive glasses ideally allows the design and development of a huge number of BG-based biomaterials with interesting textural and reactive properties [1].

In 90's, one important step in BG evolution occurred when Li *et al.* realized sol-gel bioactive glasses overcoming the limitations of traditional melt-derived BGs [3].

Indeed, sol-gel bioactive products can be obtained in a wider range of composition compared to the melt-derived ones. Melt-derived process need to respect the boundaries of 60 per cent SiO_2 silica-based systems because higher amount of silicate in the composition inhibits the biomaterial dissolution and apatite formation due to the more rigid glassy network [4][5]. Thanks to their greater surface area and porosity, sol-gel BGs exhibit higher bone bonding rates coupled with excellent degradation and resorption properties even using compositions with SiO_2 contents up to 90 per cent [3][6][7][8].

Although their higher compositional versatility and bioactivity performances compared to melt-derived products, sol-gel BGs are limited by poor uniformity of pores structure which makes them not suitable for some clinical applications, as drug loading and release [3][9].

At the beginning of XXI century, a new field of applications started considering surgeons request for a material able to solve the frequent side effects due to bacterial infections after bone reconstruction surgery, as osteomyelitis [1]. Traditionally, patients can be treated with systemic antibiotic administration, surgical debridement, wound drainage or even implant removal, but these techniques have important limitations and may lead to additional surgical interventions [1][10].

In 2001, Vallet Regì and co-workers focused their attention on the possibility to use silica mesoporous materials in biomedical applications [11][12].

Ordered mesoporous silica materials were first reported in 1990s Mobil Oil Corporation researchers and scientists from Waseda University and their physio-chemical properties were soon broadly applied in different fields, as heavy-metal adsorption, catalysis or energy storage [11].

Vallet Regì *et al.* systematically investigated the *in vitro* apatite formation of mesoporous silica materials, as Mobil composition of matter (MCM)-48, hexagonal mesoporous silica (SBA-15), phosphorous-doped MCM-41 and bioactive glasses containing MCM-41 [3][13]. These extensive studies show that mesoporous silica presents unique mesoporous texture and porosity features making it an attractive material in biomedicine thanks particularly to the good biocompatibility, low cytotoxicity and huge possibilities of functionalization [3][9][14]. Although these appealing features, pure mesoporous silica materials suffer from poor bioactivity performances to be considered for bioactive bone grafts [3][15][16].

Based on the concept studied by Vallet Regì *et al.*, in 2004 Yu and co-workers realized the first mesoporous bioactive glass (MBG) combining the sol-gel method and the supramolecular chemistry of surfactants, which opened a new direction in the field of regenerative medicine [1][17][18].

In the last two decades, MBGs are becoming increasingly important in both mesoporous material and biomaterial research opening up new opportunities in drug delivery, implanting and as coating-materials in tissue engineering [17].

2. MBG Properties

Surprisingly and in contrast with Hench's theory about bioactivity [19], pure mesoporous silica forms low amount of apatite once soaked into Simulated Body Fluid (SBF) solution although the absence of Na^+ and Ca^{2+} ions [20]. The mechanism at the basis of this phenomenon is still object of study and partially explained by the unique texture of mesoporous materials [20][15][21].

The mesoporous bioactive glasses are the latest evolution of sol-gel BGs and belong to the class of *mesoporous or mesostructured materials characterized by porosity in the range from 2 to 50 nm*, according to IUPAC nomenclature [20].

As cited before, MBGs exhibit peculiar properties which make them very attractive for biomedical applications:

1) Ultrahigh specific area (above 100 m^2/g [20])
2) Ordered meso-structure
3) Tunable and narrow pore size (2-30 nm [11])
4) High pore volume (ca 1 cm^3/g [11])
5) Well-defined surface properties characterized by high silanol density which allows further modifications [3], [11].

MBG textural properties can be properly tailored setting different parameters during the synthesis processes [22].

As previous stated, MBGs maintain also advantages of sol-gel derived bioactive glasses over melt-derived products, such as:

1) Lower temperature for the synthesis
2) Relatively easy powder technology production
3) Improved homogeneity and purity of ion-doped powder
4) Wider range of bioactive compositions (with increased bioactivity of compositions up to 90 mol% SiO_2)
5) Presence of tunable mesoporosity
6) Ability to form mesoporous scaffolds [23].

3. MBG Synthesis

As above mentioned, the first mesoporous bioactive glass derived from the intuition of Yan *et al.* to combine sol-gel synthesis with the supramolecular chemistry of surfactants (**Figure 26**) [3], [23].

Figure 26. Production of MBGs by the so-called "wet" method. The image shows, on the left side, a gel-derived glass and, on the right side, mesoporous silica by sol-gel and supramolecular arrangement routes respectively. As the image illustrates, MBGs are formed by a combination of these two routes (middle image) [23].

The result of this combination is a mesoporous material with composition similar to that of a conventional glasses but showing additional value of an ordered mesoporous configuration [23].

Surfactants are defined, according IUPAC nomenclature as:

"A substance which lowers the surface tension of the medium in which it is dissolved, and/or the interfacial tension with other phases, and, accordingly, is positively adsorbed at the liquid/vapour and/or at other interfaces. [24]*"*

In MBGs synthesis, surfactant molecules incorporated into sol-gel process act as **structure-directing agents (SDA)**, essential for obtaining well-ordered structures and for the formation of mesopores [3], [23].

Under appropriate synthesis conditions, surfactants are dissolved in a common medium with glass precursors obtaining a homogenous mixture. The surfactant molecules organize themselves into micelles which are able to link with the hydrolysed precursors (e.g., TEOS

and TEP) forming an ordered mesophase, where a constant ratio of network former, precursors and surfactant is kept [1]. The surfactant molecules link the BGs precursors (mainly hydrolysed silica resulted from TEOS hydrolysis) through the hydrophilic components while the hydrophobic parts are set out inside the micelle interior structure [1], [3], [23].

Similarly to traditional sol-gel synthesis, the gel forms by conventional hydrolysis, condensation and aging where micelles represent the structure template [23]. During the following steps, the surfactant removal may occur through calcination or extraction methods. These processes leave empty holes and lead to the formation of the mesoporous materials, characterized by well-ordered structure which exhibits high surface area and porosity [6].

MBGs are realized in different forms, such as powders, particles [17], fibres [25], spheres [26], three dimensional scaffolds and composite, all characterized by highly ordered mesoporous structure and excellent bioactivity [3][27]. The realization of MBG particles is the easiest preparatory method of MBG materials. They were first produced in 2004 by Yan *et al.* who realized MBG particles with dimensions of which around several tens of nanometers [3][17]. These particles were characterized by well-ordered mesoporous channels of 5 nm, high surface area and pore volume.

In 2009, Lei *et al.* produced MBG powders [28] which exhibit highly specific surface area using acetic acid as structure directing agent [3]. Therefore, other MBG powders were next realized showing excellent *in vitro* bioactivity [29][30].

MBG fibres were prepared by combining surfactant and electron spin techniques. By an accurate control on electrospinning parameters, it is also possible to realize MBG fibres with hollow cores and mesoporous walls which are highly bioactive, especially for drug delivery applications [3][25].

MBG spheres are realized using other special methods, as alginate cross-linking, co-template and hydrothermal methods [26]. Yun *et al.* performed hierarchical mesoporous-microporous MBG spheres with dimensions of which around several hundred micrometres and characterized by well-interconnected pore structure and appealing bioactivity performances [31].

Two main routes, known as **Hydrothermal Method** and **Evaporation Induced Self Assembly**, used to synthetize MBGs will be describe in the following paragraphs.

3.1 Hydrothermal Method

The hydrothermal method was the first technique used to synthetize mesoporous silicate. This synthesis improves mesoscopic regularity of resulted products. In fact, after the solution reaction, meso-structures are subjected to a re-organization, growth and crystallization during the hydrothermal treatment [32].

In this method the synthetic temperature goes from -10 °C up to 130°C [32]. Sometimes 170°C may be reached by the introduction of a surfactant containing fluoride [32]. Higher temperatures could lead to micro-structures formation because of degradation of ordering and decomposition of surfactants [32].

The hydrothermal procedure involves seven main steps:

1. **Mixing** surfactants in a solvent, typically water, at high temperature (up to 130 °C).
2. Addition of silicate **precursors** into the solution, in this step hydrolysis of precursors occurs through the action of an acid or base catalyst.
3. Formation of a **sol** composed by silicate oligomers.
4. Condensation of a **gel** thanks to interactions between silicate oligomers and surfactants and precipitation of mesoporous silicate.
5. **Hydrothermal treatment**, such as cooling down to room temperature leads suddenly to a solidification of a ordered meso-structure.
6. **Filtering, washing and drying** of resulted mesoporous materials.
7. **Surfactant removal** shows final mesoporous products [32].

Meso-structures are assembled before hydrothermal treatment, while this process is necessary to improve mesopore regularity [32]. This results in the need of a long treatment in which the hydrothermal step can last up to seven days [32].

This synthesis can be conducted under acidic or basic conditions. On the contrary, neutral conditions (pH ranging from 6.0 to 8.5) do not allow mesoporous production because of polymerization and cross-linking rates of silicates impede the control of surfactant assembly [32].

With pH comprises between 9.5 to 12.5 (basic conditions), polymerization and cross-linking of silicate are reversible. For this reason, acidic conditions (ranging from 1.0 to 3.0)

are often preferred to synthetize mesoporous materials [32]. Therefore, acid environment reports faster precipitation rate [32].

Synthesis parameters adopted in hydrothermal treatment, such as high temperature in acidic conditions and relatively slow procedures, make this treatment dangerous to workers. For this reason, Evaporation Induced Self Assembly (EISA) process has more recently been preferred for the synthesis of mesoporous materials.

3.2 Evaporation Induced Self Assembly (EISA)

Self-Assembly is generally defined as follow:

> *"Self-assembly is the spontaneous organization of materials through noncovalent interactions, (such as hydrogen bond, Van der Waals forces, electrostatic forces, π- π interactions, etc.), with no external intervention.* [33]*"*

In self-assembly process typically asymmetric molecules (most commonly amphiphilic surfactants) are engaged and pre-programmed to assemble into well-ordered supra molecular structures. Once in contact with the aqueous solution, surfactant molecules spontaneously organize themselves exposing hydrophilic parts to the surrounding medium while shielding hydrophobic part within micellar interior [33].

In 1992, researchers of Mobil Oil Company investigated surfactant self-assembly in aqueous solutions of soluble silica discovering the existence of a spontaneous co-assembly process of silica-surfactant mesophases. In the following years, lot of research groups developed and studied mesoporous silica structure highlighting surfactants importance in synthesis process [9].

The knowledge of chemical mechanism which regulate a surfactant/silicate solution is a fundamental prerequisite to understand the synthesis and processes responsible for the formation of mesoporous silica and, then its evolution mesoporous bioactive glasses [33].

Behaviour of Surfactant Molecules in an Aqueous Solution

Considering a simple binary system represented by water and surfactant, SDA molecules are to be considered as very active components which can exist in different structures according to their concentration (**Figure 27**).

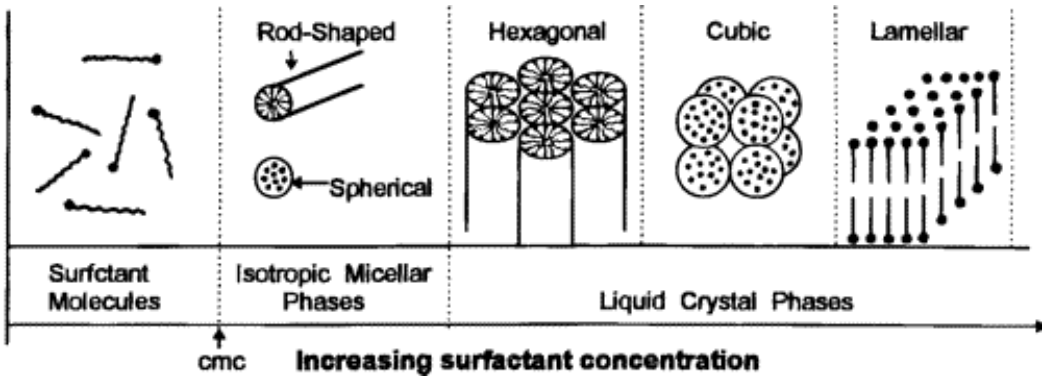

Figure 27. Phase sequence of water-surfactant binary system following surfactant concentration [13].

At low concentrations, surfactant molecules are monomolecules but, increasing their amount in the solution, they begin to aggregate in micelles to decrease system entropy. It has been defined **critical micellization concentration (cmc)** the surfactant concentration at which monomolecules aggregate to form micelles. As molecules concentration continuously grows, surfactants exhibit different forms, such as hexagonal packed arrays which produced *hexagonal phases*. Sometimes, it has been observed that surfactants can organize themselves also in *cubic phases*, characterized by complex networks of rod-shapes aggregates. Thereafter, coalescence of adjacent phases begins and *lamellar phase*, which consists in mutually parallel cylinders, appears in the system [13].

The exhibition of one of these phases in the final glassy product depends on the solvents-Pluronic® ratio, as the ternary phase diagram water-ethanol-P123 (**Figure 28**) shows. This diagram will be deeper analysed in *Chapter 4* where several considerations about it will be reported to optimize synthesis processes.

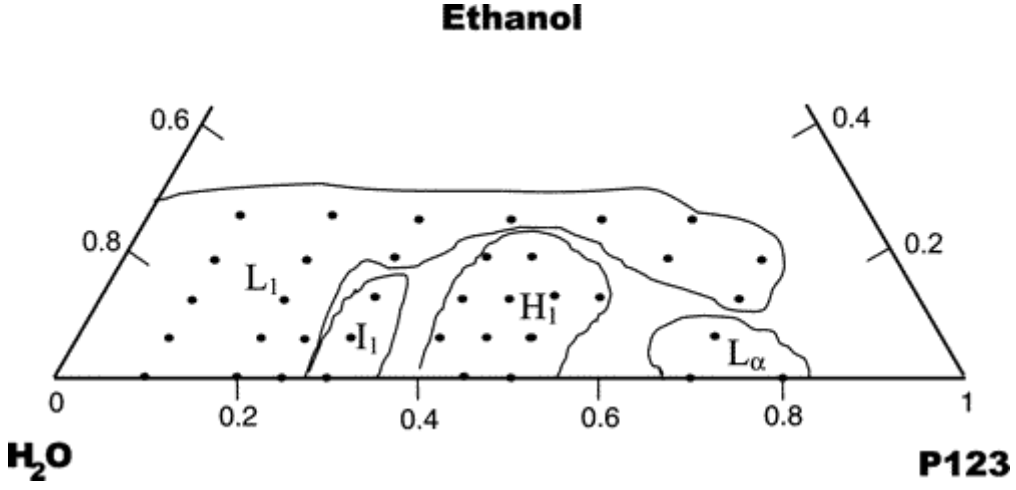

Figure 28. Ternary phase diagram of P123/water/ethanol at T=23 °C. L1 denotes region with isotropic solution (water rich), I1 refers to isotropic gels, H1 to cylindrical micelles arranged in a 2D hexagonal lattice, and Lα is the lamellae-planner micelles. The region boundaries are traced by solid lines [34].

In 1994, a study of Steel *et al.* reported different NMR spectra of surfactant in aqueous solution with different surfactant concentration (**Figure 29**).

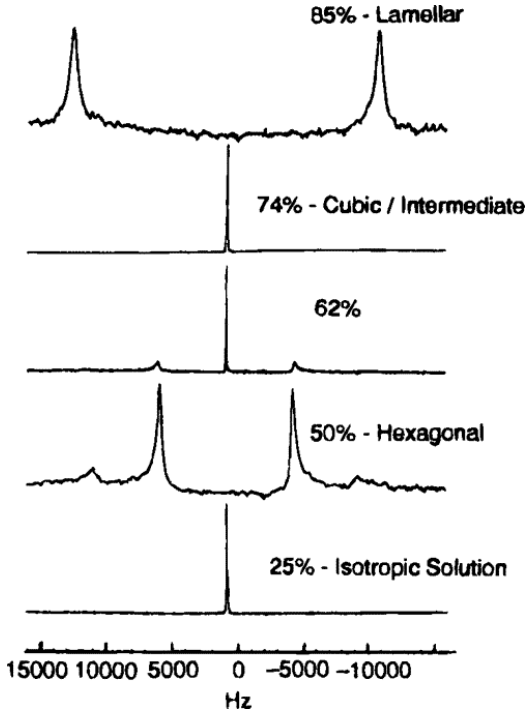

Figure 29. NMR spectra of CTAC1 aqueous solution with different concentrations ad 90°C (Steel *et al.,* 1994) [13].

EISA Process in MBG Synthesis

Now, it has been considered a more complex system, composed by homogenous solution of soluble silica and surfactant mixed in ethanol/water solvent, with initial surfactant concentration (c_o) lower than *cmc*. The preferential evaporation of ethanol induces the deposition of a film, formed by non-volatile surfactant and silica species, in water [33]. Then, surfactant concentration progressively increases driving self-assembly processes of silica-surfactant micelles organized into liquid-crystalline mesophases. The final result of this mechanism is the rapid formation of ultra-thin film mesophases well orientated according to the substrate surface [33].

As illustrated before, mesoporous bioactive glasses have highly interconnected pore structure which is realized adopting the supramolecular chemistry of surfactants [22]. Indeed, the newest approach for MBG synthesis is the **Evaporation Induced Self-Assembly (EISA)** process which implicates the use non-ionic block copolymer surfactants as structure directing agents thanks to their unique self-assembly properties (**Figure 30**) [22].

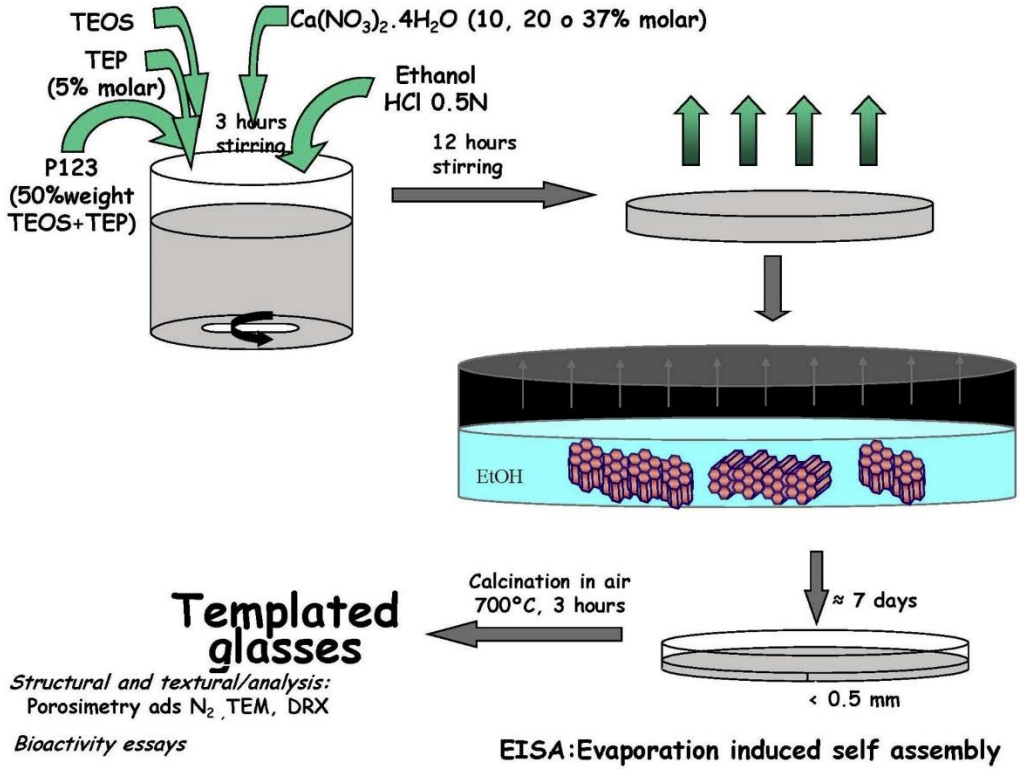

Figure 30. Example of stages of the EISA process [6].

In MBG synthesis, the mechanism is similar to the one previously explained, so a diluted solution which contains surfactant and precursors is realized by mixing in ethanol/water solvent [35]. At room temperature, solvent evaporation begins increasing surfactant concentration. Once critical micelle concentration *cmc* of the surfactant molecules is reached, self-assembly process into micelles is triggered and further organization into liquid crystalline mesophase occurs. The typical step of EISA process is the 'evaporation induced' stage in which the template is forcibly eliminated giving birth to the final product. Indeed after surfactant is completely removed by thermal treatment, such as calcination, empty holes are in the glass networks and MBG, characterized by well-ordered structure, are obtained [35].

Evaporation temperature in the EISA synthesis is another important parameter to control MBG textural properties. It has been demonstrated that, using the same MBG composition, the mesostructure can change form 3D cubic to 2D hexagonal in relation of a decrease in the solvent evaporation temperature, for example from 40 °C to 20 °C [35]. These two arrangements can both coexist for intermediate temperature. When solvent evaporation is conducted at higher temperatures, micelle size increases reducing hydrogen interaction between micelles and water and leads to the formation of 3D cubic mesostructure [35]. Contrary, 2D hexagonal structures are realized when the synthesis is conducted at low evaporation temperatures [35].

The textural features of MBGs are also strongly influenced by both surfactant nature, such as copolymer molecular structure, and synthesis conditions, as solvent compositions, temperature, medium of reaction, etc. [22].

4. Effects of Surfactants and Precursors

As previously seen, MBG synthesis results from the combination of sol-gel process and supramolecular chemistry of surfactants. Surfactant molecules act as structure directing agents which template glass network and leave empty holes in MBG structure once they are removed [24].

Generally an homogenous solution of surfactants in solvent is necessary to produce ordered meso-structures [32].

Surfactants can be classified into three categories as cationic, anionic and non-ionic surfactants [32]. Cationic surfactants exhibit excellent solubility, high critical micelle temperature (cmc) values and may be used in both acidic and basic media [32]. On the other side, they are often toxic and expensive [32]. In anionic salt surfactants are included carboxylates, sulfates, sulfonates, phosphates, etc. Non-ionic surfactants are also widely available in different chemical structures [32]. Therefore, they are non-toxic, available at low prices and biodegradable. For all these reasons, they are largely employed for industrial applications [32].

4.1 Brief Review of Main Commercial Surfactants

The particular phase present in a solution containing surfactant at a given concentration depends not only on the template concentrations but also on its properties, i.e the length of the hydrophobic carbon chain, hydrophilic head group and counterion [13].

Most used surfactants in MBG synthesis are CTAB, Pluronic® P123 and Pluronic® F127.

It follows a brief review of these three templates useful to better understand how their use influences MBG architecture.

CTAB

Cetyltrimethylammonium bromide (CTAB) is a quaternary ammonium surfactant which is one of the main components of some buffers for the extraction of DNA. Therefore, CTAB is widely used in the synthesis of gold nanoparticles, as spheres and rods, and mesoporous silica materials [36].

Chemical formula of CTAB is $C_{16}H_{33}N(CH_3)_3Br$ (**Figure 31**) which corresponds to a molecular weight of 364,45 g/mol.

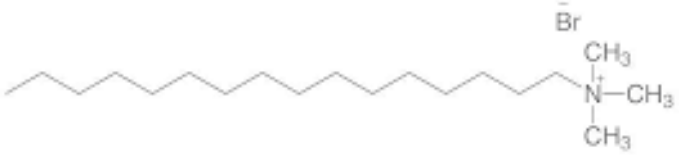

Figure 31. Cetyltrimethylammonium bromide (CTAB) chemical representation.

As other surfactants, CTAB forms micelles in aqueous solutions when a temperature of 30 °C is reached. The formed micelles have aggregation number between 75-120 and degree of ionization α= 0,2 -0,1.

For this properties CTAB is the first template that was used for the synthesis of mesoporous materials. The products of sol-gel synthesis combined with CTAB used possess regular arrays of uniform channels, the dimensions of which can be tailored tuning different factors, as the choice of surfactant, auxiliary chemicals and reaction conditions [36].

Pluronics® represent another important class of biomedical polymers composed by PEO-PPO-PEO triblock (**Figure 32)**. This group of synthetic polymers are thermo-reversible in aqueous solutions [37]. Their sol-gel transition is influenced by the composition, molecular weight and concentration of each constituent block polymer [37].

Pluronics have an amphiphilic structure in which ethylene oxide constitutes the hydrophilic part while propylene oxide is the hydrophobic component [37]. Indeed, this class of triblock polymers is composed by a polar, water-soluble group attached to a non-polar, water-insoluble hydrocarbon chain [37].

These surfactants self-assemble into amphiphilic micelles which are able to accommodate lipophilic molecules in the central core area [38]. Thanks to this peculiarity, Pluronic micelles are effectively employed as drug carriers because their assemblies can be used as passive drug containers.

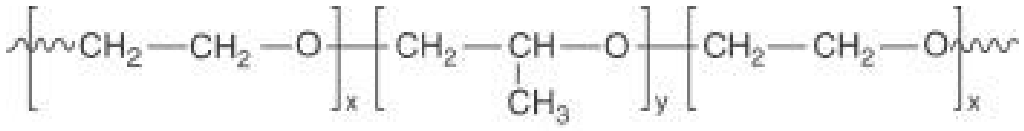

Figure 32. Pluronics triblock structure $(PEO)_x$-$(PPO)_y$-$(PEO)_z$ [38].

Pluronic micelles have also other appealing features as low *in vivo* toxicity and an appropriate size that restricts renal excretion [38].

Pluronics structures absolve the role of drug delivery carriers in a spacial and temporal controlled manner. Therefore, the shielding effect of their structure reduces drug interaction with healthy tissues [38].

The aggregation state of these micelle systems can be tuned just selecting the appropriate Pluronic size and PPO/PEO block-length ratio [38].

Pluronic ® P123

Pluronic® P123 is a symmetric triblock copolymer formed by poly(ethylene oxide) (PEO) and poly(propylene oxide) (PPO) in an alternated linear chain (**Figure 33**).

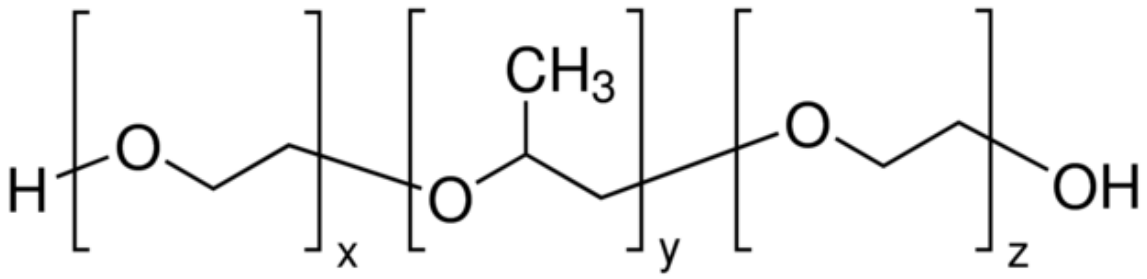

Figure 33. The structure of Pluronic P-123, where x=20, y=70 and z=20.

The chemical formula of P123 is $HO(CH_2CH_2O)_{20}(CH_2CH(CH_3)O)_{70}(CH_2CH_2O)_{20}H$ which corresponds to PEO-PPO-PEO.

The peculiar characteristic of this surfactant is influenced by PPO unit which is hydrophobic at temperature above 15 °C and soluble in water ate temperature below 15 °C, leading to the formation of micelle made up of PEO-PPO-PEO triblock copolymers. Micelles are constituted by a hydrophobic core of PPO block and a hydrophilic corona of PEO groups [34].

In acidic conditions, this phosphonated triblock copolymer is cleavable [39]. This feature allows the conversion of its terminal hydroxyl groups of the PEG block of Pluronic P123 which interact with tetraethoxysilane (TEOS) to produce mesoporous silica based materials, once the template removal occurs [39].

Pluronic® F127

Pluronic® F-127 (**Figure 34**), also known as Poloxamer 407, is a nonionic, surfactant polyol that has been often employed in tissue engineering because of its sol-gel transition near physoliological temperature and pH [37][40].

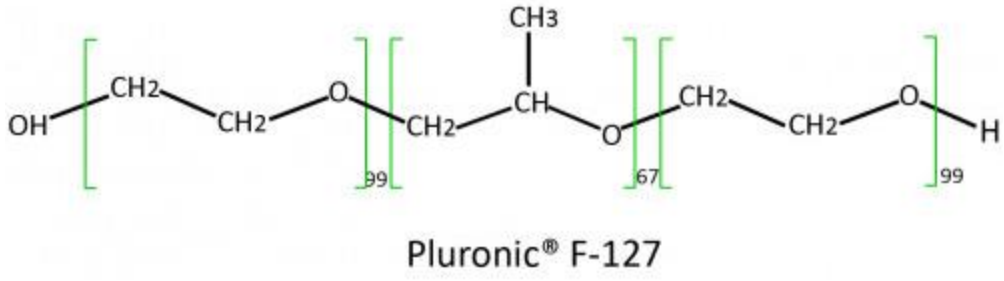

Figure 34. Pluronic F-127 structure.

4.2 Surfactant molecules as structure directing agents in MBG synthesis

It has been demonstrated that the surfactant choice directly impacts on mesopore structure, mesopore size and pore volume of mesoporous bioactive glasses [3].

Lot of studies have been conducted on the main structure directing agents for MBGs synthesis, such as CTAB, F127 (EO106- PO70- EO106) and P123 (EO20- PO70- EO20) [3]. The resulted MBGs would exhibit different final mesopore size, volume and surface area (**Table 10**), ranging from 2 to 10 nm, 0.4 to 0.7 cm^3 and 150 to 1000 m^2/g [23].

Table 10. Textural characteristics of MBGs prepared by different structure-directing agent [3].

Structure-directing agent	**Surface area (m^2g^{-1})**	**Pore volume (cm^3g^{-1})**	**Pore size (nm)**
P123	300-350 278-400 250-350 438-466 450-480 499	0.4-0.49 0.54-0.73 0.4-0.5 0.63-0.73 0.7	4.3-4.6 6.5-6.9 5 3.5-3.7 5.37-6.43 6.1
F127	520 228-300 152-310	0.51 0.36-0.42 0.235-0.356	5.4 5.0-7.1 4.2-5.0
CTAB	1040 443	1.54 0.57	1.82-2.2 2.9
P123 + CTAB	552-618	0.69-1.08	4.1-6.2

Generally, it has been noticed that P123 induces a more ordered architecture on final MBG product than CTAB, as can be seen in **Figure 35**.

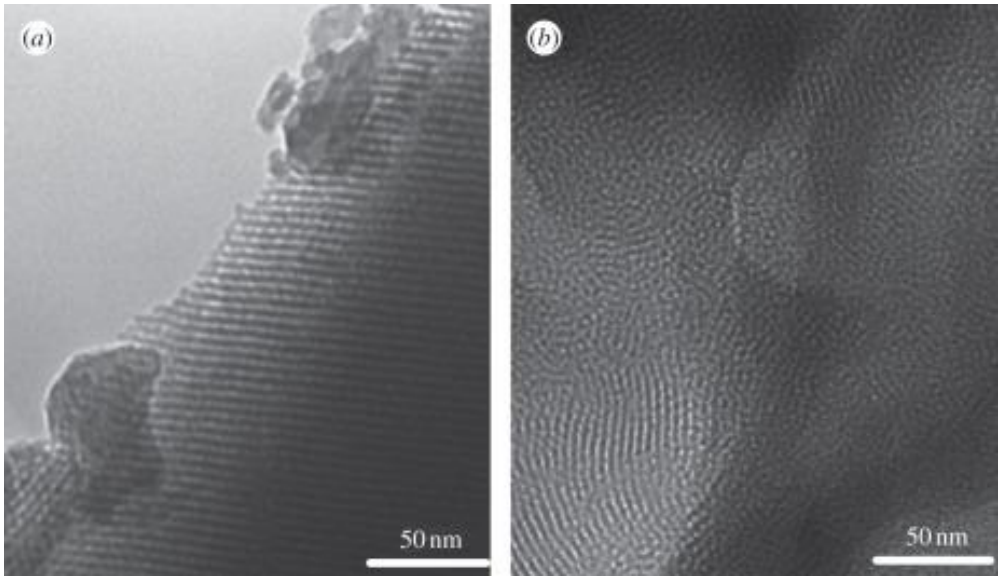

Figure 35. Transmission electron microscopy images of (*a*) P123 induced MBG and (*b*) CTAB induced MBG [3].

Also pore size is generally different in CTAB-induced MBGs and MBGs realized using Pluronics: CTAB products are characterized by lower pore size (2-3 nm) than P123 or F127 ones (4-10 nm) [3].

Therefore, SDA choice impacts on MBG architecture: P123 usually induces a 2D hexagonal mesopore structure, F127 a wormlike structure, while in CTAB-induced MBGs the orderings are substantially lower than Pluronics ones [3].

Considering pore volume, P123-MBGs exhibit higher pore volume and surface area than F127 ones. This feature is reflected on significantly higher drug load efficiency of P123-induced MBGs compared to F127-induced MBGs with same composition [3].

Arcos *et al.* study has also demonstrated that MBG realized by CTAB addition has the highest loading efficiency (10.7%) than same MBG compositions P123-induced and F127 induced (respectively 9.7% and 9.1%) [41]. For this reason, the usage of CTAB is recommended to improve drug delivery performances of MBG than other surfactants [3][42].

But concerning the preparation methods of applying each surfactants, the employment of P123 and F127 is considered much easier than that of CTAB because of its need of additional filtering and washing procedures aiming at obtaining a material able to be calcinated [3].

Before explaining precursors influence into textural properties of MBG products, it is reported a brief paragraph about chemistry and structural properties of silica-based bioactive glasses.

4.3 Chemistry and structural properties of silica-based BGs

Understand the role of each component on the bioactivity performances of a BGs is fundamental to design and develop mesoporous bioactive glasses.

Considering for example Bioglass® 45S5, it is an amorphous structure constituted by a covalent bonded network of SiO_2 together with P_2O_5 [6].

Silica oxide is considered the main network former, but both oxides are in the form of tetrahedral units, such as [SiO_4] and [PO_4], covalently bonded through the oxygen atoms present in network vertex [6].

While CaO and Na_2O are defined as network modifiers because their cations disrupt the covalent network and create ionic bonds with oxygen atoms [6].

In this way, network formers are responsible of material stability while network modifiers enhance glass reactivity and, consequently, glass bioactivity [6].

This process is reflected in a parameter called *connectivity value (Y)*. The connectivity parameter value reaches Y=4 in pure silica SiO_2 glasses, where all O atoms are bonded to tetrahedral units [SiO_4] and [PO_4] [6].

On the contrary, bioactive glasses are descripted by much lower connectivity values, i.e. Y=2.07 for Bioglass. Different studies have demonstrated that connectivity value Y<2.4 generally exhibits bioactivity behaviour [6].

4.4 Composition- mesopore structure relationship of MBG materials

Although pure mesoporous silica exhibits excellent mesoporous textural properties, it lacks in bioactivity behaviour due to its structure. Pure SiO_2 architecture is characterized by extremely rigid network which is not able to easily interact with physiological environment inhibiting the dissolution process at the base of bioactivity mechanism.

For this reason, in last two decades a huge number of multi-components MBG have been realized to improve bioactivity performances.

Compared to melt-derived BGs (which can have SiO_2 content of around 60%), sol-gel synthesis allows the production of glass composition with very high SiO_2 content (up to 90%) exploiting appealing mesoporous features. Generally, high content of silica is reflected in a more ordered mesopore structure, higher pore volume and surface area than MBG based on composition with low SiO_2 content [3].

MBGs exhibit a porosity intermediate between sol-gel derived BGs and pure mesoporous silica (**Figure 36**) [35]. Textural features of mesoporous bioactive glasses, such as porosity and surface area, are almost twice than sol-gel derived with similar composition [35].

Generally, sol-gel BGs have typical surface area in the range of 100 and 250 m^2/g, whereas pore volume values are between 0.2- 0.4 g/cm^3 [35].

MBGs typical values ranges between 200 and 500 m^2/g for surface area and from 0.5 to 0.7 g/cm^3 for pore volume [35].

Instead, pure mesoporous silica usually exhibits up to 1000 m^2/g of surface area and 1.0 g/cm^3 of pore volume [35].

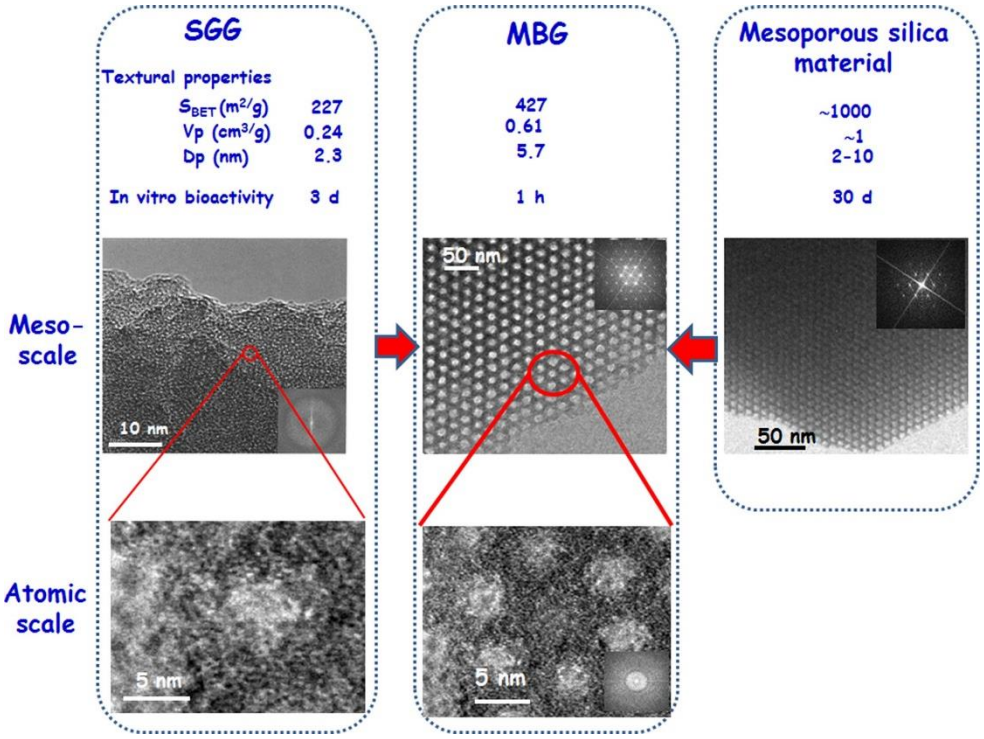

Figure 36. HRTEM images and ED patterns of typical examples of a sol-gel derived glasses, a MBG and a pure mesoporous silica material. *(HRTEM: High-resolution transmission electron microscopy; ED: electron diffraction)* [35].

Images obtained by high-resolution transmission electron microscopy confirm the intermediate porosity characteristic of MBG material.

All considered glass families have similar structure at the atomic level, exhibiting an amorphous structure, but they present substantial differences at mesoscale [35].

In fact, MBG shows an ordered mesoporous structure which, combined with its bioactivity behaviour, make them excellent candidate for tissue engineering applications.

Researchers have more recently focused their attention on MBGs based on multicomponent systems, beginning from simpler SiO_2-CaO and SiO_2-CaO-MO systems (where M is generally P) to more complex quaternary systems [3].

In fact, in sol-gel derived MBGs, the mesopore size and volume can be tailored by tuning the synthesis parameters, such as temperature of thermal treatment, but also the glass composition, particularly CaO content [2].

Calcium Oxide Role

Calcium oxide is an essential element in BGs and consequentially in mesoporous bioactive glasses.

CaO introduction into MBG composition strongly impacts the mesoporosity of the silica walls and the mesoporous structure [35].

Changing CaO amount in glass composition, different mesostructures can be realized, such as 3D cubic or 2D hexagonal arrangements [35].

As previously explained, calcium oxide is a modifier oxide which disrupts the network glass structure decreasing the network connectivity.

Thus, increase in Ca^{2+} content is directly reflected in increasing of inorganic/organic volume ratio of micelles which decreases the curvature of surfactant micelles contributing to the formation of hexagonal phases [35]. While three-dimensional cubic arrangement is exhibited when Cao content is lower.

Although a decrease in textural properties, such as surface area and pore volume, and the introduction of potential structural defects have been observed with the incorporation of CaO content, MBGs still possess high surface area and pore volume (as seen in **Figure 36**) [43].

Ca^{2+} ions are also responsible for the excellent and extremely quick *in vitro* bioactivity behaviour exhibited by MBG compositions once in contact with simulated physiological fluids [35].

This occurs because Ca^{2+} presence in the glass surface decreases pH at a value around 6.7 which allows the formation of octa-calcium phosphate, an intermediate phase for the formation of nanocrystalline HCA, accelerating bone biomineralization process [35].

Thus, other studies have shown that the increased bioactivity related on CaO content leads to enhance loading efficiency while decreases drug release rate and burst effect playing an important role in modulating the drug delivery [29].

The CaO influence on drug release abilities can be explained because drugs may be chelated with Ca^{2+} ions present in the pore walls inhibiting release process [10].

Phosphorous Oxide Role

P_2O_5 presence is not essential for the formation of mesoporous bioactive glasses but extremely beneficial in concentration < 5% mol.

Phosphorous pentoxide content has also a great impact on mesoporous structure and bioactivity performances of MBGs [35].

The presence of phosphorous atoms in the glass composition induces the formation of 3D cubic arrangements in MBGs, while in P-free compositions a 2D hexagonal nanostructure is naturally obtained [35].

Therefore, P_2O_5 spontaneously binds to CaO leading the formation of amorphous calcium phosphate clusters on the glass surface. In this way, calcium ions are ejected from the glass network affecting the structure similarly to a decrease the CaO amount, thus facilitating cubic structure formation [35].

Although phosphorous oxide impacts on structure arrangements at atomic level, its introduction not significantly compromise textural parameters value of MBGs [35].

Even if such parameters are subject to change with incorporation of Ca or P into mesoporous silica systems, MBG features remain extremely appealing for clinical applications [3]. Similarly, the introduction of divalent ions, (such as Mg, Zn, Cu, or Sr), trivalent ions (Ce, Ga or B) or tetravalent ions (Zr) into the simplest SiO2-P2O5-CaO systems negatively affects MBG mesoporous properties (**Table 11**), but these more complex MBG compositions maintains and introduces new attractive skills for medical applications [3].

Table 11. The effect of composition on the characteristics of mesopore structures [3].

MBG with different compositions	Surface area [m^2/g]	Pore volume [cm^3/g]	Pore size [nm]	References
100 Si 95Si5Ca 90Si10Ca	490 467 438		3.6 3.7 3.5	[44]
100Si 97.5Si2.5P (TEP) 97.5Si2.5P (H_3PO_4)	310 270 152	0.356 0.308 0.235	4.2 4.4 4.8	[45]
80Si15Ca5P 70Si15Ca5P 60Si15Ca5P	351 319 310	0.49 0.49 0.43	4.6 4.6 4.3	[17]
100Si 90Si5Ca5P 80Si15Ca5P 70Si25Ca5P	384 330 351 303	0.4 0.35 0.36 0.33	4.9 4.9 4.8 4.8	[46]
80Si10Ca5P5Fe 80Si5Ca5P10Fe 80Si0Ca5P15Fe	260 334 367	0.26 0.3 0.36	3.5 3.6 3.7	[47]
80Si15Ca5P 80Si10Ca5P5Mg 80Si10Ca5P5Zn 80Si10Ca5P5Cu 80Si10Ca5P5Sr	342 274 175 237 247	0.38 0.35 0.23 0.31 0.31	3.62 3.31 3.33 3.66 3.66	[30]
80Si15Ca5P 76.5Si15Ca5P3.5Ce 76.5Si15Ca5P3.5Ga	515 397 335	0.58 0.38 0.31	4.7 2.9 3.8	[48]
80Si15Ca5P 80Si10Ca5P5Zr 80Si5Ca5P10Zr 80Si5P15Zr	317 287 278 277	0.37 0.32 0.33 0.27	4.1 3.7 4.1 3.4	[49]
80Si15Ca5P 75Si15Ca5P5B 70Si15Ca5P10B	265 234 194	0.33 0.24 0.21	5.29 5.28 5.09	[50]

Indeed, although Si, Ca and P may be considered the main elements of MBG compositions, a lot of other components have been recently introduced into MBG systems, as it will be illustrated in paragraph 8.

5. MBG clinical applications

Similarly to BGs, MBG applications invest different fields thanks to their attractive properties, such as angiogenic, cementogenic, antibacterial effects.

Therefore, BGs represented a substantial evolution thanks to their ability of creating a bond with the host tissue without scar formation but promoting bone regeneration. However bone infections frequently occur after bone surgeries for which MBG-based clinical devices may represent a potential solution [29].

Bone regeneration applications

The intrinsic characteristics of MBG materials indicate them as appealing biomaterials for bone regeneration applications [3].

In the last decade, a huge number of studies has been conducted to evaluate the *in vitro* bioactive potential and reaction kinetics of different MBG-based products in contact with body fluids.

Apatite formation on the surface of MBG particles and scaffolds was first studied by Yan *et al.* who reported HCA presence *in vitro* after only 4 hours immersion in SBF [17]. The extraordinary MBG ability to induce apatite mineralization significantly faster than NBGs, is the result of the high surface area and pore volume, which strongly enhance the surface reactivity of the material due to an increased number of exposed silanol groups (Si-OH) at the interface with the external environment [17][3].

Other studies conducted by Garcia *et al.* investigated the mechanism of apatite mineralization through nuclear magnetic resonance (**Figure 37**) [51]. This analysis confirmed the significant difference on apatite formation between NBGs and MBGs. This phenomenon could be explained underlining the differences of HCA mineralization process in both two class of materials [3].

In conventional NBGs, apatite formation occurs through 'three different steps' in which the glass releases M^+ ions, forms Si-OH groups and then Si-OH groups form networks by repolymerization [3]. On the other side, MBG surface appears already prepared to execute faster these three steps accelerating and increasing the whole process of HCA mineralization [51].

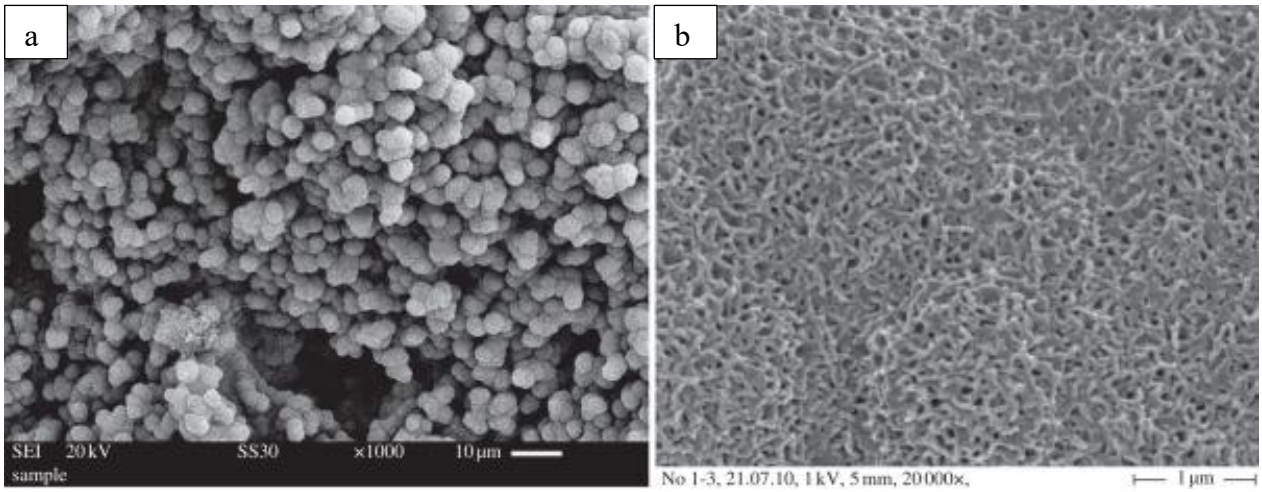

Figure 37. Nanoapatite mineralization on the surface of three-dimensional MBG scaffolds. Image (a) is a low magnification image, (b) high magnification image [3].

Drug delivery systems

Osteomyelitis incidence is one of the most important causes of surgeries failure and traditional techniques are applied just in order to prevent further complications, once the infection is already underway. Treatments, as systemic antibiotic administration, surgical debridment, wound drainage and implant removal, cause to patient extra traumas. Furthermore, conventional drug administration, such as injection or oral pill, shows variable drug concentration during the assumption reaching toxic peaks and declining rapidly to ineffective values [2], [29], [52].

Hence, continuous evolutions and improvements characterise the study and development of systems to improve drug delivery efficacy and reduce toxicity [1].

Controlled drug release has gained crescent attention aiming at the development of targeted sustained drug delivery systems able to release effective drug concentration in injured sites and limiting all side effects associated to conventional drug administration.

As seen before, one of the most appealing features of MBG materials is their very high surface area and pore volume. These two characteristics are strictly correlated with the loading efficiency of drugs and growth factors in a material. For this reason, MBG-based devices are considered potentially attractive for clinical applications, as drug delivery systems (**Figure 38**) [3]

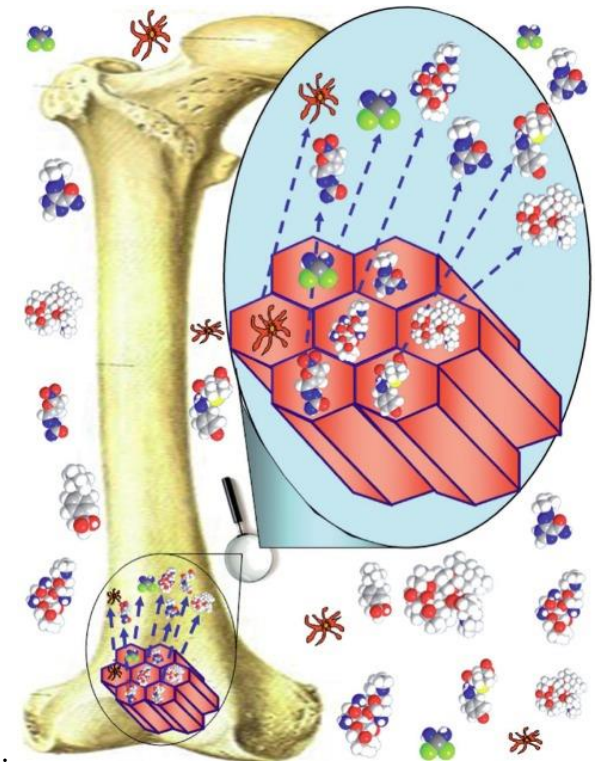

Figure 38. Schematic concept of MBG for drug delivery and bone regeneration [14].

Drug loading efficiency and release kinetics strictly depend on environmental conditions but also on mesopore characteristics. MBGs can be finely tailored through synthesis parameters and are suitable as carriers of different drug compounds. This characteristic makes MBGs an attractive and versatile tool for drug delivery applications [23].

The high density of Si-OH groups on MBG surface plays a fundamental role in interaction with drugs and protein exhibiting an appealing mechanism of slow and sustained drug release kinetics [29].

Extensive researches have demonstrated that, compared to no mesoporous bioactive glasses (NBG), drug release in MBGs is more efficient (**Table 12**) because of Fickian diffusion mechanism which regulates MBG dissolution.

"Fickian diffusion refers to the solute transport process in which the material relaxation time is much greater than the characteristic solvent diffusion time [53]. *"*

Table 12. Example of structural parameters of the MBGs and BGs scaffolds before and after loading gentamicin drug (Gen) and their drug loading efficiency [54].

Samples	Surface (BET) [m2/g]	Pore Volume [cm3/g]	Pore Diameter [nm]	Drug loading

MBGs	334.4	0.348	4.8	-
MBGs-Gen	208.9	0.216	4.4	12.33
BGs	86.7	0.099	-	-
BGs-Gen	53.1	0.081	-	5.03

Furthermore, different studies have shown that the apatite formation on MBG surface also improves drug-loading efficiency and decrease burst release and release rate [55][26].

5.1 MBGs as Multifunctional Platforms

Recent studies have investigated the role of mesoporous bioactive glasses as multifunctional platforms which can absolve to different functions through release of therapeutic ions and drug/growth factors [52].

MBG multifunctionality has been casually discovered by the observation of drug delivery experiments. For example, it was recently found in MBGs loaded with dimethyloxally glycine (commonly used as neuroprotective agent) an increased osteogenic and angiogenic activity of stem cells while doxorubicin-loaded MBGs (doxorubicin is an antibiotic and anthraclyne drug) inhibited viability of cancer cells [52].

Therefore, it has demonstrated that the dissolution of ions from the bioactive material stimulates osteogenic differentiation and bone tissue regeneration [56].

Different studies have been conducted about the incorporation of different therapeutic ions combined with the loading of drugs or growth factors. All results agreed to confirm the MBGs ability to simultaneously induce multifunctional effects once in contact with biological fluids [52].

Indeed, both therapeutic ions and drug/growth factors may be efficiently delivered from MBG system which now represent the perfect candidate as multifunctional and targeted platform for clinical applications.

Anti-bacterial effects, stimulation of osteogenesis/ cementogenesis and angiogenesis are all demonstrated effects carried by these extremely appealing biomaterials.

In the last decade, different therapeutic ions, such as monovalent ions (Ag and Li), divalent ions (Sr, Mg, Zn, Cu and Co), trivalent ions (Ce, Ga, B and Fe) and tetravalent (Zr) ion have been added in MBG compositions aiming at deeper study multifunctional features of MBG biomaterials (**Table 13**).

Table 13. Positive effects of the release of therapeutic ions and corresponding properties [52].

Therapeutic ions released from MBG		Concentration level (mg/L)	Functional properties				Ref.
			Osteogenesis	Cementogenesis	Angiogenesis	Antibacterial Effect	
monovalent	Ag Li	0.014 <17.28	✓	✓	[48]	✓	[57] [58]
Divalent	Sr Zn Mg Cu Co	<22 <0.75 <100 <152 <25	✓ ✓ ✓ ✓	✓	✓ ✓	✓	[59] [60] [61]
Trivalent	Ce Ga B Fe	0.2% mol 1% mol <50 5% mol	✓ ✓ ✓ ✓			✓ ✓	[48]
Tetravalent	Zr	<15% mol	✓				[49]

6. MBG Doped Scaffolds

Mesoporous bioactive glasses exhibit excellent bioactivity and drug delivery performances combined with effective ionic release in the body fluids thanks to its specific mesoporous architecture and high surface area [52].

Hence, functional ions, drug/growth factors and bone morphogenetic protein have been recently incorporated into MBGs creating new attractive multifunctional devices for biomedical applications.

Recently, the need of an interconnected and porous structure for the realization of an ideal scaffolds suggests to focus the research on **MBG-based scaffolds**.

Fabrication of hierarchical MBG-based scaffolds is one of the most attractive actual challenge in material science and biomedicine. In fact, mesopore size is almost three orders magnitude lower than that of osteoblast and, for this reason macroporosity must be introduced in the final device with the aim to allow cell colonization and tissue regeneration [62].

Three-dimensional porous scaffolds based on MBG materials can be realized by combination of structure-directing agent and other special techniques [3].

Several methods are used for preparing MBG scaffolds.

The first MBG scaffold was realized by the **porogen method** [3]. In 2008, Yun *et al.* used methylcellulose as porogen to create porous MBG scaffolds characterized by large pore size (about 100 μm) [3].

Another widely used method is the **polymer template method** which consists in the usage of a polyurethane sponge as porous template. For the first time, in 2008 Wu *et al.* successfully realized hierarchically porous 3D MBG scaffolds with different glass compositions by polyurethane sponge, as template for macroporous structure, and P123 surfactant, as structure directing agent for the synthesis of MBGs (**Figure 39-40**) [46].

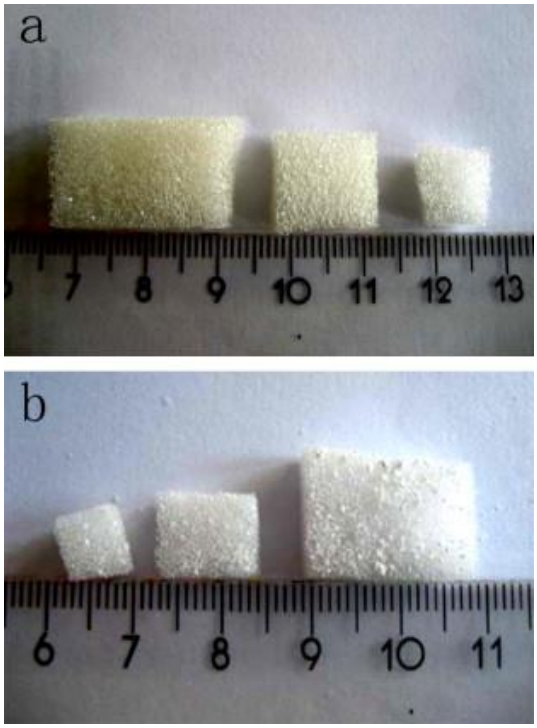

Figure 39. Photographs of the polyurethane sponges used as template (a) and the sample of MBGs 80S15C realized by Wu *et al*. [46].

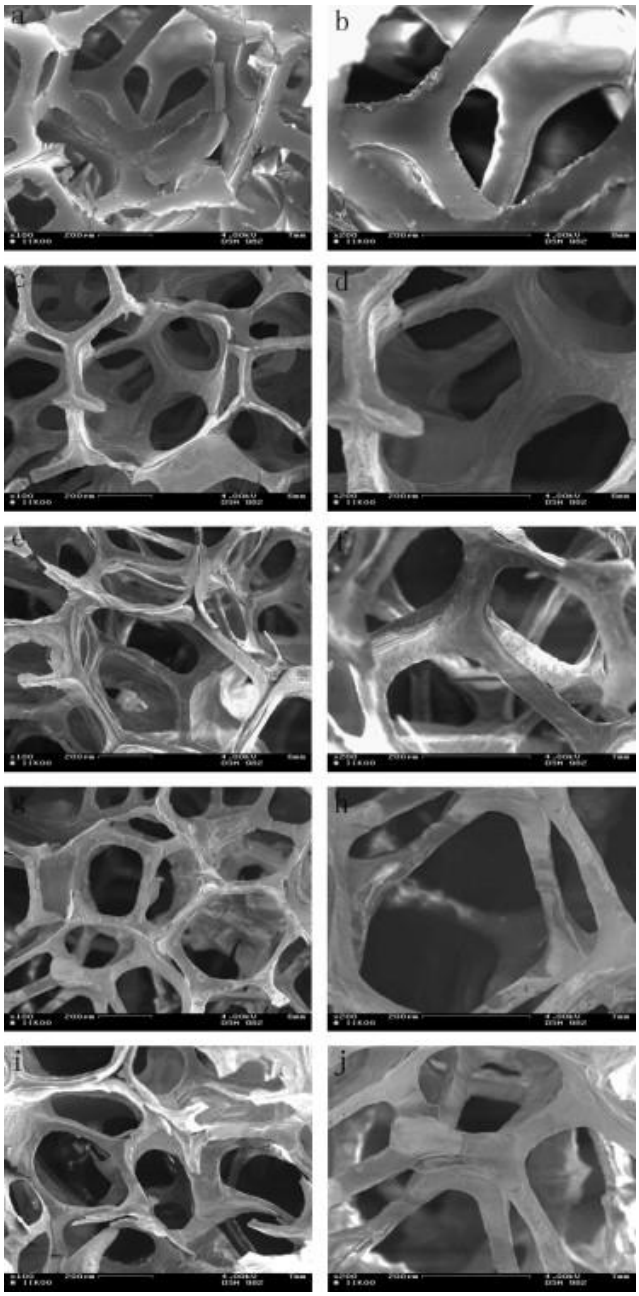

Figure 40. SEM analysis of polyurethane sponges (a,b) and the MBGs scaffolds MBGs 100S (c,d), MBGs 90S5C (e,f), MBGs 80S15C (g,h) and MBGs 70S25S (i,j) [46].

At the same time, Li *et al.* also prepared MBG scaffolds using a similar method, combining polyurethane foam, responsible of final product macroporosity, and P123 surfactant, as template for mesoporosity (**Figure 41- 42**) [63]. The foams exhibit a hierarchical structure characterized by interconnected macropores (about 200-400 or 500-700 μm) which allows *in vivo* cell colonization and tissue regeneration [63].

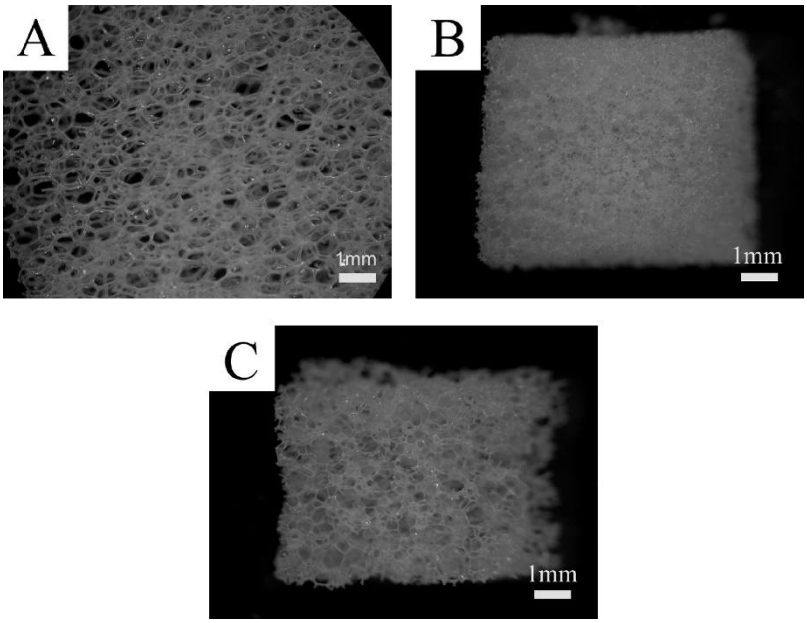

Figure 41. Optical micrographs of (A) the polyurethane foam used for preparing the scaffold-S, (B) hierarchically porous bioactive scaffold-S, (C) scaffold-L realized in 2008 by Li *et al.* [63].

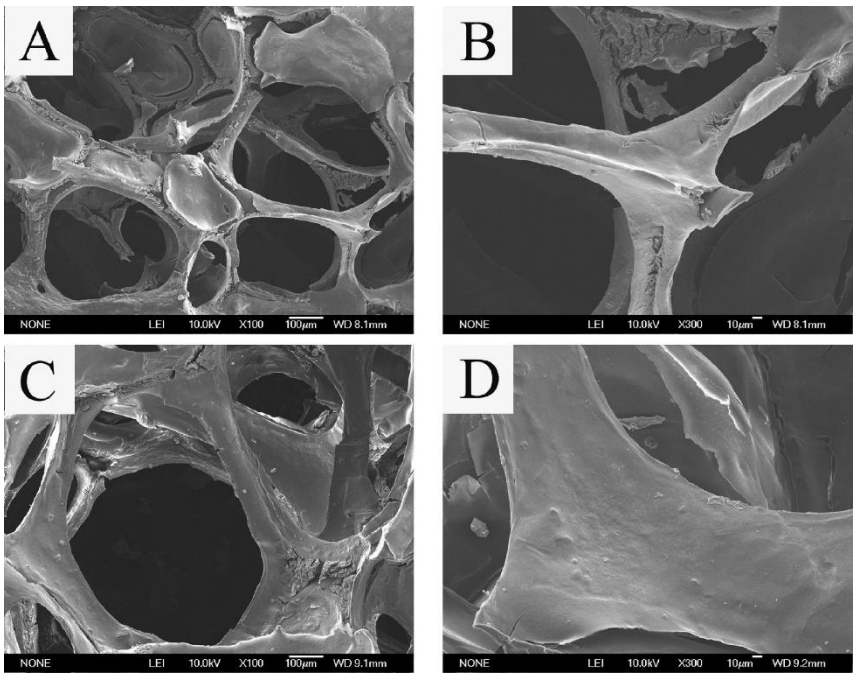

Figure 42. Representative FE-SEM images of the sample scaffold-S (A-B), and scaffold-L (C,D) after calcination at 700 °C realized in 2008 by Li *et al.* [63].

Both these studies reported excellent results in bioactivity performances during SBF immersion *in vitro*.

The other advantages in the use of polyurethane sponge template method for the realization of MBG scaffolds are the high interconnected pore structure and tunable pore size of the polymer. Mechanical properties of the material, as mechanical strength and resistance, are still quite low [3].

Another important method for the fabrication of MBG derived scaffolds is a three dimensional plotting technique, referred as **direct writing** or **printing**, which allows to better control the pore morphology, pore size and porosity [3].

In this technique, the control on final product structure occurs concisely layer by layer during the plot under mild conditions (**Figure 43**). Both Yun *et al.* and *Garcia et al.* [64] realized hierarchical 3D porous MBG scaffold using a combination of double polymer template and rapid proptyping methods. In these experiments, MBG gel was mixed with methylcellulose, then the resulted viscous solution was printed in the desired structure and finally sintered at 500-700 °C to remove polymer templates and obtained the final MBG scaffolds [3][64].

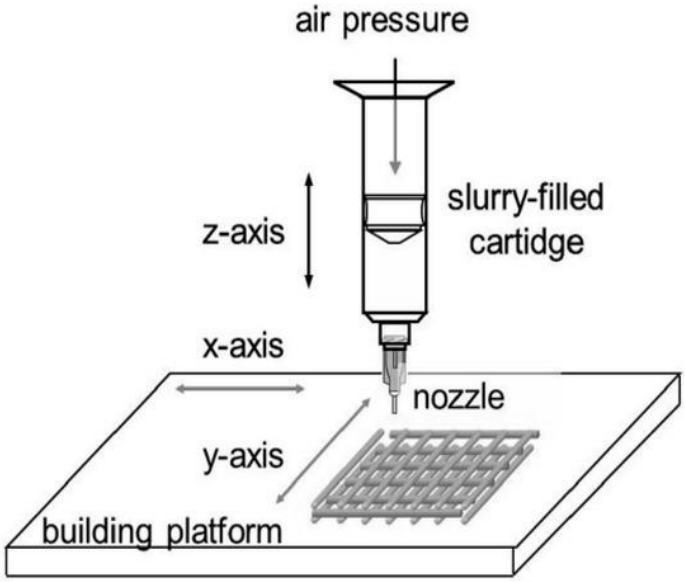

Figure 43. Schematic representation of 3D printing technique [62].

The results of these experiments shown MBG scaffolds characterized by uniform pore structure but weakened mechanical properties, as low mechanical strength value because of micropores in the structure due to the use of methylcellulose. In fact, main disadvantages of this method are the need of methylcellulose of an additional sintering procedure. For this reason, a new application of 3D printing technique was realized substituting polyvinylalcohol to methylcellulose. The MBG scaffolds resulted from this method are

characterized by excellent mechanical strength (200 times higher than MBG scaffolds realized with methylcellulose) and mineralization ability which make them perfectly suitable for bone regeneration applications [35].

Compared with non-mesopore bioactive glass (NBG), MBG has significantly improved specific surface area and pore volume which is reflected in greater *in vitro* bioactivity and degradation [65].

A lot of experiments have been recently conducted about MBG scaffolds increasing more and more the performances these devices.

For all these reasons, researchers are focusing their attention on the design and realization of MBG scaffolds for regenerative medicine, understanding how these systems represent new appealing devices for clinical applications.

6.1 Brief review of MBG-doped scaffolds

During last decade, lot of experiments have been conducted about multifunctional ability of MBG scaffolds. This appealing peculiarity of MBG-derived three-dimensional scaffold has opened a new frontier in innovative and targeted medicine [66].

It follows a short review of different MBG-doped scaffolds.

Considering monovalent oxides, silver and lithium are therapeutic ions used for doping biomaterials to develop innovative clinical applications [67].

The study of MBGs for antibacterial strategies have seen **Silver (Ag)** as one of the most appealing elements to be introduced in doped composition [23].

Silver has the highest level of antibacterial activity among all heavy metal elements generally employed for this purpose [23].

Ag antibacterial effect is produced because Ag^+ ions strongly interact with disulfide (S-S) and sulfhydryl (-SH) groups exposed on microbial cells surface leading to the formation of a S-Ag bond [23]. Once the silver ions are bonded to the surface protein of microbial walls, they inhibit respiration process of bacteria triggering the cascade of rescue mechanisms which ultimately lead to bacteria cell death [23].

Ag^+ ions absolve their antibacterial role also causing the proton leakage in the membrane of bacteria which causes its disruption and allows Ag^+ entry into cell cytoplasm where silver ions provoke conformational changes leading to cell apoptosis (**Figure 44**) [23].

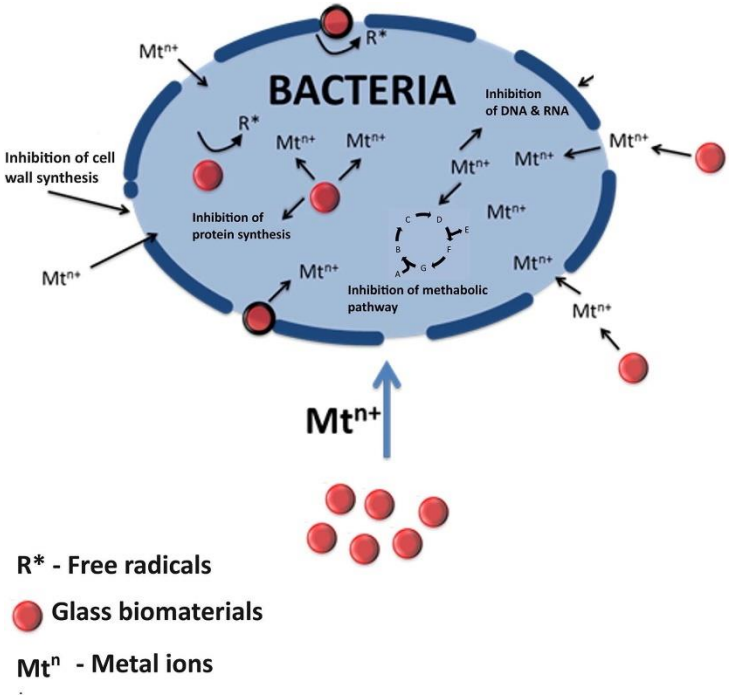

Figure 44. Schematic representation of the hypothesized mechanisms related to the antibacterial activity of metal ions release from MBG-scaffolds [68].

The attractive antibacterial property of Ag induces different researches to develop MBG-based scaffolds with the introduction of silver as doping elements [23].

Several experiments conducted about Ag-doped MBG scaffolds have shown how the introduction of this element cause some change in structural, morphological and textural properties compared to Ag-free MBG [23].

For example, Vulpoi *et al* reported a progressive decrease in surface area and change in mesoporous features with the increasing of silver amount into MBG composition [69].

The antibacterial effects of Ag-doped MBG scaffolds have been deeply analysed by Zhu *et al*. showing a strong dependence on surface glass modifications [70]. The functionalization of MBG surface improves both antibacterial effect and loading capability of Ag-doped scaffolds [23].

Lithium-doped MBG scaffolds will be separately treated in the next paragraph.

Divalent ions, such as Mg, Zn and Sr, have been used for the realization of MBG-doped scaffolds to study bone formation *in vivo* and *in vitro* [52][60].

Indeed, **magnesium** absolves an essential role in bone metabolism processes and its leaked is correlated to resorption phenomenon in bone tissue [71].

Zinc is one of the most fundamental trace elements present in human organism. It is involved into the structure and function of many macromolecules and it participates to up than 300 enzymatic reactions [72].

Strontium is naturally present in the liver, muscles and body fluids but its highest amount is revealed into bone tissue [59].

For example, Wang and co-workers successfully synthesized Mg-, Zn- and Sr-doped scaffolds using Pluronic P123 by polyurethane sponge method [60].

The resulted scaffolds show no evident differences in phase composition, macroporous structure or pore volume comparing them with no-doped scaffolds [60].

Therefore, cytotoxic effects have been not revealed in Mg-, Zn- and Sr- MBG-doped scaffolds.

Moreover, the release of these therapeutic ions into the culture medium from the scaffolds has contributed to enhance both proliferation of mesenchymal stem cells (MSC) and alkaline phosphate (ALP) activity which are at the base of bone regeneration process [60].

These results have confirmed that the addition of magnesium, strontium or zinc as therapeutic ions into MBG composition confers to MBG scaffolds multifunctional properties and enhance bioactivity performances [71].

Copper (Cu) has also been employed as therapeutic ion for doping MBG-derived scaffolds. *In vitro* culture has in fact shown that Cu^{2+} ions enhance the proliferation of endothelial cells in a dose dependent manner [73].

Therefore, *in vivo* experiments have confirmed the intervention of Cu^{2+} ions in vascular endothelial growth factors (VEGF) regulation which promote wound healing [61].

For these reasons, Cu introduction into MBG composition expands biological effects of MBG scaffolds, conferring additional angiogenesis and antibacterial properties [61].

The characterization of Cu-MBG scaffolds has shown lower surface area, pore volume and pore size respect to Cu-free scaffolds; however the value of these textural properties are still sufficient [61].

The prepared Cu-doped scaffolds possess good biocompatibility and show no cytotoxic effects. Experimental results have also confirmed Cu introduction improves angiogenesis capacity, hypoxia mimicking ability and VEGF secretion indicating the fundamental role of Cu^{2+} ions as trigger agents of hypoxia effects [61].

Therefore, another interesting result indicates that copper ions doping into MBG materials significantly improves the osteogenic differentiation and bone-related gene expression [61]. These multifunctional characteristics of Cu-doped MBG scaffolds are suggested to be of great potential to regenerate defected bone [61].

Although MBG are not magnetic, the introduction of **iron (Fe)** in their composition can add magnetic properties into MBG-derived scaffolds skills [74].

Iron plays a fundamental role in several organism processes and it can be found in red blood cells, tissues and plasma [74].

In such way, Fe-doped MBGs constitute an appealing multifunctional platform for several clinical applications, such as targeted drug delivery and thermal treatment of tumoral sites.

For this reason, Wu *et al.* realized MBG scaffolds with 0% Fe, 5% mol. Fe and 10% mol. Fe in MBG composition using polymer sponge method.

Increasing Fe amount in MBG materials, the mesoporous structures of scaffolds appeared more random [43]. The 5Fe-MBG scaffolds maintained hexagonal structure characterized by mesopore size of 5nm, while 10Fe-MBG scaffolds presented a lack of order in mesopores distribution [43].

Textural features of Fe-doped MBG scaffolds are good: surface area is high and mesopore size was not affected by the doping.

A significative difference had been reported in the shapes of MBG-doped scaffolds but this change do not compromise MBG functionality [43].

The realized scaffolds no shown cytotoxic effects and the incorporation of Fe did not impact mechanical strength [43]. They are strong enough to absolve the role of cell carriers

without being comprised during the handle and the implant into defected site meeting the requirements of 3D scaffolds for bone tissue engineering [43].

Therefore, the results of *in vitro* tests into Kokubo's solution shown excellent bioactivity.

Becoming magnetic biomaterials, Fe-doped MBG scaffolds represent potential candidates as multifunctional platform for several clinical applications, such as bone regeneration, drug delivery and hyperthermia treatments [43].

6.2 Lithium-doped MBG scaffolds

As seen in Chapter 1, lithium has been generally considered as a mysterious but attractive element because it can absolve multiple functions.

Li has been widely employed for the past 50 years in the cure of depressive disorders, playing a role of mood stabilizer [75][67].

The mechanism behind lithium as drug used for psychiatric pathologies remains partially unknown.

It is thought that Li effect is caused by the activation of Wtn signaling pathway thanks to lithium compounds interactions which enhances remyelination of peripheral nerves and increases proliferation of neuronal progenitor cells [75].

Therefore, lithium has been recently studied for its effects on bone density reporting that this trace element interferes with calcium transport and improves the proliferation, differentiation and cementogenic gene expression in bone cells [52][67], [76], [77].

For this reason, several studies have been conducted about Li introduction as trace element into bioactive glasses composition aiming at confirming bone regeneration abilities of lithium.

In this perspective, in last few years, researchers have developed Li-doped MBG scaffolds with the aim to realize a multifunctional bioactive device for tissue engineering applications.

The first study on this topic was conducted by Han and coworkers who realized MBG scaffolds doped which were intended as possible solution to be employed for periodontal disease [58].

Architecture of Li-doped MBG scaffolds still maintains mesoporous features, exhibiting highly porous structures composed by well-ordered and uniform mesoporous channel with pore size of 5 nm (**Figure 45**).

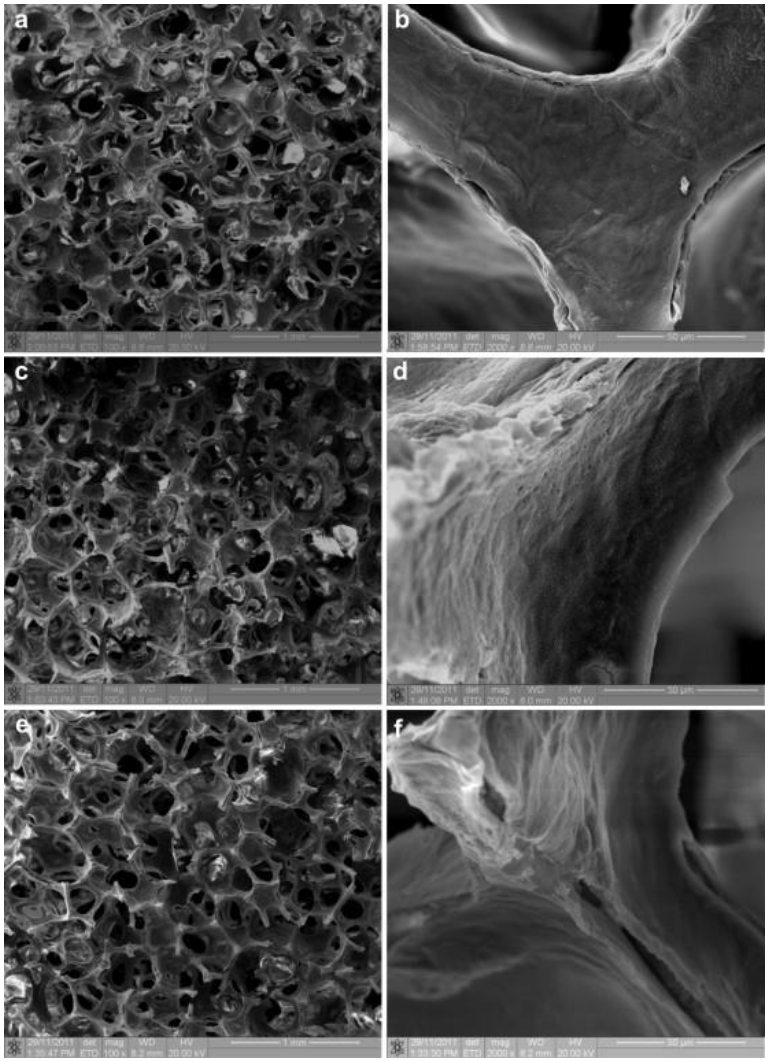

Figure 45. SEM analysis for 0Li-MBG (a,b), 2Li-MBG (c,d) and 5Li-MBG (e,f) scaffolds. (b), (d) and (f) are high magnification images [58].

Further studies have been conducted on Li-MBG scaffolds capability of stimulating human cells attachment to the surface of the pore walls (**Figure 46-47**).

Comparing different Li-doped scaffolds to Li-free MBG scaffolds, both number of cells attached to scaffold walls and cell proliferation rate were greater in doped MBGs with the highest Li content (5% mol.) [58].

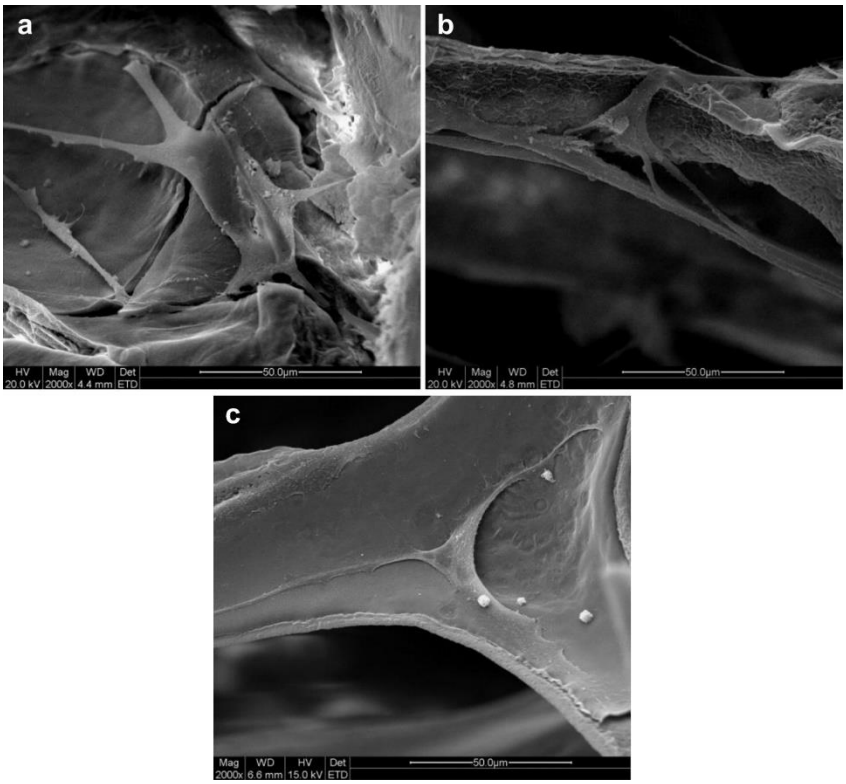

Figure 46. SEM analysis shows cell attachment on 0Li-MBG (a), 2Li-MBG (b) and 5Li-MBG (c) scaffolds after culturing for seven days [58].

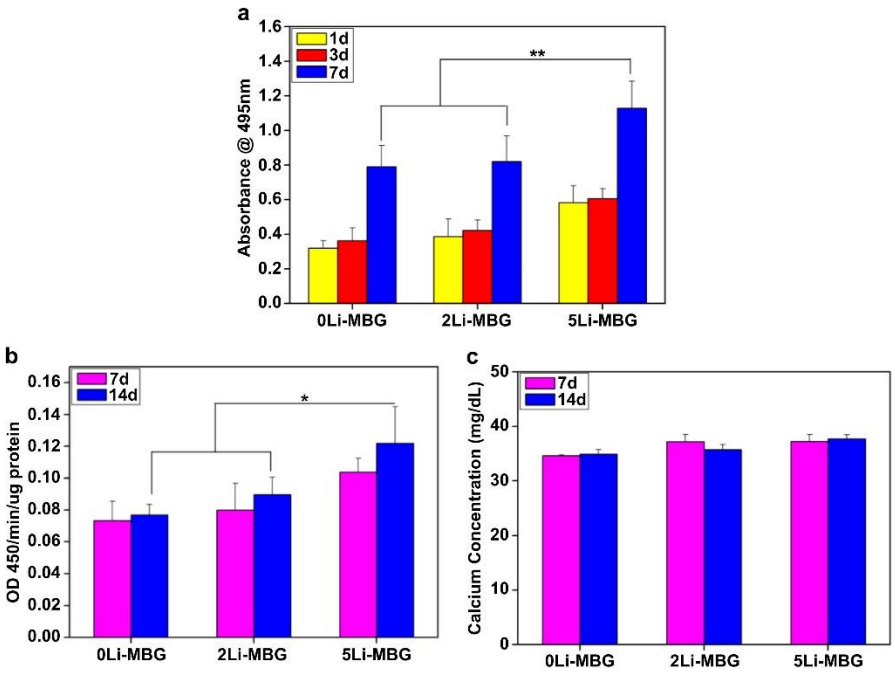

Figure 47. MTT assay is a colorimetric assay for assessing cell metabolic viability. It shows the cell proliferation (a), relative ALP activity (b) and calcium mineralization concentration (c) of cells on three scaffolds (0-Li MBG, 2-Li MBG and 5Li-MBG) [58].

Appropriate lithium content in MBG composition significantly enhances cell proliferation and cementogenic differentiation [52], [58].

Indeed, lithium itself is known to promote all these mechanisms.

For this reason, introduction of lithium ions in biomaterials constitutes an important innovation in the field of multifunctional scaffolds representing a great potential for application of bone and dental tissue engineering.

Bibliography

[1] I *et al.*, "We are IntechOpen , the world ' s leading publisher of Open Access books Built by scientists , for scientists TOP 1 %," *Intech*, vol. i, no. tourism, p. 13, 2012, doi: 10.1016/j.colsurfa.2011.12.014.

[2] M. Vallet-Regí, C. Victoria Ragel, and A. J. Salinas, "Glasses with medical applications," *Eur. J. Inorg. Chem.*, no. 6, pp. 1029–1042, 2003, doi: 10.1002/ejic.200390134.

[3] C. Wu and J. Chang, "Mesoporous bioactive glasses: Structure characteristics, drug/growth factor delivery and bone regeneration application," *Interface Focus*, vol. 2, no. 3, pp. 292–306, 2012, doi: 10.1098/rsfs.2011.0121.

[4] J. R. Jones, "Review of bioactive glass: From Hench to hybrids," *Acta Biomater.*, vol. 9, no. 1, pp. 4457–4486, 2013, doi: 10.1016/j.actbio.2012.08.023.

[5] F. Baino, E. Fiume, M. Miola, and E. Verné, "Bioactive sol-gel glasses: Processing, properties, and applications," *Int. J. Appl. Ceram. Technol.*, vol. 15, no. 4, pp. 841–860, 2018, doi: 10.1111/ijac.12873.

[6] D. Arcos and M. Vallet-Regí, "Sol-gel silica-based biomaterials and bone tissue regeneration," *Acta Biomater.*, vol. 6, no. 8, pp. 2874–2888, 2010, doi: 10.1016/j.actbio.2010.02.012.

[7] J. Zhong and D. C. Greenspan, "Processing and properties of sol-gel bioactive glasses," *J. Biomed. Mater. Res.*, vol. 53, no. 6, pp. 694–701, 2000, doi: 10.1002/1097-4636(2000)53:6<694::AID-JBM12>3.0.CO;2-6.

[8] M. Hamadouche *et al.*, "Long-term in vivo bioactivity and degradability of bulk sol-gel bioactive glasses," *J. Biomed. Mater. Res.*, vol. 54, no. 4, pp. 560–566, 2001, doi: 10.1002/1097-4636(20010315)54:4<560::AID-JBM130>3.0.CO;2-J.

[9] A. López-Noriega, D. Arcos, I. Izquierdo-Barba, Y. Sakamoto, O. Terasaki, and M. Vallet-Regí, "Ordered mesoporous bioactive glasses for bone tissue regeneration," *Chem. Mater.*, vol. 18, no. 13, pp. 3137–3144, 2006, doi: 10.1021/cm060488o.

[10] L. Zhao *et al.*, "Mesoporous bioactive glasses for controlled drug release," *Microporous Mesoporous Mater.*, vol. 109, no. 1–3, pp. 210–215, 2008, doi: 10.1016/j.micromeso.2007.04.041.

[11] M. Gisbert-Garzarán, M. Manzano, and M. Vallet-Regí, "Mesoporous silica nanoparticles for the treatment of complex bone diseases: Bone cancer, bone infection and osteoporosis," *Pharmaceutics*, vol. 12, no. 1, 2020, doi: 10.3390/pharmaceutics12010083.

[12] M. Vallet-Regi, A. Rámila, R. P. Del Real, and J. Pérez-Pariente, "A new property of MCM-41: Drug delivery system," *Chem. Mater.*, vol. 13, no. 2, pp. 308–311, 2001, doi: 10.1021/cm0011559.

[13] X. S. Zhao, G. Q. Lu, and G. J. Millar, "Advances in mesoporous molecular sieve MCM-41," *Ind. Eng. Chem. Res.*, vol. 35, no. 7, pp. 2075–2090, 1996, doi: 10.1021/ie950702a.

[14] M. Vallet-Regí, "Ordered mesoporous materials in the context of drug delivery systems and bone tissue engineering," *Chem. - A Eur. J.*, vol. 12, no. 23, pp. 5934–5943, 2006, doi: 10.1002/chem.200600226.

[15] P. Horcajada, A. Rámila, K. Boulahya, J. González-Calbet, and M. Vallet-Regí, "Bioactivity in ordered mesoporous materials," *Solid State Sci.*, vol. 6, no. 11, pp. 1295–1300, 2004, doi: 10.1016/j.solidstatesciences.2004.07.026.

[16] I. Izquierdo-Barba, L. Ruiz-González, J. C. Doadrio, J. M. González-Calbet, and M. Vallet-Regí, "Tissue regeneration: A new property of mesoporous materials," *Solid State Sci.*, vol. 7, no. 8, pp. 983–989, 2005, doi: 10.1016/j.solidstatesciences.2005.04.003.

[17] X. Yan, C. Yu, X. Zhou, J. Tang, and D. Zhao, "Highly ordered mesoporous bioactive glasses with superior in vitro bone-forming bioactivities," *Angew. Chemie - Int. Ed.*, vol. 43, no. 44, pp. 5980–5984, 2004, doi: 10.1002/anie.200460598.

[18] X. Yan *et al.*, "The in-vitro bioactivity of mesoporous bioactive glasses," *Biomaterials*, vol. 27, no. 18, pp. 3396–3403, 2006, doi: 10.1016/j.biomaterials.2006.01.043.

[19] L. L. Hench, *Bioactive Ceramics: Theory and Clinical Applications*, vol. 7, no. July. Butterworth-Heinemann Ltd, 1994.

[20] F. Baino, "Bioactive glasses – When glass science and technology meet regenerative medicine," *Ceram. Int.*, vol. 44, no. 13, pp. 14953–14966, 2018, doi:

10.1016/j.ceramint.2018.05.180.

[21] M. Vallet-regí, I. Izquierdo-barba, A. Rámila, and J. Pérez-pariente, “Phosphorous-doped MCM-41 as bioactive material,” vol. 7, pp. 233–237, 2005, doi: 10.1016/j.solidstatesciences.2004.10.038.

[22] A. Kumar, S. Murugavel, A. Aditya, and A. R. Boccaccini, “Mesoporous 45S5 bioactive glass: Synthesis,: in vitro dissolution and biomineralization behavior,” *J. Mater. Chem. B*, vol. 5, no. 44, pp. 8786–8798, 2017, doi: 10.1039/c7tb01738c.

[23] S. Kargozar, M. Montazerian, S. Hamzehlou, H. W. Kim, and F. Baino, “Mesoporous bioactive glasses: Promising platforms for antibacterial strategies,” *Acta Biomater.*, vol. 81, pp. 1–19, 2018, doi: 10.1016/j.actbio.2018.09.052.

[24] F. Kleitz, W. Schmidt, and F. Schüth, “Calcination behavior of different surfactant-templated mesostructured silica materials,” *Microporous Mesoporous Mater.*, vol. 65, no. 1, pp. 1–29, 2003, doi: 10.1016/S1387-1811(03)00506-7.

[25] B. Y. Hong *et al.*, “Preparation , Bioactivity , and Drug Release of Hierarchical Nanoporous Bioactive Glass Ultrathin Fibers,” pp. 754–758, 2010, doi: 10.1002/adma.200901656.

[26] C. Wu, Y. Zhang, X. Ke, Y. Xie, H. Zhu, and R. Crawford, “Bioactive mesopore-glass microspheres with controllable protein- delivery properties by biomimetic surface modification,” doi: 10.1002/jbm.a.32873.

[27] D. Arcos *et al.*, “Acta Biomaterialia Mesoporous bioactive glasses : Mechanical reinforcement by means of a biomimetic process,” *Acta Biomater.*, vol. 7, no. 7, pp. 2952–2959, 2011, doi: 10.1016/j.actbio.2011.02.012.

[28] B. Lei, X. Chen, Y. Wang, N. Zhao, C. Du, and L. Zhang, “Acetic acid derived mesoporous bioactive glasses with an enhanced in vitro bioactivity,” *J. Non. Cryst. Solids*, vol. 355, no. 52–54, pp. 2583–2587, 2009, doi: 10.1016/j.jnoncrysol.2009.09.014.

[29] W. Xia and J. Chang, “Well-ordered mesoporous bioactive glasses (MBG): A promising bioactive drug delivery system,” vol. 110, pp. 522–530, 2006, doi: 10.1016/j.jconrel.2005.11.002.

[30] W. Xia, “Preparation , in vitro bioactivity and drug release property of well-ordered

mesoporous 58S bioactive glass," vol. 354, pp. 1338–1341, 2008, doi: 10.1016/j.jnoncrysol.2006.10.084.

[31] H. Yun, S. Kim, and Y. Hyun, "Preparation of bioactive glass ceramic beads with hierarchical pore structure using polymer self-assembly technique," vol. 115, pp. 670–676, 2009, doi: 10.1016/j.matchemphys.2009.02.001.

[32] Y. Wan and D. Zhao, "On the Controllable Soft-Templating Approach to Mesoporous Silicates," vol. 107, no. 7, 2007, doi: 10.1021/cr068020s.

[33] C. J. Brinker, Y. Lu, A. Sellinger, and H. Fan, "ChemInform Abstract: Evaporation-Induced Self-Assembly: Nanostructures Made Easy," *ChemInform*, vol. 30, no. 28, p. no-no, 2010, doi: 10.1002/chin.199928288.

[34] S. S. Soni, G. Brotons, M. Bellour, T. Narayanan, and A. Gibaud, "Quantitative SAXS analysis of the P123/water/ethanol ternary phase diagram," *J. Phys. Chem. B*, vol. 110, no. 31, pp. 15157–15165, 2006, doi: 10.1021/jp062159p.

[35] A. J. Salinas and D. Arcos, "Tailoring the Structure of Bioactive Glasses : From the Nanoscale to Macroporous Scaffolds," vol. 205, pp. 195–205, 2016, doi: 10.1111/ijag.12205.

[36] Y. Ma, C. Zhang, C. Hou, H. Zhang, and H. Zhang, "Cetyl trimethyl ammonium bromide (CTAB) micellar templates directed synthesis of water-dispersible polyaniline rhombic plates with excellent processability and fl ow-induced color variation," *Polymer (Guildf).*, vol. 117, pp. 30–36, 2017, doi: 10.1016/j.polymer.2017.04.010.

[37] R. Schmelzeisen and M. Rolf, "Rapid prototyping of scaffolds derived from thermoreversible hydrogels and tailored for applications in tissue engineering," vol. 23, pp. 4437–4447, 2002.

[38] "Biological Structures," p. 2005, 2005.

[39] R. E. M. Ii *et al.*, "Solvent-Washable Polymer Templated Synthesis of Mesoporous Materials and Solic-Acid Nanocatalysts in One-Pot Solvent-washable polymer templated synthesis of mesoporous materials and solid-acid nanocatalysts in one-pot w," vol. 6203, 2009, doi: 10.1039/b913035g.

[40] P. List, "Pluronic ® F-127," 2001.

[41] D. Arcos, A. López-Noriega, E. Ruiz-Hernández, O. Terasaki, and M. Vallet-Regí, "Ordered mesoporous microspheres for bone grafting and drug delivery," *Chem. Mater.*, vol. 21, no. 6, pp. 1000–1009, 2009, doi: 10.1021/cm801649z.

[42] Y. F. Zhao, S. C. J. Loo, Y. Z. Chen, F. Y. C. Boey, and J. Ma, "In situ SAXRD study of sol – gel induced well-ordered mesoporous bioglasses for drug delivery," doi: 10.1002/jbm.a.31545.

[43] C. Wu *et al.*, "Acta Biomaterialia Multifunctional magnetic mesoporous bioactive glass scaffolds with a hierarchical pore structure," *Acta Biomater.*, vol. 7, no. 10, pp. 3563–3572, 2011, doi: 10.1016/j.actbio.2011.06.028.

[44] X. Wu, J. Wei, X. Lu, Y. Lv, F. Chen, and Y. Zhang, "Chemical characteristics and hemostatic performances of ordered mesoporous calcium-doped silica xerogels," 2010, doi: 10.1088/1748-6041/5/3/035006.

[45] A. García, I. Izquierdo-barba, C. López, D. Laorden, and M. Vallet-regí, "Acta Biomaterialia Preparation of 3-D scaffolds in the SiO 2 – P 2 O 5 system with tailored hierarchical meso-macroporosity," vol. 7, pp. 1265–1273, 2011, doi: 10.1016/j.actbio.2010.10.006.

[46] Y. Zhu, C. Wu, Y. Ramaswamy, and E. Kockrick, "Preparation , characterization and in vitro bioactivity of mesoporous bioactive glasses (MBGs) scaffolds for bone tissue engineering," vol. 112, pp. 494–503, 2008, doi: 10.1016/j.micromeso.2007.10.029.

[47] X. Li, X. Wang, Z. Hua, and J. Shi, "One-pot synthesis of magnetic and mesoporous bioactive glass composites and their sustained drug release property," vol. 56, pp. 3260–3265, 2008, doi: 10.1016/j.actamat.2008.03.013.

[48] A. J. Salinas, S. Shruti, G. Malavasi, L. Menabue, and M. Vallet-regí, "Acta Biomaterialia Substitutions of cerium , gallium and zinc in ordered mesoporous bioactive glasses," *Acta Biomater.*, vol. 7, no. 9, pp. 3452–3458, 2011, doi: 10.1016/j.actbio.2011.05.033.

[49] Y. Zhu, Y. Zhang, C. Wu, Y. Fang, J. Yang, and S. Wang, "Microporous and Mesoporous Materials The effect of zirconium incorporation on the physiochemical and biological properties of mesoporous bioactive glasses scaffolds," *Microporous Mesoporous Mater.*, vol. 143, no. 2–3, pp. 311–319, 2011, doi:

10.1016/j.micromeso.2011.03.007.

[50] C. Wu, R. Miron, A. Sculean, S. Kaskel, T. Doert, and R. Schulze, “Biomaterials Proliferation , differentiation and gene expression of osteoblasts in boron-containing associated with dexamethasone deliver from mesoporous bioactive glass scaffolds,” *Biomaterials*, vol. 32, no. 29, pp. 7068–7078, 2011, doi: 10.1016/j.biomaterials.2011.06.009.

[51] P. N. Gunawidjaja *et al.*, “Biomimetic Apatite Mineralization Mechanisms of Mesoporous Bioactive Glasses as Probed,” pp. 19345–19356, 2010, doi: 10.1021/jp105408c.

[52] C. Wu and J. Chang, “Multifunctional mesoporous bioactive glasses for effective delivery of therapeutic ions and drug/growth factors,” *J. Control. Release*, vol. 193, pp. 282–295, 2014, doi: 10.1016/j.jconrel.2014.04.026.

[53] A. Manuscript, D. R. Kinetics, D. Polymeric, and D. Systems, “NIH Public Access,” vol. 7, no. 4, pp. 429–444, 2011, doi: 10.1517/17425241003602259.Drug.

[54] Y. Zhu and S. Kaskel, “Microporous and Mesoporous Materials Comparison of the in vitro bioactivity and drug release property of mesoporous bioactive glasses (MBGs) and bioactive glasses (BGs) scaffolds,” *Microporous Mesoporous Mater.*, vol. 118, no. 1–3, pp. 176–182, 2009, doi: 10.1016/j.micromeso.2008.08.046.

[55] C. Wu, Y. Zhang, Y. Zhu, T. Friis, and Y. Xiao, “Biomaterials Structure – property relationships of silk-modified mesoporous bioglass scaffolds,” *Biomaterials*, vol. 31, no. 13, pp. 3429–3438, 2010, doi: 10.1016/j.biomaterials.2010.01.061.

[56] A. Hoppe, N. S. Güldal, and A. R. Boccaccini, “Biomaterials A review of the biological response to ionic dissolution products from bioactive glasses and glass-ceramics,” *Biomaterials*, vol. 32, no. 11, pp. 2757–2774, 2011, doi: 10.1016/j.biomaterials.2011.01.004.

[57] H. Lin, J. Zhang, F. Qu, J. Jiang, and P. Jiang, “In Vitro Hydroxyapatite-Forming Ability and Antimicrobial Properties of Mesoporous Bioactive Glasses Doped with Ti / Ag,” vol. 2013, 2013.

[58] P. Han, C. Wu, J. Chang, and Y. Xiao, “The cementogenic differentiation of periodontal ligament cells via the activation of Wnt/β-catenin signalling pathway by

Li + ions released from bioactive scaffolds," *Biomaterials*, vol. 33, no. 27, pp. 6370–6379, 2012, doi: 10.1016/j.biomaterials.2012.05.061.

[59] Y. C. Fredholm, N. Karpukhina, R. V Law, and R. G. Hill, "Strontium containing bioactive glasses : Glass structure and physical properties," *J. Non. Cryst. Solids*, vol. 356, no. 44–49, pp. 2546–2551, 2010, doi: 10.1016/j.jnoncrysol.2010.06.078.

[60] X. Wang, X. Li, A. Ito, and Y. Sogo, "Acta Biomaterialia Synthesis and characterization of hierarchically macroporous and mesoporous CaO – MO – SiO 2 – P 2 O 5 (M = Mg , Zn , Sr) bioactive glass scaffolds," vol. 7, pp. 3638–3644, 2011, doi: 10.1016/j.actbio.2011.06.029.

[61] C. Wu *et al.*, "Biomaterials Copper-containing mesoporous bioactive glass scaffolds with multifunctional properties of angiogenesis capacity , osteostimulation and antibacterial activity," *Biomaterials*, vol. 34, no. 2, pp. 422–433, 2013, doi: 10.1016/j.biomaterials.2012.09.066.

[62] M. B. Glasses, M. Fundamentals, F. Baino, and E. Fiume, "materials 3D Printing of Hierarchical Sca ff olds Based on," 2020.

[63] X. Li, X. Wang, H. Chen, P. Jiang, X. Dong, and J. Shi, "Hierarchically Porous Bioactive Glass Scaffolds Synthesized with a PUF and P123 Cotemplated Approach," no. 5, pp. 4322–4326, 2010, doi: 10.1021/cm0708564.

[64] F. Baino *et al.*, "Processing methods for making porous bioactive glass-based scaffolds—A state-of-the-art review," *Int. J. Appl. Ceram. Technol.*, vol. 16, no. 5, pp. 1762–1796, 2019, doi: 10.1111/ijac.13195.

[65] C. Wu *et al.*, "Biomaterials Hypoxia-mimicking mesoporous bioactive glass scaffolds with controllable cobalt ion release for bone tissue engineering," *Biomaterials*, vol. 33, no. 7, pp. 2076–2085, 2012, doi: 10.1016/j.biomaterials.2011.11.042.

[66] F. Baino *et al.*, "Fe-doped sol-gel glasses and glass-ceramics for magnetic hyperthermia," *Materials (Basel).*, vol. 11, no. 1, 2018, doi: 10.3390/ma11010173.

[67] A. L. B. Maçon *et al.*, "Lithium-silicate sol–gel bioactive glass and the effect of lithium precursor on structure–property relationships," *J. Sol-Gel Sci. Technol.*, vol. 81, no. 1, pp. 84–94, 2017, doi: 10.1007/s10971-016-4097-x.

[68] J. S. Fernandes, P. Gentile, R. A. Pires, R. L. Reis, and P. V Hatton, “Acta Biomaterialia Multifunctional bioactive glass and glass-ceramic biomaterials with antibacterial properties for repair and regeneration of bone tissue,” vol. 59, pp. 2–11, 2017, doi: 10.1016/j.actbio.2017.06.046.

[69] A. Vulpoi, L. Baia, S. Simon, and V. Simon, “Silver effect on the structure of SiO 2 -CaO-P 2 O 5 ternary system,” *Mater. Sci. Eng. C*, vol. 32, no. 2, pp. 178–183, 2012, doi: 10.1016/j.msec.2011.10.015.

[70] H. Zhu *et al.*, “Preparation and antibacterial property of silver-containing mesoporous 58S bioactive glass,” *Mater. Sci. Eng. C*, vol. 42, pp. 22–30, 2014, doi: 10.1016/j.msec.2014.05.004.

[71] H. Zreiqat, P. Evans, and C. R. Howlett, “Effect of surface chemical modification of bioceramic on phenotype of human bone-derived cells,” 1998.

[72] P. Balasubramanian, L. A. Strobel, U. Kneser, and A. R. Boccaccini, “Zinc-containing bioactive glasses for bone regeneration, dental and orthopedic applications,” *Biomed. Glas.*, vol. 1, no. 1, pp. 51–69, 2015, doi: 10.1515/bglass-2015-0006.

[73] G. F. Hu, “Copper stimulates proliferation of human endothelial cells under culture,” *J. Cell. Biochem.*, vol. 69, no. 3, pp. 326–335, 1998, doi: 10.1002/(SICI)1097-4644(19980601)69:3<326::AID-JCB10>3.0.CO;2-A.

[74] K. Yamasaki and H. Hagiwara, “Excess iron inhibits osteoblast metabolism,” *Toxicol. Lett.*, vol. 191, no. 2–3, pp. 211–215, 2009, doi: 10.1016/j.toxlet.2009.08.023.

[75] V. Miguez-Pacheco *et al.*, “Development and characterization of lithium-releasing silicate bioactive glasses and their scaffolds for bone repair,” *J. Non. Cryst. Solids*, vol. 432, pp. 65–72, 2016, doi: 10.1016/j.jnoncrysol.2015.03.027.

[76] R. J. Kavitha, B. Subha, S. Shanmugam, and K. Ravichandran, “Synthesis and Invitro Characterisation of Lithium Doped Bioactive Glass through Quick Alkali Sol - Gel Method,” *IJIRSE) Int. J. Innov. Res. Sci. Eng. ISSN (Online)*, pp. 2347–3207.

[77] P. K. Khan *et al.*, “Influence of single and binary doping of strontium and lithium on

in vivo biological properties of bioactive glass scaffolds," *Sci. Rep.*, vol. 6, no. February, pp. 1–18, 2016, doi: 10.1038/srep32964.

Chapter 3 – Materials and Methods

Introduction

This experimental works draws inspiration from the desire to design MBG materials derived from six-oxides system with the aim to develop 3D-scaffolds exhibiting multifunctional properties.

In last decade, many research teams have already developed MBG scaffolds derived from complex systems, underlining the effect of doping elements on both mechanical and biological properties [1]. However, to date, no publications about systems based on six different oxides have been reported.

The present experimental activity deals with the design of mesoporous bioactive glasses based on a complex six-oxide composition in the system SiO_2-P_2O_5-CaO-MgO-Na_2O-K_2O, named as 47.5B, designed at the Department of Applied Science and Technology of Politecnico di Torino. Previous studies showed that both melt-derived and sol-gel bioactive glasses based on 47.5B system exhibited excellent reactivity in Simulated Body Fluid and an exceptional apatite-forming ability [2].

The introduction of several former and modifier oxides further complicates synthesis processes pointing out new problems in 47.5B MBG realization, such as solubility limits or complications due to ion recombination mechanisms.

The experimental activity carried out at the Department of Applied Science and Technology at Politecnico di Torino was organized into two different phases.

The preliminary part regards the optimization of MBG composition of 47.5B system through analytical and chemical calculations. In this phase, the role of each reagent in the wet synthesis was deeply investigated.

Secondary, different syntheses were conducted in laboratories turning several parameters with the aim to highlight the impact of such factors in MBG products. The obtained samples have been analysed and characterized through different methods, such as Differential Thermal Analysis (DTA), X-Ray Diffraction (X-RD), Scanning Electron Microscopy (SEM) and BET analysis.

The aim of this chapter is to describe the materials and methods used to carry out the syntheses and the characterization techniques employed to define physiochemical and biological properties of the obtained materials.

1 Glass Synthesis

1.1 Synthesis I

First attempt to develop MBG biomaterial based on 47.5B composition was conducted based on a study with a similar composition and excellent mesoporous structure.

Shoaib *et al.* synthesized a five-oxide mesoporous bioactive glass by sol-gel procedure, according to the composition reported in **Table 14** [3].

Mathematical calculations to adapt the synthesis to 47.5B composition were previously done.

Table 14. Comparison between the composition of MBG produced by Shoaib *et al.* [3] and 47.5B bioactive glass realized by Vernè *et al.* [3]

Glass Composition	**SiO_2 [mol.%]**	**CaO [mol.%]**	**Na_2O [mol.%]**	**K_2O [mol.%]**	**P_2O_5 [mol.%]**	**MgO [mol.%]**
Shoaib MBG [3]	51	20	20	5	4	-
47.5B	47.5	20	10	10	2.5	10

The first synthesis was conducted at room temperature under acidic conditions in a mixed solution, with water/ethanol molar ratio 32: 1 (mol.) and water/TEOS ratio 162: 1 (mol.).

1. 20 ml of H_2O and 2 ml of EtOH were mixed.
2. 2 ml of HNO_3 (0.1 M) were added to the mixture under continuous stirring (200 rpm).
3. 0.32 g of Pluronic® P123 was dissolved in the solution.
4. TEOS was added to it and stirred for 1 hour at room temperature.

Then other precursors were added to this mixture with time interval of 30 minutes along with continuous stirring (200 rpm), following the order reported in **Table 15**.

Table 15. Reagents required in synthesis I

Reagent	**Molecular Weight [g/mol]**	**Density [g/ ml]**	**Amount**
Water	18.015	0.997	20 ml
Ethanol	46.07	0.789	2 ml
HNO_3 (0.1 M)	63.01	1.51	2 ml
TEOS	208.33	0.933	1.5094 ml

TEP	182.15	1.072	0.1212 ml
Calcium Nitrate Tetrahydrate	236.15	-	0.6761 g
Magnesium Nitrate Hexahydrate	256.41	-	0.3672 g
Sodium Nitrate	84.99	-	0.2434 g
Potassium Nitrate	101.10	-	0.2895 g

After the complete dissolution of all the precursors, a clear and transparent sol was obtained.

Afterwards, 25% ammonia solution was added dropwise as gelation catalyst, as reported by Shoaib et al[3]

However, differently from what reported in the literature, no gel formation occurred but the formation of a white precipitate was observed, as shown in **Figure 48.**

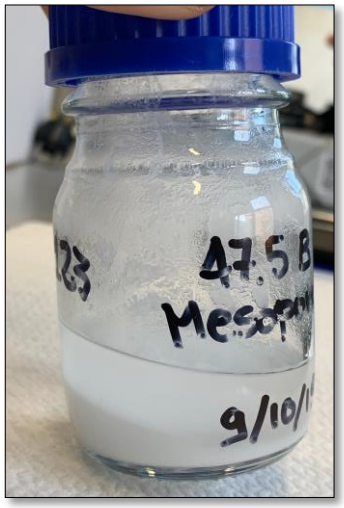

Figure 48. Phase separation observed in synthesis I.

As no gelification occurred, the synthesis was stopped in an earlier stage.

1.2 Synthesis II

The phase separation (reported in synthesis I) was supposed to be induced by ammonia addition as "supposed" gelation agent.

In order to verify ammonia role, II synthesis was conducted upon same conditions using the same reagents (**Table 15**) but without ammonia introduction and the sol was left to gel without the action of any catalyst.

After mixing all reagents, differently to **Figure 48**, solution appeared perfectly clear.

The solution was cast in a mould and left to dry at room temperature to induce gelation process.

Although this attempt did not report phase separation, gelation did not occur over an observation period of 4 weeks.

1.3 Synthesis III

To investigate how H_2O: TEOS molar ratio impacts on sol-gel route, another synthesis was conducted realizing traditional 47.5B sol-gel derived aiming at deeply studying gelation process without introduction of structure directing agent as Pluronic® P123.

This synthesis was realized at room temperature under acidic conditions, in aqueous environment, following indication of a previous synthesis on such a multicomponent system conducted at Politecnico di Torino by Fiume *et al.* [2], but changing H_2O: TEOS molar ratio to 40:1 (mol.).

1. 30 ml of H_2O were used as unique solvent.
2. 5 ml of HNO_3 (2 M) were added to the mixture under continuous stirring (200 rpm).
3. TEOS was added to the solution and stirred for 1 hour at room temperature.
4. Then other precursors (**Table 16**) were added to this mixture with time interval of 30 minutes along with continuous stirring (200 rpm).

Table 16. Reagents required in synthesis III.

Reagent	**Molecular Weight [g/mol]**	**Density [g/ ml]**	**Amount**
Water	18.015	0.997	30 ml
HNO_3 (2 M)	63.01	1.51	5 ml
TEOS	208.33	0.933	9.294 ml
TEP	182.15	1.072	0.744 ml
Calcium Nitrate Tetrahydrate	236.15	-	4.136 g
Magnesium Nitrate Hexahydrate	256.41	-	1.30 g
Sodium Nitrate	84.99	-	1.489 g
Potassium Nitrate	101.10	-	1.771 g

Once all reagents were mixed, solution appeared clear as seen in **Figure 49**.

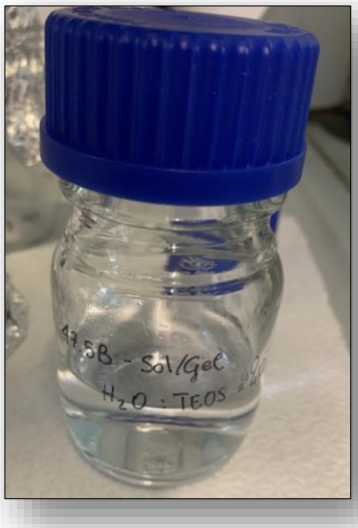

Figure 49. 47.5B solution after mixing in synthesis III.

The following traditional steps of sol-gel route was conducted in synthesis III.

The sol was versed in a mould and left drying at room temperature.

Gelation occurred after ten days and the resulted gel appeared clear and homogenous.

The gel was aged heating at 60 °C for three days and then dried at 120 °C for two days.

1.4 Synthesis IV

In order to solve the problems derived from too long gelation step and phase separation occurred during previous syntheses, another synthesis was developed based on literature research.

According to Vallet Regì's studies [4], the fourth synthesis was at room temperature in alcoholic environment with the introduction of Pluronic® P123 as structure directing agent and ethanol-TEOS ratio 40:1 (mol.) and EtOH: P123= 30g: 2g (wt.).

1. 76.066 ml of EtOH were used as unique solvent.
2. 1 ml of HCl (0.5 M) was added to the mixture under continuous stirring (200 rpm).
3. Pluronic® P123 was stirred for 40 minutes and it completely dissolved in ethanol.
4. TEOS and other precursors (**Table 17**) were added to this mixture with time interval of 1 hour along with continuous stirring (200 rpm).

Table 17. Reagents required in synthesis IV.

Reagent	**Molecular Weight [g/mol]**	**Density [g/ ml]**	**Amount**
Ethanol	46.07	0.789	76.066 ml
HCl (0.5 M)	36.46	1.49	1 ml
Pluronic P123	5800	1.018	4 g
TEOS	208.33	0.933	7.149 ml
TEP	182.15	1.072	0.581 ml
Calcium Nitrate Tetrahydrate	236.15	-	3.235 g
Magnesium Nitrate Hexahydrate	256.41	-	1.014 g
Sodium Nitrate	84.99	-	1.163 g
Potassium Nitrate	101.10	-	1.383 g

After the mixing, the solution appeared clear until the addition of the last reagent.

Potassium nitrate never dissolved, and solution presented the formation of a precipitate (**Figure 50**).

Precipitation was dried and prepared to qualitative analysis with the aim to understand if its formation was due to solubility limits or ion recombination problem.

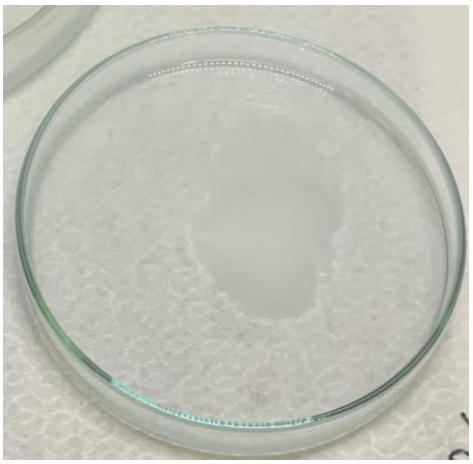

Figure 50. Precipitate formation in synthesis IV following the addition of Potassium nitrate.

Compositional analysis of the precipitate was conducted by Energy- Dispersive Spectroscopy (EDS) Analysis and their results will be reported in the Chapter 4.

1.5 Synthesis V

The fifth synthesis was designed with the aim to avoid precipitation within the sol. Bibliographic researches on reagent solubility and ternary phase diagram of P123-water-ethanol were previously conducted and they will be exhaustively explained in *Chapter 4*.

On this basis, the fifth synthesis was realized at room temperature in a mixed alcoholic and aqueous environment using ethanol: water = 35: 5 (mol.), while solvents/TEOS ratio was still 40: 1 (mol).

1. 35 mol of ethanol and 5 mol of water were used as co-solvents for dissolving reagents.
2. Nitric acid was added to the mixture under continuous stirring (200 rpm) to catalyse reagent hydrolysis and poly-condensation.
3. Pluronic® P123 was stirred for 40 minutes until complete dissolution.
4. TEOS and other precursors (**Table 18**) were added to this mixture with time interval of 1 hour along with continuous stirring (200 rpm).

Table 18. Reagents required in synthesis V.

Reagent	**Molecular Weight [g/mol]**	**Density [g/ ml]**	**Amount**
Ethanol	18.015	0.997	76.066 ml
Water	46.07	0.789	3.36 ml
HNO_3 (2M)	63.01	1.51	0.25 ml
Pluronic P123	5800	1.018	4 g
TEOS	208.33	0.933	8.24 ml
TEP	182.15	1.072	0.666 ml
Calcium Nitrate Tetrahydrate	236.15	-	3.70 g
Magnesium Nitrate Hexahydrate	256.41	-	1.157 g
Sodium Nitrate	84.99	-	1.33 g
Potassium Nitrate	101.10	-	1.583 g

During the synthesis, it was observed that the addition of the first four reagents (TEOS, TEP, calcium nitrate tetrahydrate and magnesium nitrate tetrahydrate) still maintained the solution clear, but when sodium nitrate was added to the solution its appearance changed.

The powder of sodium nitrate never dissolved into the solution and the synthesis was interrupted because the solvents were not able to dissolve all the reagents and form the final ‘sol’.

1.6 Synthesis VI

The major difference introduced in VI synthesis is the ethanol-water molar ratio which turned into 1: 1 (mol.) while P123: (water + P123) = 50: 50 (w.t.%) aiming at solving the impossibility to dissolve the reagents into mixed solution.

Every reagent solubility was calculated before beginning the synthesis, particularly focusing on sodium nitrate and potassium nitrate which had reported solubility problems in previous synthesis (**Table 19**).

Table 19. Analytical calculations on sodium nitrate and potassium nitrate solubility in mixed synthesis.

	Solubility Limit	**Used Amount**
Sodium nitrate	1.75 g	0.497 g
Potassium nitrate	1.55 g	0.59 g

1. Equal mol of ethanol and water were used as solvents for dissolving reagents.
2. Nitric acid was added to the mixture under continuous stirring (200 rpm) to catalyse reagent hydrolysis and poly-condensation.
3. Pluronic® P123 was stirred for 40 minutes and it completely dissolved in ethanol.
4. TEOS and other precursors (**Table 20**) were added to this mixture with time interval of 1 hour along continuous stirring (200 rpm).

Table 20. Reagents required in synthesis VI.

Reagent	**Molecular Weight [g/mol]**	**Density [g/ ml]**	**Amount**
Ethanol	18.015	0.997	16.2 ml
Water	46.07	0.789	5 ml
HNO_3 (2M)	63.01	1.51	0.053 ml
Pluronic P123	5800	1.018	5 g
TEOS	208.33	0.933	3.075 ml
TEP	182.15	1.072	0.246 ml
Calcium Nitrate Tetrahydrate	236.15	-	1.382 g
Magnesium Nitrate Hexahydrate	256.41	-	0.433 g
Sodium Nitrate	84.99	-	0.497 g
Potassium Nitrate	101.10	-	0.59 g

The synthesis was conducted in a controlled thermal bath at a temperature of 35 °C.

The pH and temperature of the solution were measured before adding each reagent to the solution (**Table 21**).

Table 21. Check of pH and temperature during the addition of each reagent VI synthesis.

Reagent	**pH**	**°C**
P123	2.46	32.2
TEOS	2.31	32.5
TEP	2.32	32.3
Calcium Nitrate	2.30	32.4
Magnesium Nitrate	2.27	32.4
Sodium Nitrate	2.35	32.6
Potassium Nitrate	-	-

Despite solubility prescriptions, sodium nitrate did not dissolve in the solution and the synthesis was interrupted at this stage.

1.7 Synthesis VII

This synthesis was conducted using the same solvent ratios and reagents (**Table 21**) of synthesis VI but changing system conditions. In order to solve problems emerged from previous synthesis, VII synthesis was conducted using two different batches in parallel **(Figure 51)**. Solvents (water and ethanol) were used separately to dissolve different reagents, thus aiming at eliminating precipitation problems.

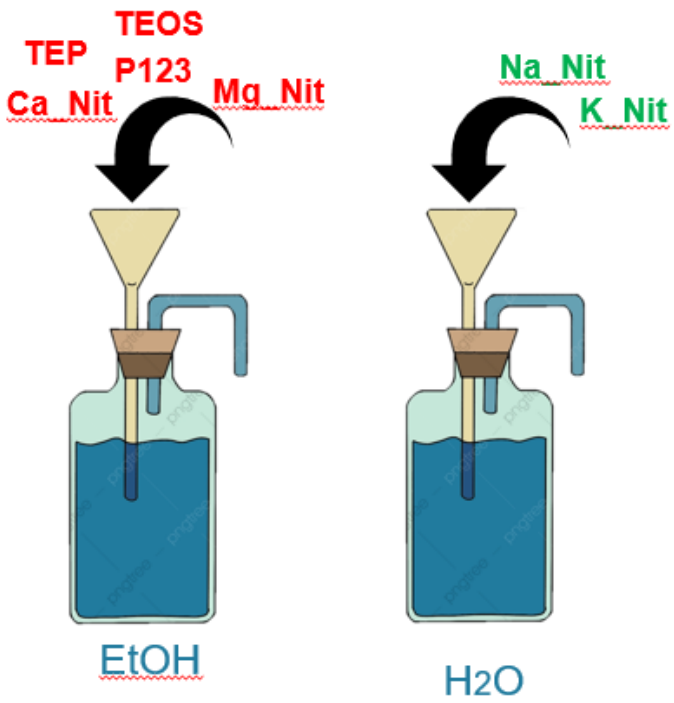

Figure 51. Schematic representation of two parallel systems with water and ethanol used in synthesis VII.

Both systems were in a controlled water bath at 38 °C.

In this synthesis two different mixing steps were simultaneously conducted:

1. In a batch containing 16.2 ml of ethanol and 0.053 ml of nitric acid:

- Pluronic® P123 was added and stirred for 30 minutes at 200 rpm
- TEOS was added and stirred (200 rpm) for 1 hour
- TEP was added and stirred (200 rpm) for 1 hour
- Calcium nitrate tetrahydrate was added and stirred (200 rpm) for 1 hour
- Magnesium nitrate hexahydrate was added and stirred (200 rpm) for 1 hour.

1. At the same time, in a batch containing 5 ml of water:

- Sodium nitrate was added and stirred (200 rpm) for 1 hour
- Potassium nitrate was added and stirred (200 rpm) for 1 hour.

2. After stirring in separate systems, solutions were mixed adding dropwise water solution into the ethanol one (**Figure 52**).

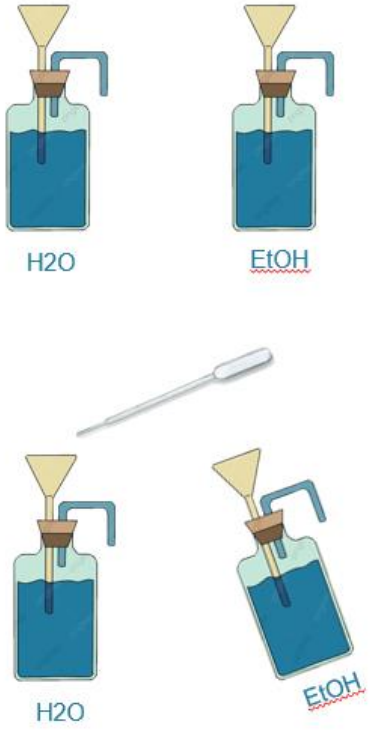

Figure 52. Schematic representation of second step in VII synthesis.

While water solution was added drop by drop, ethanol solution changed its aspect: some nanoparticles began to appear in the mixed solution.

The new solution was milky differently from the two starting solutions which were perfectly clear.

3. Anywhere, the obtained sol was poured in a Petri dish and left at room temperature to induce solvent evaporation.
4. Gelation occurred after three days (**Figure 53**).

Figure 53. Gel after three days at room temperature.

5. Gel was dried in a furnace at temperature of 120 °C for 24 hours (**Figure 54**).

Figure 54. Gel after drying step at T= 120 °C and t= 24h.

6. Dry gel was calcinated at temperature of 625 °C for three hours in an electrical furnace (Nabertherm 1300 Manfredi) (**Table 22- Figure 55**) (**Figure 56**).

Table 22. Process parameters for air calcination.

Furnace Model	**Treatment conditions**	**Heating rate ↑ (°C/ min)**	**T1 (°C)**	**Heating rate ↓ (°C/min)**	**T2 (°C)**
Nabertherm 1300	Air	1	625	10	20

Figure 55. Nabertherm 1300 electrical furnace.

Figure 56. Calcinated gel at T= 625 °C and t= 3h.

The results of the seventh synthesis were analysed with Scanning Electron Microscopy (SEM), Differential Thermal Analysis (DTA) and Brunauer- Emmet- Teller (BET) Analysis, they will be showed in the next paragraph.

1.8 Synthesis VIII

VIII synthesis involved imposing a water/ethanol volume ratio of 10: 1 and changing sodium nitrate with sodium carbonate because its solubility limit is higher than nitrate's one.

Every reagent solubility was calculated before beginning the synthesis.

The synthesis was conducted at room temperature.

1. Water and ethanol were used as solvents for dissolving reagents.
2. Nitric acid was added to the mixture under continuous stirring to catalyse reagent hydrolysis and poly-condensation.
3. Pluronic® P123 was stirred for 40 minutes and it completely dissolved in ethanol.
4. TEOS and other precursors (**Table 23**) were added to this mixture with time interval of 30 minutes along continuous stirring.

Table 23. Reagents required in synthesis VIII.

Reagent	**Molecular Weight [g/mol]**	**Density [g/ ml]**	**Amount**
Ethanol	18.015	0.997	11.66 ml
Water	46.07	0.789	116.66 ml
HNO_3 (0.5 M)	63.01	1.51	3.33 ml
Pluronic P123	5800	1.018	4 g
TEOS	208.33	0.933	6.287 ml
TEP	182.15	1.072	0.507 ml
Calcium Nitrate Tetrahydrate	236.15	-	2.817 g
Magnesium Nitrate Hexahydrate	256.41	-	0.885 g
Sodium Carbonate	84.99	-	3.007 g
Potassium Nitrate	101.10	-	1.206 g

Although sodium nitrate was substituted with sodium carbonate, once sodium carbonate was added to the solution, it changed immediately colour and began milky (**Figure 57**).

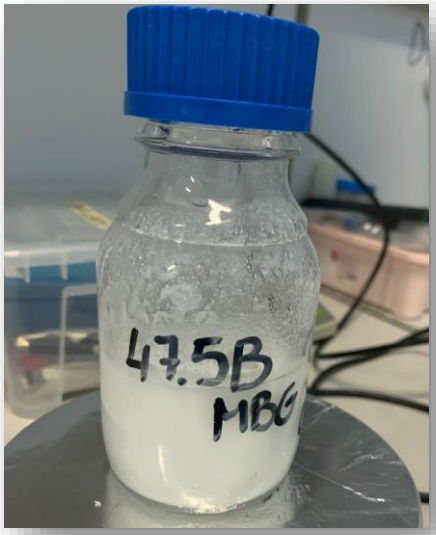

Figure 57. Solution after the addition of all reagents synthesis VIII.

However, even if colour of the solution changed, the solution appeared homogenous and the synthesis was carried on.

To improve gelation, ammonia was added dropwise until reaching the amount of 15 ml.

The complete gelation occurred after three days (**Figure 58**), after that the gel was dried in a furnace at temperature of 200 °C for four hours.

Figure 58. Gel after 3 days in synthesis VIII.

The dry gel was calcinated at temperature of 700 °C for five hours in a tubular furnace used for the calcination in air (Carbolilte) (**Table 24- Figure 59**)(**Figure 60**).

Table 24. Process parameters for air calcination.

Furnace Model	Treatment conditions	Heating rate ↑ (°C/ min)	T1 (°C)	Heating rate ↓ (°C/min)	T2 (°C)
Lenton LTF 16/50/450 Carbolite	Air	5	700	15	20

Figure 59. Lenton LTF 16/50/450 Carbolite tubular furnace.

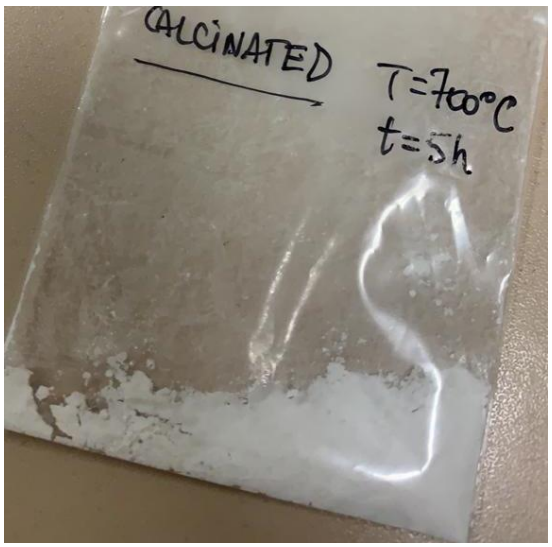

Figure 60. Glass powder obtained in synthesis VIII after 3 days of gelation, gel drying at T= 200 °C and t= 4h, calcination at T= 700 °C and t= 5h.

The resulted glass powder was milled and prepared to be analysed through X-Ray Diffraction (XRD) Analysis and Brunauer- Emmet- Teller (BET) Analysis, as will be reported in the next paragraph.

2 Characterizations

Although some of previous presented syntheses were interrupted and did not achieve the final step, results coming from synthesis IV, synthesis VII and synthesis VIII were deeply analysed by characterizing the products obtained from these processes.

2.1 Differential Thermal Analysis (DTA)

As its name suggests, Differential Thermal Analysis (DTA) is a thermo-analytic analysis that measures endothermic and exothermic transitions of a material as function of temperature, providing information about material transformations, such as glass transition, crystallization and melting temperatures.

In DTA, the temperature of the test material is measured relative to that of an adjacent inert material, such as alumina (Al_2O_3).

The material under study and an inert reference are made to undergo identical thermal cycles, at example the same heating programme, while any temperature difference between sample and reference are recorded.

This differential temperature is then plotted against time, or against temperature (DTA curve or thermogram), permitting the calculation of the heat flow difference. Therefore, change in the sample which lead the absorption or evolution of heat can be detected relative to the inert reference.

Conventionally, peaks in negative verse of y-axis are indicative for endothermic reactions, while positive spikes are associated to exothermic ones.

Weight of the sample and heating rate also influence shape of DTA peaks, for example higher sample weights correspond to sharper peaks.

A generic DTA device is composed of:

1. Sample holder, which includes a ceramic or metallic block to provide a homogenous heat distribution in the chamber, sample holders and two thermocouples.
2. Heating chamber, in which thermal cycle occurs following temperature programme indications.
3. Computer system able to precisely programme and record thermal cycles guaranteeing constant heating rates [5].

In the production of BG or MBG products by sol-gel route, DTA analysis represents a fundamental requirement for configuring appropriate calcination parameters.

DTA analyses have been performed using DTA device (DTA 404 PC- NETZSCH) (**Figure 61**).

Figure 61. DTA device (DTA 404 PC- NETZSCH).

Before each analysis, a baseline was performed analysing 50 mg of Al_2O_3 at heating rate of 10 °C/min with the aim of reducing the noise derived from environmental interferences. In

post processing operations, the baseline has been subtracted from the obtained curve to extract the denoised data of the sample.

The analysis was conducted in air using 50 mg of Al_2O_3 and 50 mg of dried and milled powders obtained in synthesis VII, at heating rate of 10 °C/min.

2.2 Scanning Electron Microscopy (SEM) and Energy Dispersive Spectroscopy (EDS)

Scanning Electron Microscopy (SEM) Analysis is a powerful investigative tool which uses a focused beam of electrons to produce complex, high magnification images of a sample's surface topography.

In addition to surface evaluation, SEM analysis is utilized for particle characterization. The high magnification, high-resolution imaging of SEM analysis supports also of the number, size, and morphology of small particles.

Therefore, signals reported in this analysis provide information about texture, crystalline structure and chemical composition. Such signals derive from the interaction between samples and electron beam which causes dissipation of kinetic energy [6].

The signals are produced from the backscattering process of photons and electrons (**Figure 62**), which are particularly useful to provide information regarding composition shifts in multiphase samples.

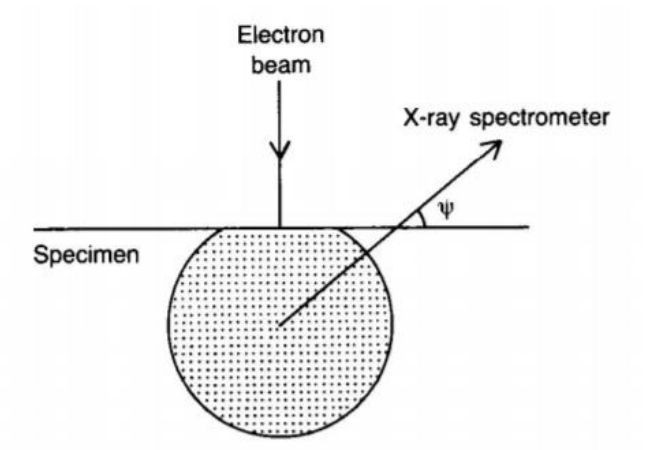

Figure 62. Signals derived from backscattering electron beam [6].

Generally, a SEM device (**Figure 63**) is composed of:

1. Electron beam sources
2. Electron lenses
3. Sample stage
4. Signals detectors
5. Output device.

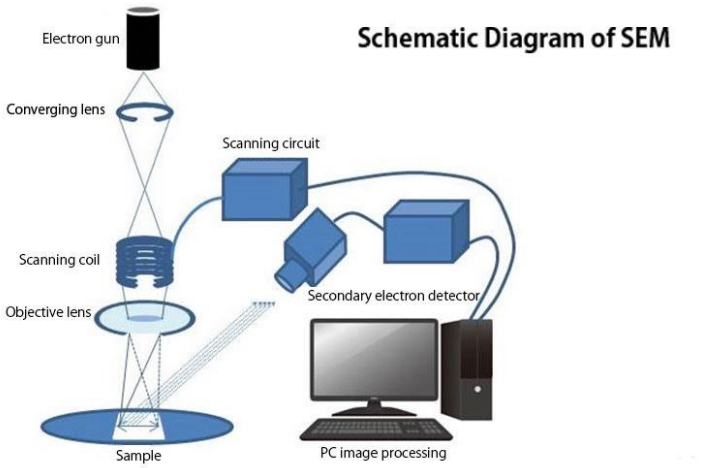

Figure 63. Schematic diagram of SEM device.

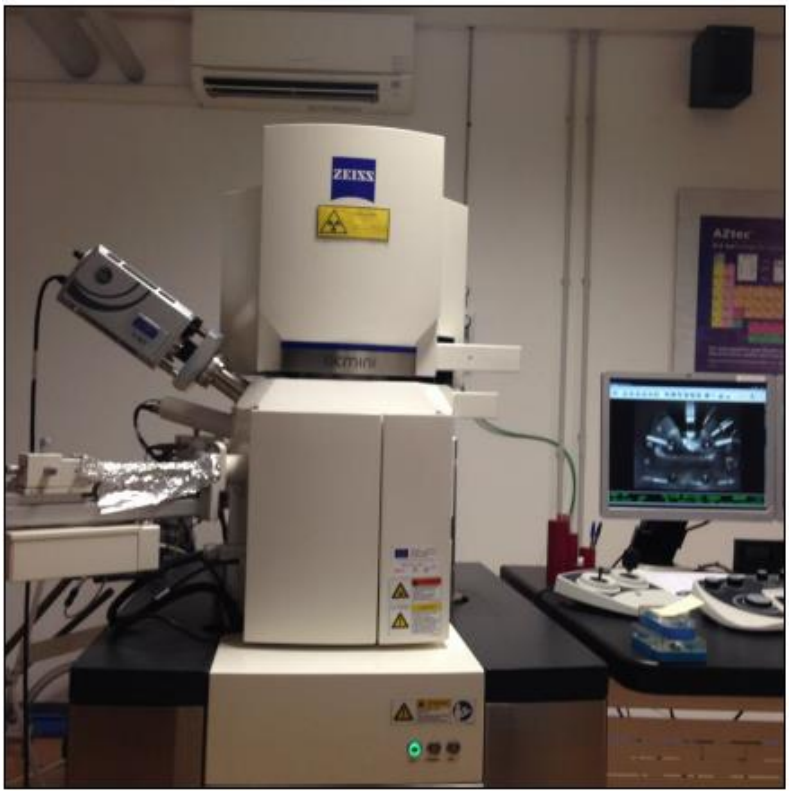

Figure 64. SEM device (ZEISS MERLIN) used for morphological and chemical characterization.

Preparation of the sample constitutes a critical step in SEM analysis because depending on its nature could be minimal or elaborate and may be necessary to introduce a protective coating with a thin layer of conducting materials [6]. In fact, samples need particular requirements to be correctly analysed, such as solid matter, suitable size able to enter in SEM chamber and stability in a vacuum.

Although pre-processing steps, SEM analysis is considered as a conservative analysis because sample characteristics are not perturbated by analysis processes.

Conventionally, the analysed area ranges from 1 cm to 5 μm in width with a spatial resolution of 50 to 100 nm [6].

Compositional characteristics are evaluated by Energy Dispersive Spectroscopy, an analytical technique which uses X-ray spectrum emitted by the interaction from the sample and the focused beam of electrons to achieve a localized chemical analysis.

EDS approach both permits qualitative analysis involving identification of the spikes present in the spectrum, and quantitative analysis measuring spike intensity which detect element concentrations [6][7].

These techniques have been used to analyse both precipitate powders in synthesis IV and glass powder obtained in synthesis VII.

2.3 X-Ray Diffraction (XRD) Analysis

X-Ray Diffraction (XRD) is a non-destructive technique that provides detailed information about the crystallographic structure, chemical composition and physical properties of materials.

Therefore, it provides information on structures, phases, texture, such as preferred crystal orientation and other parameters, as grain size, strain and crystal defects.

In this analysis, X-rays, produced by a cathode, are filtered to obtain a monochromatic beam which interferes with the powdered sample. The constructive interference derived from this interaction generates examined signals.

XRD pattern is characteristic of the substance under investigation. In fact, atomic positions within substance structure determine peak intensities allowing quick phase identification for a large variety of crystalline samples.

This technique is based on Bragg's law:

$$n\lambda = 2d\ sin\theta$$

In this equation, λ indicates the wavelength of the radiation, d is the lattice spacing in a crystalline sample and θ is the diffraction angle. The incognita of this formula is the d parameter, from which individuation is possible to univocally determine the mineral phase. In fact, each mineral is characterized by its own d-spacing.

During the analysis process, X-ray beam is appropriately collimated and deviated toward the powder sample (**Figure 65**). Once the beam hits sample surface, the radiation is diffracted, and this signal is detected.

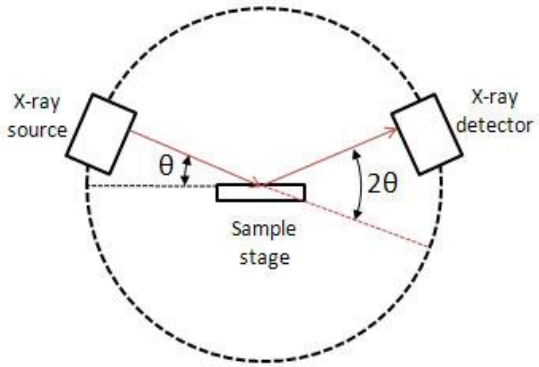

Figure 65. Schematic representation of X-ray diffraction process.

In post processing steps, diffracted ray is showed in form of a diffraction spectra which is characterized by peaks correspondent to the detected mineral phase.

A typical X-ray diffractometer is composed of:

1. X-ray source, typically a X-ray tube which contains a copper block anode bearing a metal target made of metals such as, molybdenum, tungsten, copper, rhodium, etc. the cathode is a tungsten filament.
2. Sample stage, usually four circle goniometers because circles help position of the crystal planes for optimum X-ray diffraction.
3. Detector, which can include more sensitive options as gas filled transducers, scintillation counters and semiconductor transducers.

XRD analysis was performed on glass powders obtained by synthesis VII and VIII (**Figure 66**).

Figure 66. Diffratometer X'Pert.

2.4 Brunauer- Emmet- Teller (BET) Analysis

BET analysis takes its name from the theory stipulated by Brunauer, Emmet and Teller in 1938 about adsorption mechanism [8].

These scientists extensively studied process on the base of physical adsorption of gas molecules on a solid surface. The BET theory is applied to systems of multilayer adsorption using probing gases which do not interact with material surfaces [9].

BET analysis was developed basing on theory of Brunauer, Emmet and Teller and allows the determination of the specific surface area by physical adsorption of a gas on the surface of the material. Nitrogen is the most commonly employed gas used for surface probing by BET methods because of its availability in high purity and its strong interaction with most solids [9].

The amount of adsorbed gas molecules is revealed to determine the mass of the gas adsorbed monolayer through the equation:

$$\frac{1}{W(\frac{p}{p_0}-1)} = \frac{1}{W_m C} + \frac{C-1}{W_m C}\left(\frac{p}{p_0}\right)$$

Where:

W: weight of gas adsorbed;

W_m: weight of adsorbate constituting monolayer surface;

C: BET constant which indicates interaction magnitude between gas molecules (adsorbate) and solid particles surface (adsorbent) [10].

In BET analysis, known amount of nitrogen gas are released stepwise into sample surface[11].

A precise quantity of sample (> 100 mg) is introduced in glass burettes and purified by degassing process under vacuum conditions[11].

In each analysis, sample weight is recorded both before and after degas process detecting a mass reduction [10].

In biomedical applications, BET device allows a fundamental approach for detection of surface area, pore volume and pore size (**Figure 67**). These features are particularly interesting for the evaluation of bioactivity behaviour of BG and MBG materials, as function of their dissolution rate, typically proportional to the specific surface area [10].

Figure 67. ASAP 2020 Plus BET device.

Chapter 4 – Analysis and discussion of results

1. Introduction

The aim of the present work is the design and development of mesoporous bioactive glasses based on a complex six-oxides system. In particular, the realization of MBG based on 47.5B composition, which was developed by Vernè *et al.*[2], at Politecnico di Torino. Although this glass was previously developed by melt-quenching and traditional sol-gel routes, attributing mesoporous features to 47.5B composition constitutes an attractive challenge.

As introduced in *Chapter 2* and described in *Chapter 3*, the optimization of MBG synthesis involves several factors and is a very challenging task. For this reason, the experimental activity has been based on two distinct parts: preliminary theoretical calculations, aimed at optimizing synthesis parameters , and practical experimental realization of several syntheses with their characterization.

The study of Pluronic® P123 - solvents state diagram and solubility calculations has been fundamental to solve solubility problems which occurred during the syntheses of a such complex system.

Another important part has been represented by the thermal, morphological and chemical characterization of synthesis precipitate and product. Differential Thermal (DTA), X-Ray Diffraction, Scanning Electron Microscopy and Brunauer-Emmet-Teller (BET) analyses were conducted to interpret synthesis results.

2. Synthesis Design

MBG synthesis is the combination of sol-gel route and supramolecular chemistry of surfactants [4].

Different preliminary calculations to establish reagent amount were conducted for the optimization of every synthesis conducted in this study.

The quantity of each reagent needed for obtaining the 47.5 SiO_2- 20 CaO- 10 MgO -10 Na_2O -10 K_2O – 2.5 P_2O_5 composition was calculated on the basis of the following chemical reactions.

$$(1)\ Si(OC_2H_5)_4 + 2\,H_2O \rightarrow SiO_2 + 4\,C_2H_5OH$$

$$(2)\ 2\,(C_2H_5O)_3PO + 18\,O_2 \rightarrow 12\,CO_2 + P_2O_5 + 15\,H_2O$$

$$(3)\ Mg(NO_3)_2 \times 6\,H_2O \rightarrow 2\,NO_2 + MgO + 6\,H_2O$$

$$(4)\ 10\,Ca(NO_3)_2 \times 4\,H_2O \rightarrow 20\,NO_2 + 10\,CaO + 4\,H_2O$$

$$(5)\ 2\,NaNO_3 + H_2O \rightarrow Na_2O + 2\,HNO_3$$

$$(6)\ 2\,KNO_3 + H_2O \rightarrow K_2O + 2\,HNO_3$$

From *Equation 1*, number of mol needed had been derived and it was used to proportionally calculate the mol needed of other reagents (*Equation 2-5*). Amount of TEOS mol was calculated from TEOS/solvents ratio, important and impacting parameter on sol gel synthesis, which had been varied during the design of different syntheses. Once TEOS mol had been fixed, mol of the other reagents had been calculated following proportions of 47.5B composition and *Equations 2-5* in respect of reagent/oxide ratio.

Once reagent quantity was obtained, supplementary considerations about synthesis realization had been necessary.

A fundamental role for the development of mesoporous materials is played by structure directing template (SDA).

As previously seen in *Chapter 2*, poly (ethylene oxide)-poly (propylene oxide)-poly (ethylene oxide) PEO-PPO-PEO block copolymers (commercially available as Pluronics®) exhibit different phases depending on several factors, such as block copolymer molecular weight and PEO/PPO block ratio, solvent type and, more importantly, the block copolymer/solvent composition [12].

To get a better understand of MBG synthesis and to optimize the design of 47.5B MBG synthesis, a deep study has been conducted investigating the phase diagram of triblock copolymers in the presence of selective solvents such as water and ethanol.

As mentioned before, Pluronic® triblock copolymers are characterized by a CMC (critical micelle concentration) above which surfactant molecules aggregate in micelles. Since the PPO blocks are more hydrophobic than the PEO ones, Pluronics® micelles are constituted by a PPO core surrounded by a hydrate PEO shell [12].

Micellization of Pluronics is characterized by CMC, critical micelle temperature (CMT), molecular weight of the micelle and the aggregation/ association number. Micelles are also characterized on the basis of their size and shape which are described by the radius of gyration (R_g), radius of core (R_c), thickness of corona (L), hydrodynamic radius (R_h) and the ratio R_g/R_h [13].

Thermodynamics of micelle formation is essentially entropy driven. When the unimers of Pluronic system form aggregates, the hydrogen bonding structure in water is restored and the entropy of water increases outweighing the entropy loss due to localization of monomers [13].

Therefore, the formation of micelles depends on the aqueous solubility of the PPO and PEO segments, dependent on the solvents used and the temperature. In fact, as the hydrophobic effect increases with temperature, the tendency to form micelles at higher temperatures increases, too. As the temperature increases above CMT the solubility of PEO group decreases and becomes more hydrophobic because of the conformational changes in EO segments. Therefore, at a certain temperature PEO groups aggregate giving rise to phase separation [13].

In fact, the formation of micelles is a spontaneous process (characterized by negative free energy $\Delta G < 0$) caused by the interaction between the solvophobic segments of the amphiphiles and the solvent used [14]. The PPO block is water soluble at low temperature (4 °C) but becomes insoluble at room temperature, while PEO block still remains soluble at temperatures up to 100 °C [14]. But at low temperatures, when both PPO and PEO blocks are more soluble, the PEO-PPO- PEO block copolymers are present as un-associated unimers [14]. Upon a temperature increase, the solvophobic PPO blocks tend to associate to minimize contact with the solvent [14].

As Pluronics® can exist in a large range of molecular weight and hydrophilic lipophilic balance (HLB), a nomenclature is given to differentiate different commercial available Pluronics® [13].

In this study, all syntheses have been conducted using Pluronic® P123. **Table 25** shows P123 properties.

Table 25. Properties of Pluronic P123. A: commercial name, B: average molecular weight, C: PEO wt.%, D: melting pout point (°C), E: viscosity, F: surface tension at 0.1% 25 °C, G: foam height (mm), H: cloud point in aqueous solution 1%, I:HLB (hydrophilic- lipophilic balance)[13].

Commercial name	Average molecule weight	PEO wt %	Melting pout point (°C)	Viscosity	Surface tension at 0.1% 25 °C	Foam height (mm)	Cloud point in aqueos solution 1%	Hydrophilic - lypophilic balance
P123	5750	30	31	350	34	45	90	7-12

The possibility to obtain surfactant phases in relation to block copolymer/solvent composition is perfectly showed by ternary phase diagram water- P123- ethanol (**Figure 68**).

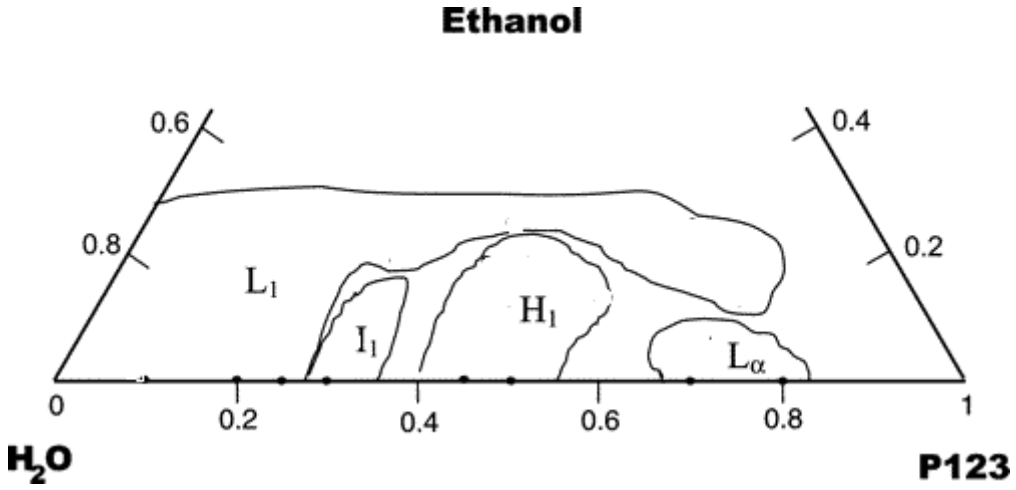

Figure 68. Ternary phase diagram of P123/water/ethanol [12].

Ternary phase diagram clearly illustrates four different regions, corresponding to four different possible phases exhibited by Pluronic®, with the aim to evidence the role of three components on the morphology of final mesoporous products.

In **Figure 1,** L_1 denotes region with isotropic solution (water rich), I_1 denotes the clear isotropic gels and mixture of cubic and HCPS lattice, H_1 indicates cylindrical micelles arranged in 2D hexagonal lattice, and L_α is referred to the lamellae- planner micelles.

P123 triblock copolymers have a CMC in pure water about 4.0 x 10^{-3}% (w/w). Water is a PEO block selective solvent, so PEO chains are expected to be solvated by water creating a homogenous medium while PPO block are not solvated. For this reason, Pluronic P123 dissolution in pure water is quite difficult at low temperatures and not recommended.

Bibliographic researches about MBG syntheses show the existence of both alcoholic and mixed syntheses.

Following Vallet Regì *et al.*[4] indications, IV synthesis was conducted using only ethanol as solvent and keeping ethanol- TEOS ratio 40:1, while ethanol – P123 proportion was 30 g of ethanol to 2 g of P123.

Although the parameters of IV synthesis were set up according to Vallet Regì studies[4], [15]–[17], in this synthesis potassium nitrate never dissolved and the presence of a precipitate was observed. Such powder precipitation was analysed with the intent to discover its nature and analysis results will be shown in *paragraph 3*.

The addition of several oxides and the major complexity of 47.5B system introduce a solubility challenge in the design of a such articulate synthesis.

The major issue in 47.5B MBG synthesis optimization is represented by the necessity to find a compromise between Pluronic® P123 to be dissolved in ethanol and solubility problems mainly related to potassium and sodium nitrate use (**Table 26**).

Table 26. Theorical solubility limits of sodium nitrate and potassium nitrate in pure water and ethanol at 25°C.

	H_2O	**EtOH**
Sodium Nitrate	91.2 g/ 100 ml	0.22 g/ 100 ml
Potassium Nitrate	31.9 g/ 100 ml	0.6 g/ 100 ml

In fact, sodium and potassium nitrates are almost completely insoluble in pure ethanol solution while the necessary amount of Pluronic® P123 is insoluble in pure water solution at room temperature, but it is impossible to reach higher temperatures (which could solve

the solubility problem of P123 in pure water) because of the need of precise temperature and concentration parameters to induce surfactant micellization.

For this reason, mixed syntheses were designed and developed studying reagent behaviour with mixed solvents (**Table 27- Figure 69-70**).

Table 27. Solubilities of sodium nitrate at different mass fractions (W) of ethanol [18].

Temperature	**Mass fraction of ethanol (W)**	**Mole fraction of ethanol (X)**	**S (g/ 100g solvent)**	**M (mol/kg solvent)**
20.4 °C	0	0.00	89.58	10.54
	0.0549	0.02	78.39	9.22
	0.1359	0.06	63.08	7.42
	0.1909	0.08	54.54	6.42
	0.3	0.14	39.77	4.68
	0.4	0.21	28.63	3.37
	0.5	0.28	19.97	2.35
	0.6	0.37	12.92	1.52
	0.9	0.78	1.06	0.13
30.0 °C	0	0.00	95.61	11.25
	0.05	0.02	85.82	10.10
	0.2	0.09	59.64	7.02
	0.4	0.21	33.49	3.94
	0.6	0.37	14.81	1.74
	0.7	0.48	8.27	0.97
	0.9	0.78	1.24	0.15
40.0 °C	0	0.00	104.10	12.25
	0.08	0.03	88.48	10.41
	0.26	0.12	57.69	6.79
	0.428	0.23	35.67	4.20
	0.651	0.42	13.43	1.58
	0.872	0.73	2.20	0.26

As **Table 27** shows, the design of a mixed water- ethanol synthesis introduces some new aspects which should be considered. The mass fraction of ethanol strongly impacts on sodium nitrate solubility. In fact, an increasing percentage of ethanol introduced in the synthesis induces a strong decrease in mass of sodium nitrate that the solvent system (ethanol-water) is able to solvatate.

	[HCl], mol kg_{solv}^{-1}												
	0			1			2			3			4		
solvent	b^{exp}	b^{calc}	RD, %	b^{exp}	b^{calc}	RD, %	b^{exp}	b^{calc}	RD, %	b^{exp}	b^{calc}	RD, %	b^{exp}	b^{calc}	RD, %
Temperature = 313.15 K															
40 wt % ethanol	1.201	1.2122	−0.93	0.9898	0.9961	−0.64	0.8518	0.8307	2.48	0.7215	0.7006	2.89	0.5892	0.5968	−1.29
50 wt % ethanol	0.7607	0.7695	−1.16	0.6088	0.6214	−2.07	0.5014	0.5095	−1.62	0.4233	0.4233	−0.01	0.3663	0.3563	2.73
60 wt % ethanol	0.459	0.4517	1.59	0.3685	0.3602	2.24	0.2974	0.2885	3.00	0.2402	0.2346	2.32	0.1930	0.1941	−0.55
70 wt % ethanol	0.2305	0.2317	−0.50	0.1853	0.1818	1.90	0.1408	0.1411	−0.23	0.1088	0.1115	−2.45	0.0910	0.0903	0.79
80 wt % ethanol	0.0771	0.0757	1.80	0.0697	0.0688	1.35	0.0517	0.0510	1.33	0.0398	0.0388	2.60			
Temperature = 323.15 K															
pure water	8.4633	8.5234	−0.71	6.4041	6.4044	−0.01	5.1850	5.1853	−0.006	4.3982	4.3982	0.00	3.8153	3.8149	0.01
5 wt % ethanol	7.1621	7.1621	0.01	5.4283	5.4280	0.01	4.4447	4.4443	0.01	3.7875	3.7867	0.02	3.2843	3.2836	0.02
10 wt % ethanol	5.854	5.9477	−1.60	4.5714	4.5778	−0.14	3.7105	3.7884	−2.10	3.2508	3.2368	0.43	2.8557	2.8023	1.87
20 wt % ethanol	3.9294	4.0139	−2.15	3.2132	3.2134	−0.01	2.6994	2.6986	0.03	2.3057	2.3055	0.01	1.9836	1.9828	0.04
30 wt % ethanol	2.629	2.6829	−2.05	2.2568	2.2094	2.10	1.8921	1.8592	1.74	1.5988	1.5764	1.40	1.3395	1.3411	−0.12
40 wt % ethanol	1.778	1.7776	0.02	1.4704	1.4701	0.02	1.2235	1.2231	0.03	1.0228	1.0219	0.09	0.8582	0.8582	0.01
50 wt % ethanol	1.0742	1.0789	−0.44	0.9257	0.9257	0.01	0.7537	0.7537	0.002	0.6177	0.6177	−0.01	0.5109	0.5109	0.01
60 wt % ethanol	0.6727	0.6727	0.007	0.5316	0.5311	0.10	0.4207	0.4207	0.008	0.3371	0.3370	0.03	0.2738	0.2737	0.02
70 wt % ethanol	0.3062	0.3049	0.42	0.2592	0.2592	0.01	0.1992	0.1992	0.02	0.1552	0.1552	−0.03	0.1234	0.1234	−0.02
80 wt % ethanol	0.1071	0.1071	−0.01	0.0903	0.0927	−2.61	0.0675	0.0686	−1.65	0.0504	0.0517	−2.56	0.0396	0.0400	−1.05
90 wt % ethanol	0.0118	0.0118	−0.36	0.0149	0.0149	0.03	0.0104	0.0104	0.01	0.0075	0.0075	0.30	0.0056	0.0056	0.07
Temperature = 333.15 K															
pure water	10.858	10.861	−0.03	8.0121	8.0118	0.01	6.7592	6.7593	−0.01	6.0309	6.0304	0.01	5.4822	5.4818	0.01
5 wt % ethanol	9.3280	9.3276	0.01	6.9802	6.9798	0.01	5.9653	5.9654	−0.01	5.3408	5.3396	0.02	4.8437	4.8432	0.01
10 wt % ethanol	7.9469	7.9032	0.55	5.9480	6.0455	−1.64	5.2570	5.2307	0.50	4.7512	4.6894	1.30	4.1258	4.2372	−2.70
20 wt % ethanol	5.5152	5.4744	0.74	4.4536	4.4533	0.01	3.9261	3.9257	0.01	3.5095	3.5089	0.02	3.1327	3.1322	0.02
30 wt % ethanol	3.7315	3.6778	1.44	3.229	3.1844	1.38	2.8317	2.8238	0.28	2.5128	2.4922	0.82	2.192	2.1839	0.37
40 wt % ethanol	2.4262	2.4263	−0.01	2.1804	2.1799	0.02	1.9127	1.9123	0.02	1.6516	1.6509	0.05	1.4158	1.4148	0.07
50 wt % ethanol	1.5438	1.5469	−0.20	1.3922	1.3918	0.03	1.1893	1.1888	0.04	0.9982	0.9982	−0.01	0.8373	0.8370	0.04
60 wt % ethanol	0.9046	0.9046	0.01	0.7932	0.7931	0.01	0.6544	0.6544	0.01	0.5349	0.5349	−0.01	0.4405	0.4405	0.01
70 wt % ethanol	0.4117	0.4053	1.55	0.3752	0.3752	0.01	0.3005	0.3005	0.01	0.2403	0.2403	0.01	0.1951	0.1951	0.01
80 wt % ethanol	0.1349	0.1349	−0.02	0.1265	0.1280	−1.20	0.1007	0.1005	0.23	0.0783	0.0789	−0.72	0.063	0.0633	−0.55
90 wt % ethanol	0.0137	0.0137	−0.02	0.0202	0.0200	1.00	0.0154	0.0154	−0.27	0.0121	0.0121	0.15	0.0098	0.0098	0.34

[a]Standard uncertainties u are: $u(T) = 0.1$ K, $u([HCl]) = 0.03$ mol kg_{solv}^{-1} and $u(b) = 0.03$ mol kg_{solv}^{-1}, where the subscript solv (solvent) accounts for (water + ethanol).

Figure 69. Potassium nitrate solubility in mixed solvents (water+ ethanol) with different temperatures [19].

	[HCl], mol kg_{solv}^{-1}												
	0			1			2			3			4		
solvent	b^{exp}	b^{calc}	RD, %	b^{exp}	b^{calc}	RD, %	b^{exp}	b^{calc}	RD, %	b^{exp}	b^{calc}	RD, %	b^{exp}	b^{calc}	RD, %
Temperature = 313.15 K															
40 wt % ethanol	1.201	1.2122	−0.93	0.9898	0.9961	−0.64	0.8518	0.8307	2.48	0.7215	0.7006	2.89	0.5892	0.5968	−1.29
50 wt % ethanol	0.7607	0.7695	−1.16	0.6088	0.6214	−2.07	0.5014	0.5095	−1.62	0.4233	0.4233	−0.01	0.3663	0.3563	2.73
60 wt % ethanol	0.459	0.4517	1.59	0.3685	0.3602	2.24	0.2974	0.2885	3.00	0.2402	0.2346	2.32	0.1930	0.1941	−0.55
70 wt % ethanol	0.2305	0.2317	−0.50	0.1853	0.1818	1.90	0.1408	0.1411	−0.23	0.1088	0.1115	−2.45	0.0910	0.0903	0.79
80 wt % ethanol	0.0771	0.0757	1.80	0.0697	0.0688	1.35	0.0517	0.0510	1.33	0.0398	0.0388	2.60			
Temperature = 323.15 K															
pure water	8.4633	8.5234	−0.71	6.4041	6.4044	−0.01	5.1850	5.1853	−0.006	4.3982	4.3982	0.00	3.8153	3.8149	0.01
5 wt % ethanol	7.1621	7.1621	0.01	5.4283	5.4280	0.01	4.4447	4.4443	0.01	3.7875	3.7867	0.02	3.2843	3.2836	0.02
10 wt % ethanol	5.854	5.9477	−1.60	4.5714	4.5778	−0.14	3.7105	3.7884	−2.10	3.2508	3.2368	0.43	2.8557	2.8023	1.87
20 wt % ethanol	3.9294	4.0139	−2.15	3.2132	3.2134	−0.01	2.6994	2.6986	0.03	2.3057	2.3055	0.01	1.9836	1.9828	0.04
30 wt % ethanol	2.629	2.6829	−2.05	2.2568	2.2094	2.10	1.8921	1.8592	1.74	1.5988	1.5764	1.40	1.3395	1.3411	−0.12
40 wt % ethanol	1.778	1.7776	0.02	1.4704	1.4701	0.02	1.2235	1.2231	0.03	1.0228	1.0219	0.09	0.8582	0.8582	0.01
50 wt % ethanol	1.0742	1.0789	−0.44	0.9257	0.9257	0.01	0.7537	0.7537	0.002	0.6177	0.6177	−0.01	0.5109	0.5109	0.01
60 wt % ethanol	0.6727	0.6727	0.007	0.5316	0.5311	0.10	0.4207	0.4207	0.008	0.3371	0.3370	0.03	0.2738	0.2737	0.02
70 wt % ethanol	0.3062	0.3049	0.42	0.2592	0.2592	0.01	0.1992	0.1992	0.02	0.1552	0.1552	−0.03	0.1234	0.1234	−0.02
80 wt % ethanol	0.1071	0.1071	−0.01	0.0903	0.0927	−2.61	0.0675	0.0686	−1.65	0.0504	0.0517	−2.56	0.0396	0.0400	−1.05
90 wt % ethanol	0.0118	0.0118	−0.36	0.0149	0.0149	0.03	0.0104	0.0104	0.01	0.0075	0.0075	0.30	0.0056	0.0056	0.07
Temperature = 333.15 K															
pure water	10.858	10.861	−0.03	8.0121	8.0118	0.01	6.7592	6.7593	−0.01	6.0309	6.0304	0.01	5.4822	5.4818	0.01
5 wt % ethanol	9.3280	9.3276	0.01	6.9802	6.9798	0.01	5.9653	5.9654	−0.01	5.3408	5.3396	0.02	4.8437	4.8432	0.01
10 wt % ethanol	7.9469	7.9032	0.55	5.9480	6.0455	−1.64	5.2570	5.2307	0.50	4.7512	4.6894	1.30	4.1258	4.2372	−2.70
20 wt % ethanol	5.5152	5.4744	0.74	4.4536	4.4533	0.01	3.9261	3.9257	0.01	3.5095	3.5089	0.02	3.1327	3.1322	0.02
30 wt % ethanol	3.7315	3.6778	1.44	3.229	3.1844	1.38	2.8317	2.8238	0.28	2.5128	2.4922	0.82	2.192	2.1839	0.37
40 wt % ethanol	2.4262	2.4263	−0.01	2.1804	2.1799	0.02	1.9127	1.9123	0.02	1.6516	1.6509	0.05	1.4158	1.4148	0.07
50 wt % ethanol	1.5438	1.5469	−0.20	1.3922	1.3918	0.03	1.1893	1.1888	0.04	0.9982	0.9982	−0.01	0.8373	0.8370	0.04
60 wt % ethanol	0.9046	0.9046	0.01	0.7932	0.7931	0.01	0.6544	0.6544	0.01	0.5349	0.5349	−0.01	0.4405	0.4405	0.01
70 wt % ethanol	0.4117	0.4053	1.55	0.3752	0.3752	0.01	0.3005	0.3005	0.01	0.2403	0.2403	0.01	0.1951	0.1951	0.01
80 wt % ethanol	0.1349	0.1349	−0.02	0.1265	0.1280	−1.20	0.1007	0.1005	0.23	0.0783	0.0789	−0.72	0.063	0.0633	−0.55
90 wt % ethanol	0.0137	0.0137	−0.02	0.0202	0.0200	1.00	0.0154	0.0154	−0.27	0.0121	0.0121	0.15	0.0098	0.0098	0.34

[a]Standard uncertainties u are: $u(T) = 0.1$ K, $u([HCl]) = 0.03$ mol kg_{solv}^{-1} and $u(b) = 0.03$ mol kg_{solv}^{-1}, where the subscript solv (solvent) accounts for (water + ethanol).

Figure 70. Potassium nitrate solubility in mixed solvents (water+ ethanol) with different temperatures [19].

As can be seen in **Figure 69-70**, also potassium nitrate solubility is strongly influenced by both temperature and water/ethanol proportions in mixed synthesis.

These impacting factors make more difficult calculations and design of a such complex synthesis.

Another factor to be considered in the synthesis optimization is the exigence to set up solvents-P123 ratio aiming at obtaining cylindrical micelles arranged in 2D hexagonal lattice, named as region H_1, (**Figure 71**).

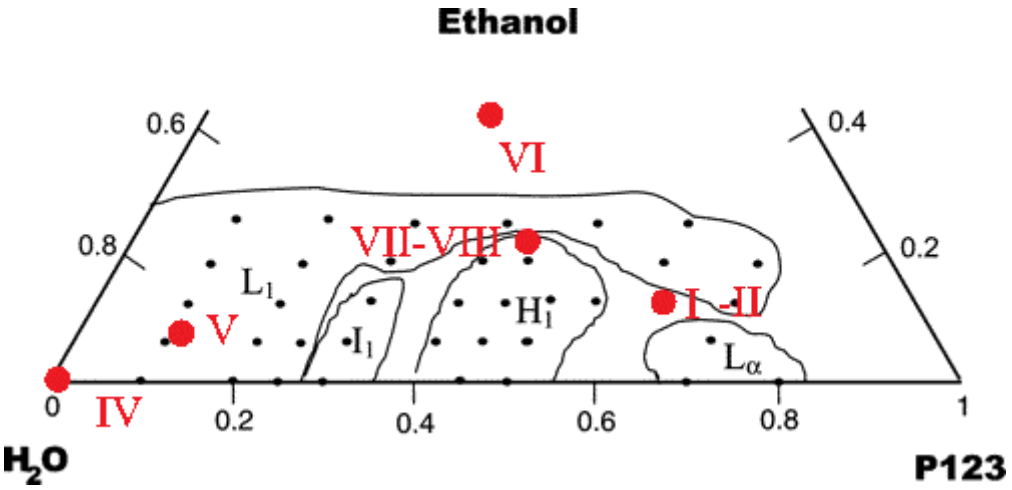

Figure 71. Red points in ternary phase diagram indicate were syntheses were conducted.

In synthesis VI, although solubility prescriptions were followed, sodium nitrate never dissolved in the solution. For this reason, following syntheses were performed using two different parallel systems of ethanol and water to separately dissolve Pluronic P123, TEOS, TEP, calcium and magnesium nitrate in ethanol while sodium and potassium nitrate, water insoluble, were solved in ethanol.

3. Precipitate Analyses

Syntheses I-II were interrupted because of the impossibility to proceed for the solubility problems of reagents.

Synthesis III role was to investigate influence of TEOS/solvent ratio in traditional sol gel synthesis aiming to properly design the correct ratio for mesoporous synthesis.

Synthesis IV had also reported precipitation problems, in this case to better understand mechanisms at the basis of precipitation, the powder precipitate was collected, stored in a Petri dish and let drying in a stove at 60 °C for seven days. Then, the powders were prepared to be analysed to assess the nature of the precipitate in order to better understand the chemical process which cause the matter precipitation.

First analysis conducted on this sample was Energy- Dispersive Spectroscopy (EDS), an analytical technique used for the elemental analysis or chemical characterization of a sample.

Particularly, in this case the analysis goal was to identify the chemical composition of precipitate sample (**Figure 72- 73**).

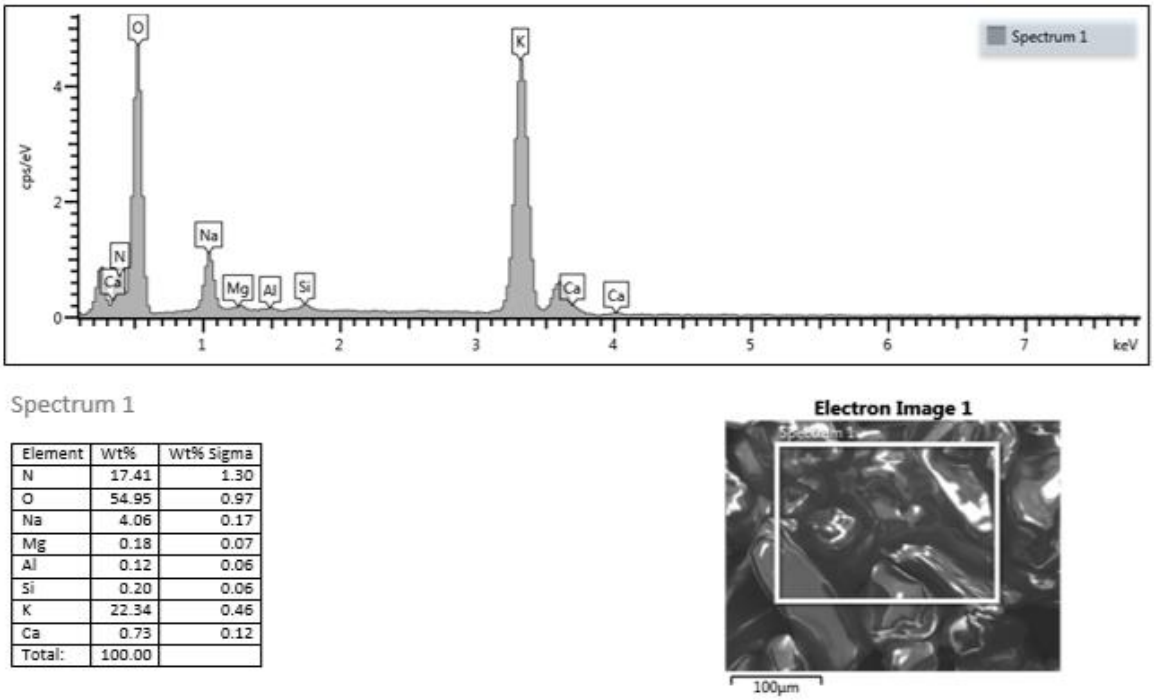

Figure 72. Energy Dispersive Spectroscopy Analysis of precipitate collected in synthesis IV.

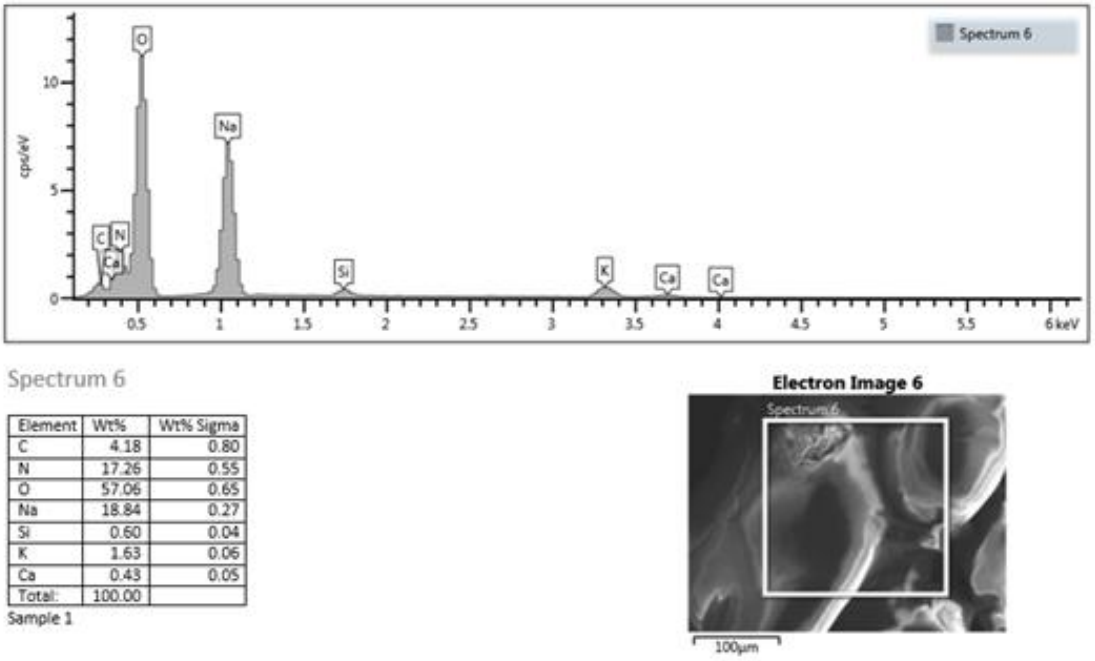

Spectrum 6

Element	Wt%	Wt% Sigma
C	4.18	0.80
N	17.26	0.55
O	57.06	0.65
Na	18.84	0.27
Si	0.60	0.04
K	1.63	0.06
Ca	0.43	0.05
Total:	100.00	

Sample 1

Figure 73. Energy Dispersive Spectroscopy Analysis of precipitate collected in synthesis IV.

These analyses reported the presence of high amount of potassium and sodium in the sample. These results could be explained because of the presence of six different reagent which are involved together into synthesis processes. The complexity of 47.5B system combined with the supramolecular chemistry of surfactants revealed a disparity between theoretical calculations about solubility limits and the real amount of salts that the system is simultaneously able to dissolve. Therefore, **Figure 72** and **Figure 73** had shown a sample characterized by high lack of homogeneity. In fact, spectra obtained by two different spots of the same sample revealed completely different compositions: in **Figure 72** spectrum 1 is characterized by high value of K (22.34 w.t.%) in comparison with 47.5B composition and by the absence of phosphorous, which is instead present in 47.5B system. The analysis of spectrum 6 (**Figure 73**) shown a completely different element distribution: phosphorous is still absent, but there is a significative presence of sodium. These results confirmed the hypothesis of potassium and sodium salts precipitation due to solubility problems of potassium and sodium nitrates.

4. Glass Analyses

4.1 Morphological and Chemical Characterization

The products derived from synthesis VII were characterized by Scanning Electron Microscopy (SEM) analysis. SEM scans the sample with an electron beam to produce a magnified image for analysis. The electrons interact with atoms in the sample, producing various information about the surface topography and composition of the sample.

A sample of gel pre-calcination was analysed (**Figure 74**) and the image shows some cracks due to drying process.

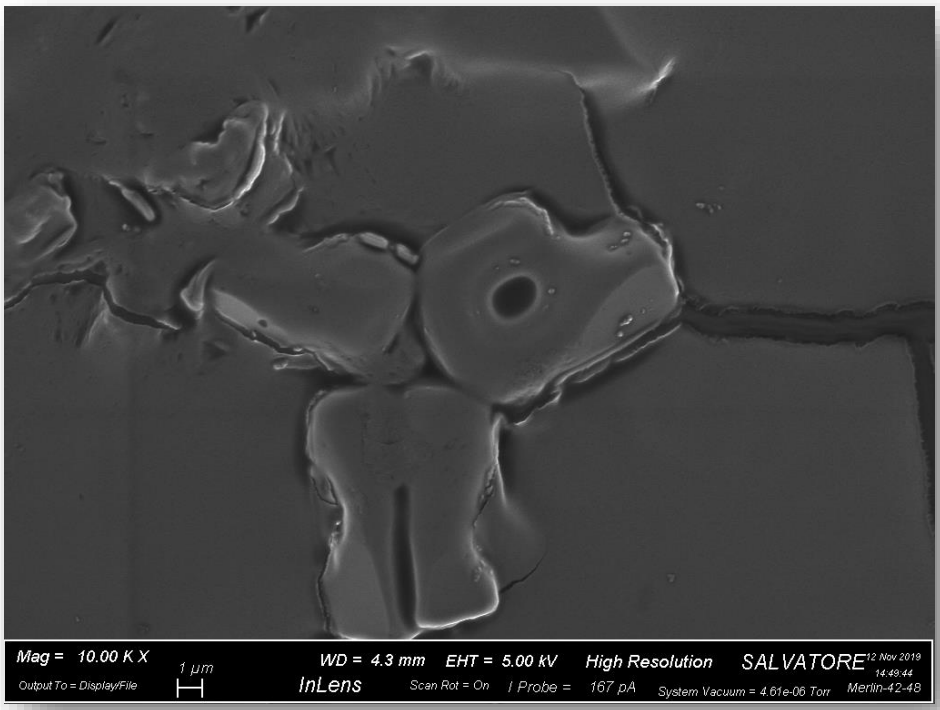

Figure 74. SEM image of gel pre-calcination obtained by synthesis VII.

The same analysis was repeated on a calcinated glass sample to investigate the glass topography (**Figure 75-76-77**).

Figure 75. SEM image of calcinated glass obtained by synthesis VII.

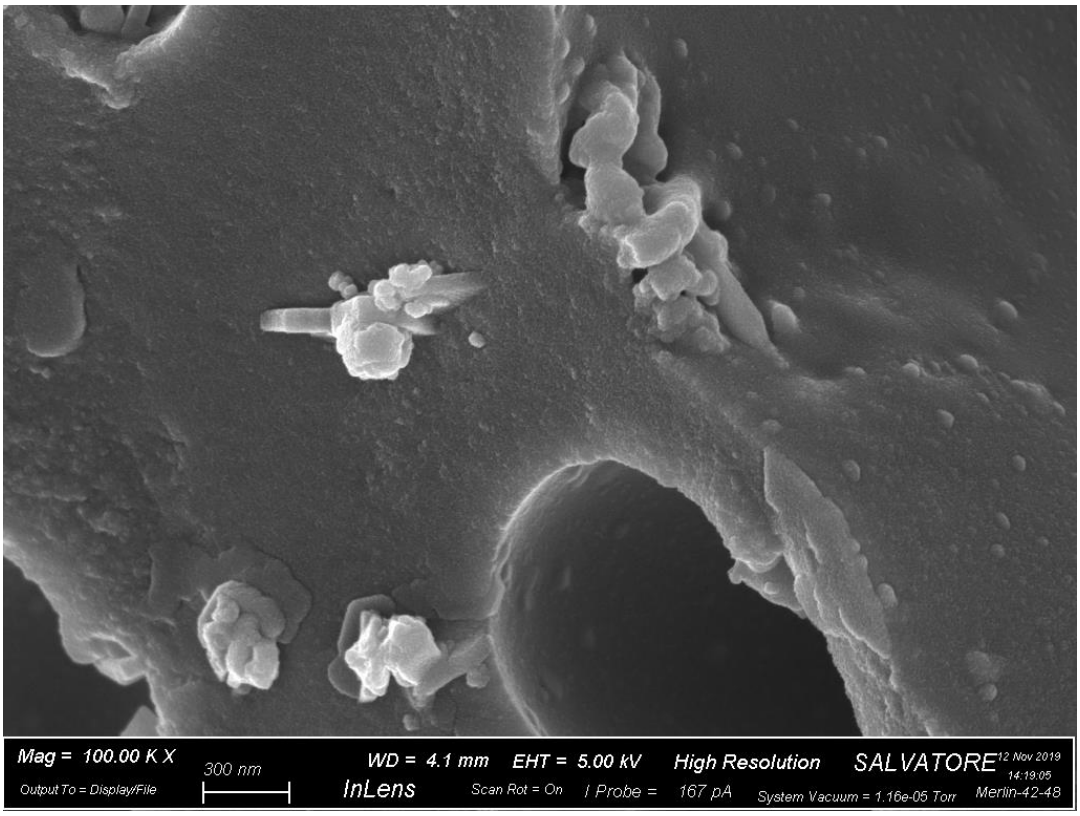

Figure 76. SEM image of calcinated glass obtained by synthesis VII.

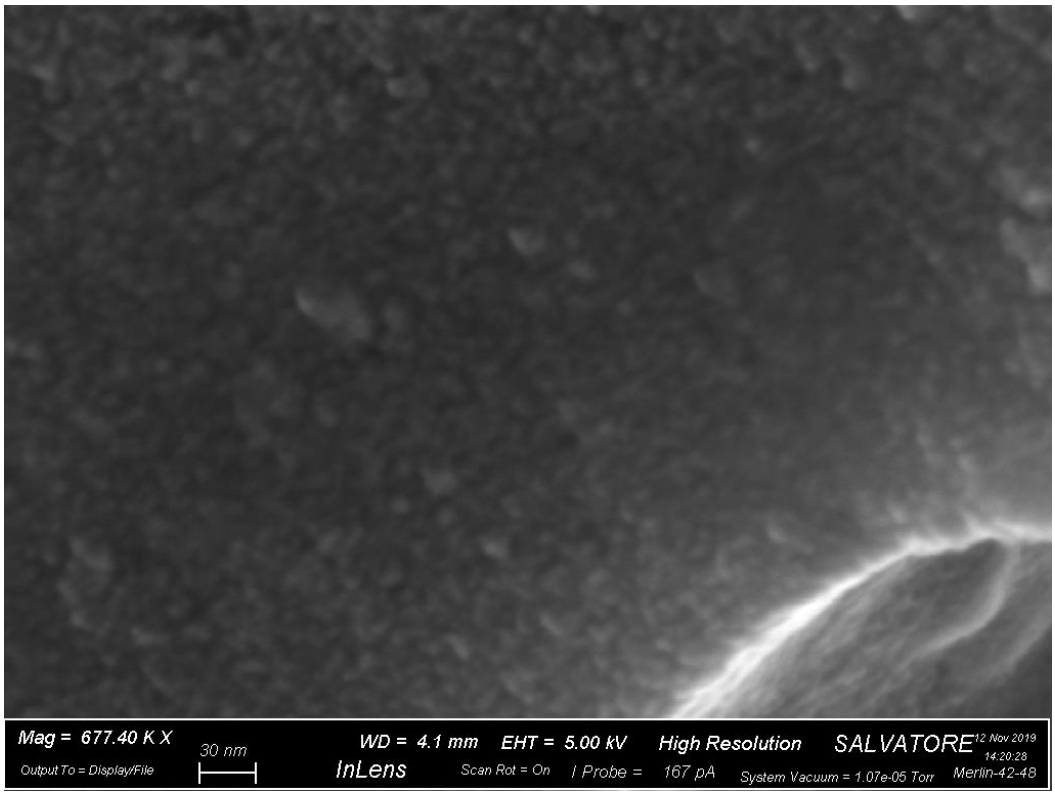

Figure 77. SEM image of calcinated glass obtained by synthesis VII.

Figure 74 had been obtained from SEM analysis of dried gel obtained in synthesis VII. In this image typical cracks of dried gel produced by sol-gel synthesis had been observed.

Figure 75 had been instead obtained from SEM analysis of calcinated powder obtained by synthesis VII. This image had shown the presence of un-common constructions compared with traditional sol-gel products. An hypothesis on the formation of these peculiar tapes-like structures could be the presence of Pluronic chains which had not been removed during calcination.

Figure 76 and **Figure 77** show the presence of clogged pores which could be due to the incomplete removal of Pluronic from the structure resulting in a lack of porosity in the material. These evidences have been confirmed by the results of Brauneur-Tellet-Emmet analysis which will be successively illustrated.

The sample were also analysed by Energy Dispersive Spectroscopy (EDS) to achieve a chemical characterization of precipitate sample.

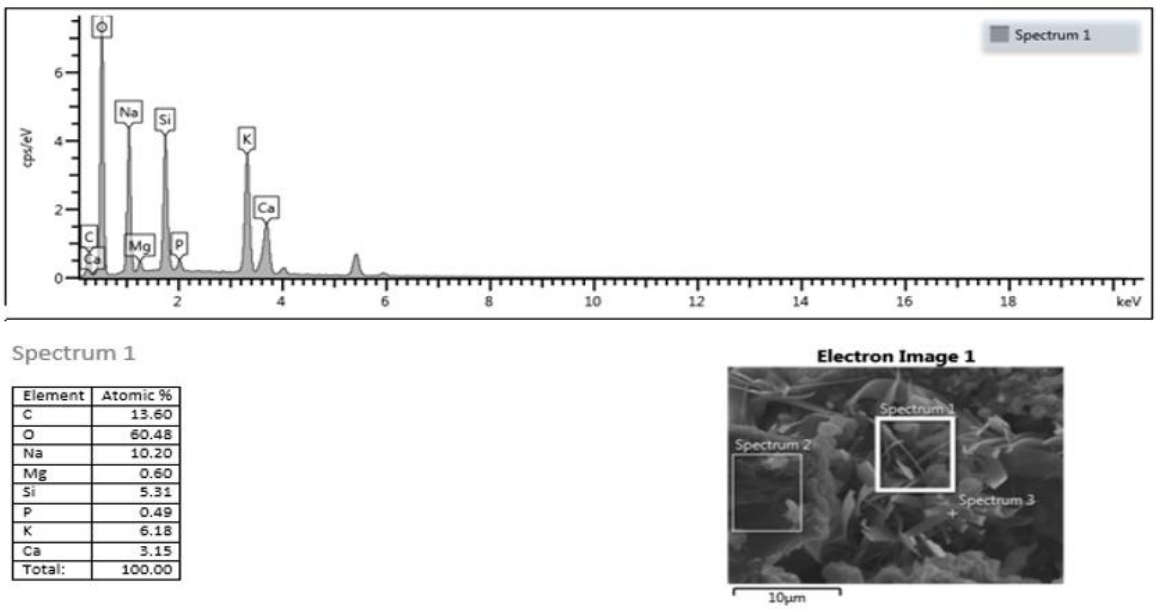

Figure 78. EDS result of sample obtained by synthesis VII.

Table obtained by EDS analysis showed weight percentages of each element in powdered glass sample. Thanks to calculations which provided to eliminate carbonium percentage which was due to impurities present in the sample because of the sample support.

Comparing EDS results with percentages obtained from 47.5B composition, they confirmed the presence of all oxides in correct proportions showing that the 47.5B composition was respected in the obtained glass.

4.2 X-Ray Diffraction

Powders obtained after the calcination of synthesis VIII have been studied by XRD analysis in order to evaluate the nucleation of crystalline phases within the material occurring as a result of the different thermal treatments performed.

Figure 79 represents the diffraction spectra obtained for the powder sample resulting from thermal treatment at 700 °C for 5 hours in a tubular furnace open in air.

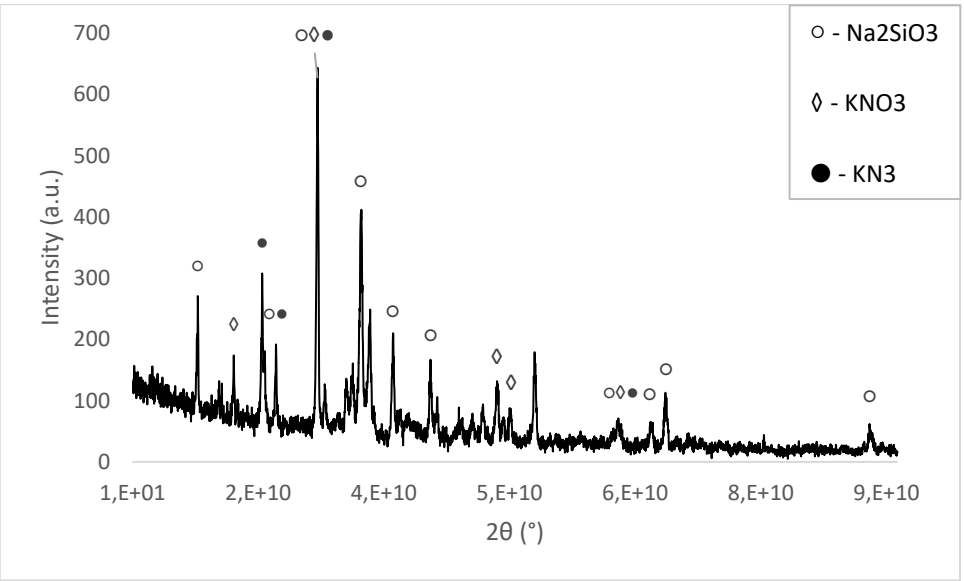

Figure 79. X-ray spectra related to powder obtained by synthesis VII after calcination at 625°C for 3 hours.

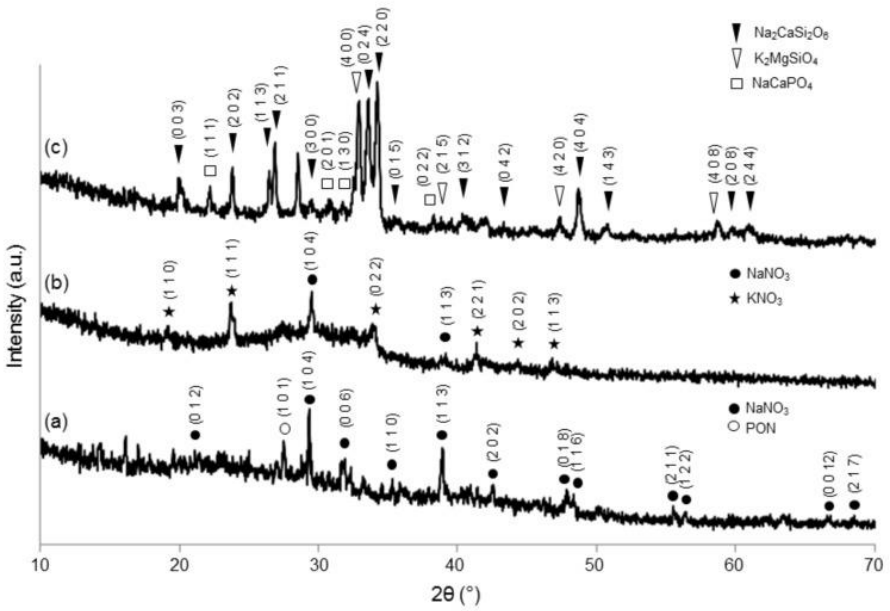

Figure 80. XRD pattern evolution upon thermal treatment of sol-gel 47.5B system at different stages of the synthesis process: dried gel at 120°C (**a**), sol-gel calcinated at 625 °C (**b**), sol-gel calcinated at 800°C (**c**) [2].

Figure 79 shows the presence of peaks which are characteristic of crystalline phases as sodium silicate (Na_2SiO_3), niter (KNO_3) and potassium azide (KN_3).

These results had been compared with XRD analyses previously obtained by melt derived (MD- 47.5B) and sol-gel derived 47.5B calcinated at 625 °C (SG- 625) and sol-gel derived 47.5B calcinated at 800 °C (SG- 800). Differently to MD-47.5b that was amorphous,

traditional sol-gel products (SG-625 and SG-800) and the sample obtained from synthesis VII through mesoporous synthesis exhibited a certain crystallinity after calcination [2]. **Figure 79** presents a XRD pattern similar to the one shown by SG-625, typical of a glass-ceramic material with an amorphous halo centered between 25° and 35° [2]. The halo is partially covered by some diffraction peaks attributable to nitrates presence, as confirmed by the detection of KNO_3 and KN_3 in our sample (**Figure 79**) and of $NaNO_3$ and KNO_3 in **figure 80 (b)** [2]. These results are compatible to with studied which still detected the presence of nitrates in sol-gel glass ceramic materials after thermal stabilization at 700 °C [20].

The list of all crystalline phases detected in sample obtained by our synthesis VII, SG-625 and SG-800, along with reference codes and formulas, are summarized in **Table 28.**

Table 28. Crystalline phases detected in SG-625, SG-800 and our glass sample obtained by synthesis VIII [2].

Detected in	**Phase Name**	**Reference Code**	**Formula**
SG-625	Niter	01-071-1558	KNO_3
	Nitratine	00-036-1474	$NaNO_3$
SG-800	Sodium calcium silicate	01-077-2189	$Na_2CaSi_2O_6$
	Potassium magnesium silicate	00-048-0900	K_2MgSiO_4
	Rhenanite	00-029-1193	$NaCaPO_4$
Sample synthesis VIII	Sodium silicate	00-016-0818	Na_2SiO_3
	Niter	00-005-0377	KNO_3
	Potassium azide	01-071-0204	KN_3

4.3 Thermal Characterization

Differential Thermal Analysis (DTA) provides information about material transformations, such as glass transition temperature and onset of crystallization. The knowledge of crystallization temperature for a given glass system is key to properly design thermal treatments, like calcination in this case, and forecast if an amorphous (glass) or glass-ceramic materials will be finally obtained..

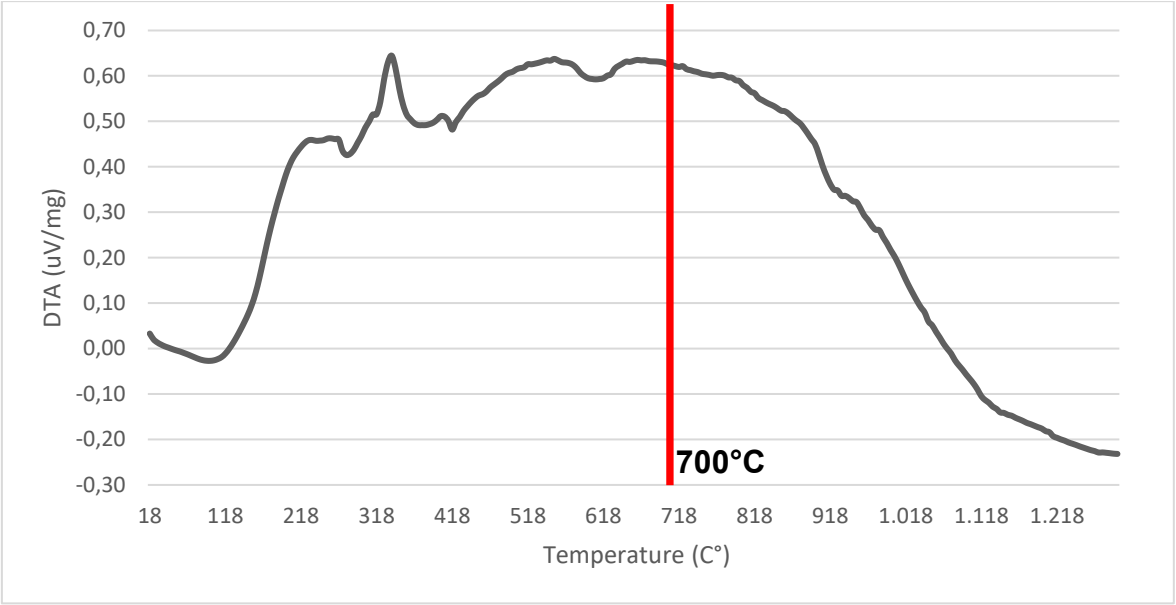

Figure 81. Graph derived from DTA analysis of dried gel sample obtained by synthesis VII.

From the study of DTA results, the setting of calcination temperature was slightly increased from 625 °C in synthesis VII up to 700 °C in synthesis VIII aiming at completely removal Pluronic residues seen in SEM analyses of sample derived by synthesis VII.

4.3 Analysis of the specific surface area and textural porosity

Brauneur-–Emmet-–Teller analysis is a fundamental analysis for MBG applications. Specific textural properties, such as porosity and specific surface area, are characteristics which allow to characterize a bioactive glass as mesoporous bioactive glass.

As seen in *Chapter 3*, this analysis is based on adsorption and desorption of nitrogen on the surface of the sample, evaluating different relative pressures. The results are isotherm curves from which pore diameter distribution can be calculated by considering the desorption branch of isotherms.

Hysteresis loops can be analysed by two different classification: IUPAC classification is given according to the different shapes that hysteresis loops could exhibit, while Stafford *et al.* classification individuate six different types (**Figure 82**) [8].

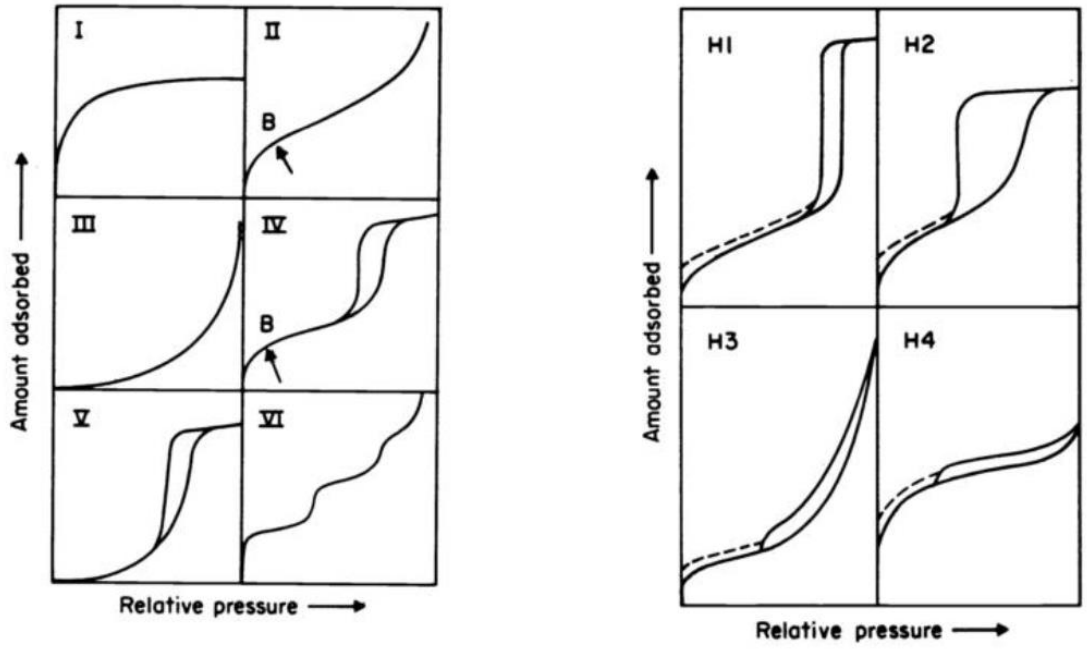

Figure 82. Stafford classification of Van der Waal adsorption isotherms on the left and IUPAC classification of hysteresis loops on the right [8].

According to the Stafford classification, physisorption isotherms could be divided into 6 categories:

- Type I: usually referred to microporous solids with small external surface, characterized by concavity to the relative pressure axis and asymptotic behaviour as $P/P_0 \rightarrow 1$.
- Type II: usually referred to non-porous or microporous materials. Point B in **Figure 12** shows the end of the formation of the first adsorbed monolayer and thus the beginning of multilayer adsorption.
- Type III: not common, is characterized by the convexity to the relative pressure axis over its entire range and it is not possible to distinguish Point B.
- Type IV: usually referred to mesoporous adsorbents characterized by an hysteresis loop caused by capillary condensation taking place within mesoporous structure. The initial part of the curve is associated to monolayer-multilayer adsorption and present analogies with type II.
- Type V: not common, usually referred to porous adsorbents where the adsorbent-adsorbate interactions are weak.

- Type VI: characterized by a multi-step trend, where each step is influenced by temperature and features of the system [8]. These isotherms are usually obtained with argon or krypton on graphitized carbon blacks at liquid nitrogen temperature.

IUPAC classification of hysteresis loops is based on the different shapes that they could exhibit (**Table 29**).

Table 29. Pore structure associated to the shape of the hysteresis loop.

Shape of hysteresis loop	**Pore structure**
H1	Porous materials consisting of agglomerates or compacts of spheres with narrow distribution of pore size
H2	Porous materials (e.g. inorganic oxide gels and porous glasses) with not well-defined pore size and shape
H3	Aggregates of plate-like particles with slit-shaped porosity
H4	Materials with narrow slit-like pores and microporous material with type I isotherms

As seen in **Table 29**, each type of hysteresis loop is associated to a specific pore structure.

The sample of glass powder obtained by synthesis VII was analysed by BET device aiming at definite its textural properties.

The hysteresis loop resulted is reported in **Figure 81**.

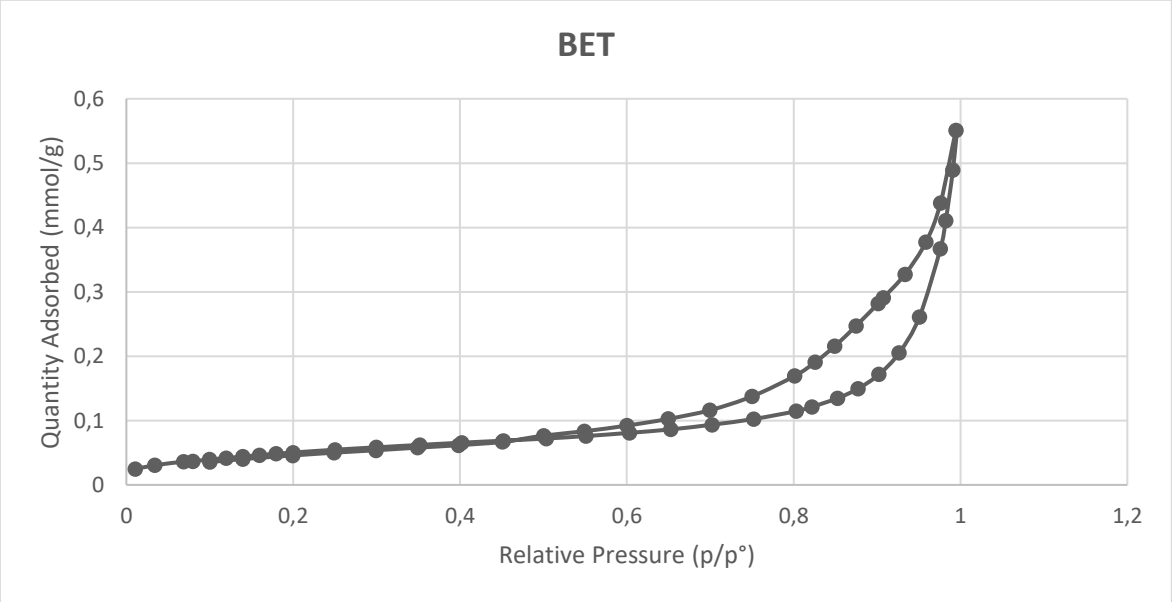

Figure 81. Hysteresis loop of glass sample obtained by synthesis VII.

BET analysis was fundamental to classify the material according to its porosity, in fact it provided information about surface area and pore volume (**Table 30**).

Sample mass	Cold free space	Analysis bath temperature	Warm free space	Sample density	Surface area	Pore volume
0.1575 g	48.2718 cm^3	77.086 K	16.2668 cm^3	1.00 g/cm^3	4.3308 m^2/g	0.016 cm^3/g

Differently to the expectations, these results have shown that the obtained material does not possess typical textural properties of mesoporous materials.

Therefore, from the comparison with previous realized melt-derived 47.5B (MD-47.5B) and sol-gel derived 47.5B (SG-47.5B) this result is in the range of bioactive glasses produced by typical sol-gel synthesis. In fact, melt derived 47.5B was characterized by 0.64 m^2/g while sol-gel products were characterized 2.23 m^2/g and 1.23 m^2/g [2]. The value obtained by BET analysis of our sample (4.33 m^2/g) is double in comparison of sol-gel 47.5B product, but it was still far away from the range which characterized mesoporous materials (until 200 m^2/g).

BET provided also results about pore volume (0.016 cm^3/g) which resulted comparable with the ones to the values obtained by MD-47.5B (0.0013 cm^3/g) and by SG-47.5B (0.016 and 0.002 cm^3/g, calcinated at 625 °C and 800 °C respectively).

Although **Figure 83** may remind to hysteresis loop of type IV, characteristic of mesoporous materials, the shape of the obtained loop is quite different from it.

Bibliography

[1] P. K. Khan *et al.*, "Influence of single and binary doping of strontium and lithium on in vivo biological properties of bioactive glass scaffolds," *Sci. Rep.*, vol. 6, no. February, pp. 1–18, 2016, doi: 10.1038/srep32964.

[2] E. Fiume, C. Migneco, E. Verné, and F. Baino, "Comparison Between Bioactive Sol-Gel and Melt- Derived Glasses / Glass-Ceramics Based on the Multicomponent SiO 2 – P 2 O 5 – CaO – MgO – Na 2 O – K 2 O System," 2020, doi: 10.3390/ma13030540.

[3] M. Shoaib, A. Saeed, M. S. U. Rahman, and M. M. Naseer, "Mesoporous nano-bioglass designed for the release of imatinib and in vitro inhibitory effects on cancer cells," *Mater. Sci. Eng. C*, vol. 77, pp. 725–730, 2017, doi: 10.1016/j.msec.2017.03.288.

[4] A. López-Noriega, D. Arcos, I. Izquierdo-Barba, Y. Sakamoto, O. Terasaki, and M. Vallet-Regí, "Ordered mesoporous bioactive glasses for bone tissue regeneration," *Chem. Mater.*, vol. 18, no. 13, pp. 3137–3144, 2006, doi: 10.1021/cm060488o.

[5] L. Magistrale and I. Biomedica, "POLITECNICO DI TORINO Corso di Laurea Magistrale in Ingegneria Biomedica Tesi di Laurea Magistrale scaffolds for clinical applications in contact with hard tissues," 2017.

[6] University of California Riverside, "Introduction to Energy Dispersive X-ray Spectrometry (EDS)," pp. 1–11, 2013, [Online]. Available: http://micron.ucr.edu/public/manuals/EDS-intro.pdf.

[7] C. Vitale-Brovarone, E. Vernè, M. Bosetti, P. Appendino, and M. Cannas, "Microstructural and in vitro characterization of SiO2-Na 2O-CaO-MgO glass-ceramic bioactive scaffolds for bone substitutes," *J. Mater. Sci. Mater. Med.*, vol. 16, no. 10, pp. 909–917, 2005, doi: 10.1007/s10856-005-4425-0.

[8] K. S. W. Sing and R. T. Williams, "Review Physisorption Hysteresis Loops and the Characterization of Nanoporous Materials," no. 1, pp. 773–782, 2004, doi: 10.1260/0263617053499032.

[9] "Brunauer-Emmett-Teller (BET) surface area analysis."

[10] M. Sudibandriyo, "A SIMPLE TECHNIQUE FOR SURFACE AREA

DETERMINATION THROUGH SUPERCRITICAL CO 2 ADSORPTION," vol. 14, no. 1, pp. 1–6, 2010.

[11] E. E. L. Sr--, J. Brame, and C. Griggs, "Surface Area Analysis Using the Brunauer-Emmett-Teller (BET) Method Scientific Operating Procedure Series : SOP-C Environmental Laboratory," no. September, 2016.

[12] S. S. Soni, G. Brotons, M. Bellour, T. Narayanan, and A. Gibaud, "Quantitative SAXS analysis of the P123/water/ethanol ternary phase diagram," *J. Phys. Chem. B*, vol. 110, no. 31, pp. 15157–15165, 2006, doi: 10.1021/jp062159p.

[13] M. A. Faiz Afzal, "A review on Pluronic block copolymer micelles: structure and dynamics," 2013, [Online]. Available: https://www.acsu.buffalo.edu/~m27/images/Pluronics_structure_dynamics_review.pdf.

[14] P. Alexandridis and Y. Lin, "5587 SANS investigation of polyether block copolymer micelle structure in mixed solvents of water and formamide, ethanol, or glycerol," *Macromolecules*, vol. 33, no. 15, pp. 5574–5587, 2000, doi: 10.1021/ma000332o.

[15] P. Horcajada, A. Rámila, K. Boulahya, J. González-Calbet, and M. Vallet-Regí, "Bioactivity in ordered mesoporous materials," *Solid State Sci.*, vol. 6, no. 11, pp. 1295–1300, 2004, doi: 10.1016/j.solidstatesciences.2004.07.026.

[16] I. Izquierdo-Barba, L. Ruiz-González, J. C. Doadrio, J. M. González-Calbet, and M. Vallet-Regí, "Tissue regeneration: A new property of mesoporous materials," *Solid State Sci.*, vol. 7, no. 8, pp. 983–989, 2005, doi: 10.1016/j.solidstatesciences.2005.04.003.

[17] D. Arcos and M. Vallet-Regí, "Sol-gel silica-based biomaterials and bone tissue regeneration," *Acta Biomater.*, vol. 6, no. 8, pp. 2874–2888, 2010, doi: 10.1016/j.actbio.2010.02.012.

[18] D. L. Herting, "Solubilities of Sodium Nitrate , Sodium Nitrite , and1 Sodium Aluminate in SimuLated Nuclear Waste," 1984.

[19] I. Dobrosz-go, J. Carlos, O. Toro, A. Miguel, C. This, and J. C. Eng, "Potassium Nitrate Solubility in (Water + Ethanol) Mixed Solvents at Di ff erent Temperatures

and Hydrochloric Acid Concentrations . Experimental Study and Modeling Using the Extended UNIQUAC Model," 2020, doi: 10.1021/acs.jced.9b00753.

[20] A. Time, "Aging Time and Temperature Effects on the Structure and Bioactivity of Gel-Derived 45S5 Glass-Ceramics €," vol. 38, no. 34704, pp. 30–38, 2015, doi: 10.1111/jace.13258.

Chapter 5 – Conclusions and Future Developments

This experimental work focused on the design and development of multifunctional mesoporous bioactive glasses for bone regeneration applications. For the first time, the sol gel synthesis combined with the supra molecular chemistry of surfactants were applied to the composition 47.5 SiO_2 -20 CaO-10 MgO-10 Na_2O- 10 K_2O- 2.5 P_2O_5 , developed on Politecnico di Torino and named as 47.5B.

As it was expected, the realization of mesoporous bioactive glasses based on a complex system of six oxide constituted a big challenge.

The theoretical work of synthesis design represented a preliminary and fundamental part in the develop of such structured system. Reagent solubility and crosstalk between chemically different precursors, surfactant need to be solute and its ability to organize itself in micelles under appropriate conditions were some of the factors which impacted on synthesis outcomes.

For these reasons, a deep study was conducted on precursors of 47.5B system (SiO_2-P_2O_5-CaO-MgO-Na_2O-K_2O) aiming at reducing problems derived from their need to be solvated in a common medium.

Another important impacting factor in the synthesis design was represented by structure directing agent. The introduction of a template in the sol-gel route was necessary for the synthesis of mesoporous bioactive glasses but involved the need to understand major concepts of supra molecular chemistry of surfactants.

Several syntheses were conducted trying to combine exigences of reagent solubility and need of precise environmental conditions to induce surfactant micellization. Each result was studied through both bibliographic support and experimental morphological, thermal, and chemical characterization.

The design of the last two syntheses allowed the realization of glass-ceramic products. These results were possible also thanks to the thermal characterization of the gel derived from the synthesis by Differential Thermal Analysis (DTA) which allowed the individuation of calcination temperature at 700 °C. The calcinated products were milled and morphological and chemical analysed.

Scanning Electron Microscopy (SEM) conducted on powdered sample showed the presence of grains in the material surface, typical of sol-gel products, while Energy Dispersive Spectroscopy (EDS) confirmed the presence of each precursors in proportions dictated by 47.5B system.

Same analyses were conducted on precipitate derived from previous synthesis to deeper understand causes of solubility problems. EDS results confirmed that the precipitate nanospheres were due to the difficulty of dissolving all reagents in the same solvent system. The high concentration of sodium, potassium and oxygen and the very low amount of silica, calcium and magnesium in the sample collected from precipitate indicated that it was constituted by sodium nitrate and potassium nitrate reagent which never dissolved in the solution. This analysis allowed to exclude the hypothesis of precipitation of 47.5B glass nanosphere.

X-Ray Diffraction (XRD) analysis was performed on sample powders to assess microstructural features of the material and identify the presence of crystalline phases deriving from the thermal treatments.

Brunauer- Emmet- Teller (BET) analysis, which is fundamental to determine material porosity, exhibited surface area value very far from the ones that characterized a mesoporous material.

All the results reported during this experimental activity were compared to the ones previously obtained in bioactive sol-gel and melt-derived glasses/ glass ceramics based on 47.5B composition [1]. Indeed, melt quenching route and sol-gel synthesis were already used to realize glasses based on the same composition in Politecnico di Torino.

Considering the melt derived 47.5B (MD-47.5B) sample, DTA termograph clearly showed the characteristic glass transition temperature (T_g), crystallization onset temperature (T_x) and maximum rate of crystallization temperature (T_c) identified at 550, 700, and 750 °C respectively.

Differently to MD- 47.5B, in sol- gel derived 47.5B (SG-47.5B) and in the product derived from this experimental activity in synthesis VIII (here referred as MBG-47.5B), it was not possible to clearly define a workability window (T_x -T_g) and so two different calcination temperatures were selected: for SG-47.5B T_{s1} and T_{s2} were 625 °C and 800 °C, while we decided to individuate as T_{s1} and T_{s2} for MBG-47.5B 625 °C and 700 °C.

Considering EDS chemical evaluation all the products (MD-47.5B, SG-47.5B and MBG-47.5B) reported the same element proportions showing that are all in compliance with the original 47.5B composition.

The BET results are the most important to classify a material according to its porosity. This analysis, in fact, reported values of textural features, such as specific surface area and pore volume. Differently to the expectations, the results from BET analysis of MBG-47.5B (4.33 m^2/g) did not show significative differences with the ones reported from MD-47.5B (0.64 m^2/g) and SG-47.5B (2.23 m^2/g and 1.23 m^2/g, calcinated at 625 °C and 800 °C respectively). This result is very far from the values needed to define a material as mesoporous (up to 200 m^2/g).

Therefore, BET provided results about pore volume (MBG-47.5B had a pore volume of 0.016 cm^3/g) and they are comparable to the ones previously obtained by MD-47.5B (0.0013 cm^3/g) and SG-47.5B samples (0.016 and 0.002 cm^3/g, calcinated at 625 °C and 800 °C respectively).

In this perspective, the possibility to realize multifunctional mesoporous scaffolds was studied exploring the introduction of different ions as doping elements in literature.

Lithium perfectly suits the desire to find an element which confers additional properties to the final bioactive device but does not report interaction problems in the synthesis of mesoporous materials. Both lithium nitrate and lithium carbonate, which are main lithium precursors, are perfectly soluble in water while lithium nitrate is also soluble in ethanol. Even if, some results have newly shown that the choose between lithium nitrate or carbonate introduction in sol gel route impacts gelation process: lithium nitrate has not impact on synthesis pH and gel is formed in three days, while lithium carbonate increases pH and gelation occurs more rapidly in just an hour [2].

Lithium has also effect on sintering temperature showing a perceptible decrease on crystallization offset temperature [3][4]. An hypothesis has been theorized upon this mechanism assuming that the silanol residues (Si-OH) are poor lithium chelators at the pH at which the synthesis was carried out [5][2].

It has also been reported that Li_2SiO_2 crystallization induces solid-phase separation and the formation of a glass-ceramic material [2]. After thermal stabilization, lithium resided in an amorphous network characterized by short range disorder. Recent studies have indeed

shown that lithium introduction in glass composition causes a change in connectivity [2]. These experimental observations have suggested that lithium acts as a network modifiers and diffuses through silica network by breaking oxygen bonds in order to balancing the charge into the structure [6].

Recently, some reports have proved the promising effect of incorporating lithium ions on bone mineral density [7]. These authors have reported that lithium might interfere with calcium transport within the body, enhancing the proliferation, differentiation, cementogenic gene expression, and osteogenic differentiation [8][9].

Therefore, lithium doped bioactive glasses have been investigated to determine their *in vitro* bioactivity. Once Li-doped bioactive glasses are immersed in Simulated Body Fluid (SBF), the formation of an apatite-like layer is exhibited on material surface after one hour of immersion [10].

Several studies have synthesized Li-BG scaffolds. Analyses obtained by SEM micrographs have confirmed lithium doped BG excellent bioactivity, indicated by the presence of cauliflower-like structures, typical of calcium phosphate formation, on scaffold surface [10].

More recently, few studies have developed MBG scaffolds doped with lithium. These experiments have reported that there is a great benefit in using MBGs to deliver active ions as lithium [2]. The release of lithium from Li-doped MBGs have shown beneficial effects on the proliferation and cementogenic differentiation of bone tissue, and their applications have been particularly investigate into dental regeneration [2][8].

Lithium action seems also to promote combinational effect, when incorporated into quaternary system containing calcium and silica, superior to the sum of the individual ionic contribution on cell metabolism [2].

In conclusion, the research on multifunctional mesoporous bioactive glasses still offers a huge number of opportunities for clinical application in tissue engineering and regenerative medicine. The possibility to properly tailor different therapeutic device continues to represent an extremely attractive challenge for biomedical investigations.

Bibliography

[1] E. Fiume, C. Migneco, E. Verné, and F. Baino, "Comparison Between Bioactive Sol-Gel and Melt- Derived Glasses / Glass-Ceramics Based on the Multicomponent SiO 2 – P 2 O 5 – CaO – MgO – Na 2 O – K 2 O System," 2020, doi: 10.3390/ma13030540.

[2] A. L. B. Maçon *et al.*, "Lithium-silicate sol–gel bioactive glass and the effect of lithium precursor on structure–property relationships," *J. Sol-Gel Sci. Technol.*, vol. 81, no. 1, pp. 84–94, 2017, doi: 10.1007/s10971-016-4097-x.

[3] B. Zhang and Æ. A. J. Easteal, "Effect of HNO 3 on crystalline phase evolution in lithium silicate powders prepared by sol – gel processes," pp. 5139–5142, 2008, doi: 10.1007/s10853-008-2736-5.

[4] F. Wang, K. Li, and C. Ning, "Sintering properties of sol – gel derived lithium disilicate glass ceramics," pp. 372–379, 2018, doi: 10.1007/s10971-018-4738-3.

[5] D. L. Dugger, J. H. Stanton, B. N. Irby, L. Bobby, W. W. Cummings, and R. W. Maatman, "The Exchange of Twenty Metal Ions with the Weakly Acidic Silanol Group of Silica," vol. 68, no. 4, pp. 5–8, 1964, doi: 10.1021/j100786a007.

[6] B. Yu *et al.*, "E ff ect of Calcium Source on Structure and Properties of Sol − Gel Derived Bioactive Glasses," 2012, doi: 10.1021/la303768b.

[7] M. Khorami, S. Hesaraki, A. Behnamghader, H. Nazarian, and S. Shahrabi, "In vitro bioactivity and biocompatibility of lithium substituted 45S5 bioglass," *Mater. Sci. Eng. C*, vol. 31, no. 7, pp. 1584–1592, 2011, doi: 10.1016/j.msec.2011.07.011.

[8] P. Han, C. Wu, J. Chang, and Y. Xiao, "The cementogenic differentiation of periodontal ligament cells via the activation of Wnt/β-catenin signalling pathway by Li + ions released from bioactive scaffolds," *Biomaterials*, vol. 33, no. 27, pp. 6370–6379, 2012, doi: 10.1016/j.biomaterials.2012.05.061.

[9] B. Liu and Q. Wu, "Lithium use and risk of fracture : a systematic review and meta-analysis of observational studies," pp. 257–266, 2019.

[10] V. Miguez-Pacheco *et al.*, "Development and characterization of lithium-releasing silicate bioactive glasses and their scaffolds for bone repair," *J. Non. Cryst. Solids*,

vol. 432, pp. 65–72, 2016, doi: 10.1016/j.jnoncrysol.2015.03.027.

Acknowledgments

Mi è doveroso dedicare questo spazio del mio elaborato alle persone che hanno contribuito, con il loro instancabile supporto, alla realizzazione dello stesso.

Un ringraziamento sincero va al mio relatore Professoressa Enrica Vernè per l'interesse nella materia che ha saputo trasmettere durante i corsi e la sua disponibilità durante lo svolgimento di tutta l'attività sperimentale.

Ringrazio infinitamente il mio correlatore Professore Francesco Baino per non avermi fatto mai mancare il suo supporto durante l'attività sperimentale e nei mesi difficili che tutti noi abbiamo passato a causa della pandemia Co-Vid19. Grazie ai suoi insegnamenti mi sono avvicinata al mondo della ricerca con entusiasmo e curiosità. La sua inesauribile tenacia e il suo ottimismo sono stati i motori che mi hanno spinta durante tutto il lavoro di tesi a credere nel progetto di ricerca e nelle mie capacità. La sua fiducia nei miei confronti è per me fonte di grande orgoglio.

È per me doveroso dedicare un grazie speciale alla Dottoressa Elisa Fiume. La tua presenza in questo percorso è stata per me fonte di inesauribile forza. Grazie per avermi accompagnato in ogni passo dal primo giorno, per avermi insegnato tanto e per avermi sempre fatta sentire sicura anche nei momenti più difficili. La mia stima e il mio sincero affetto nei tuoi confronti sono grandi. Grazie per l'esempio di donna, professionista e ricercatrice che rappresenti per me.